Geochemical Perspectives

Volume 1, number 3 | July 2012

Bjørn Jamtveit
Øyvind Hammer

Sculpting of Rocks by Reactive Fluids

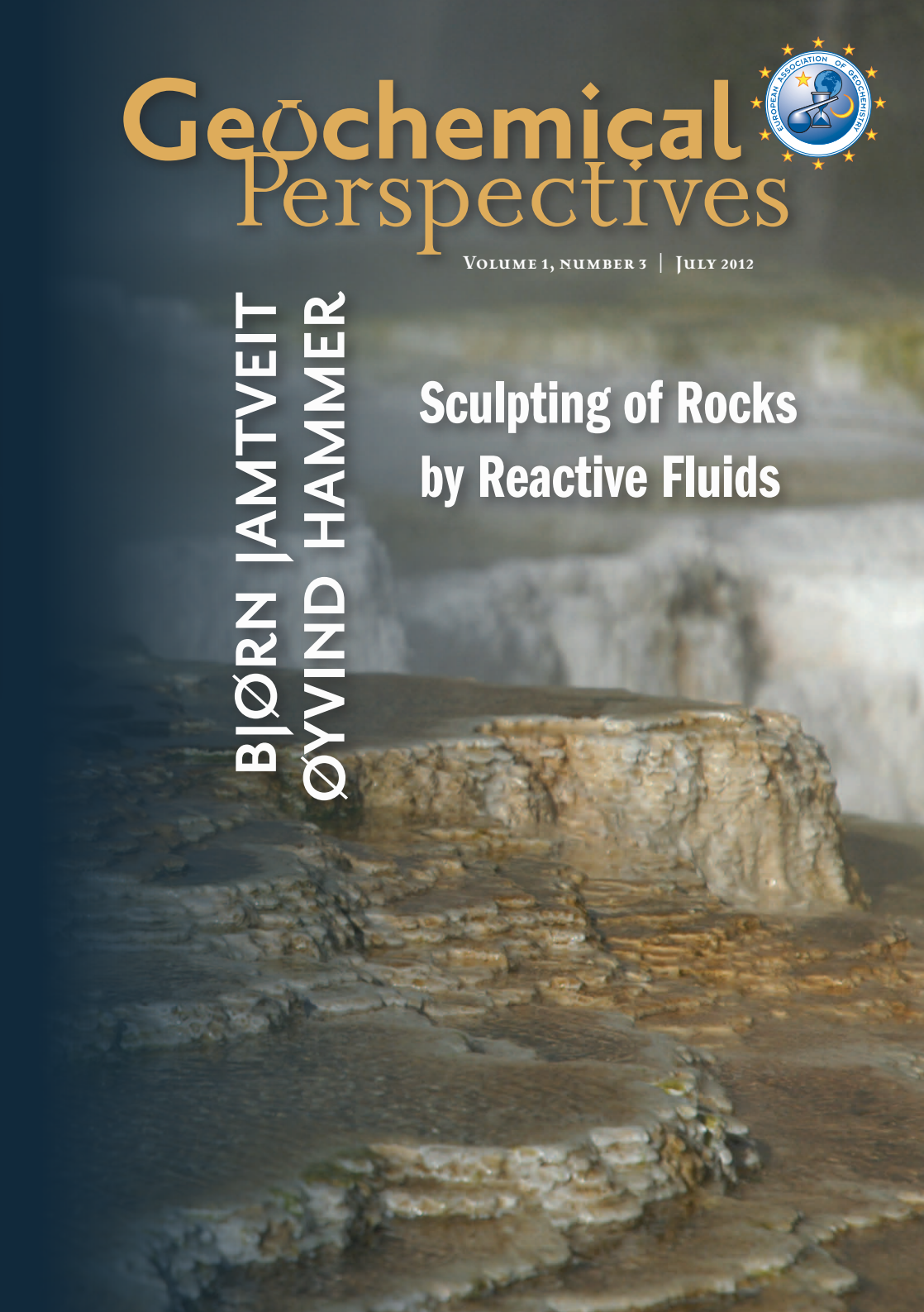

Geochemical Perspectives

Each issue of ***Geochemical Perspectives*** presents a single article with an in-depth view on the past, present and future of a field of geochemistry, seen through the eyes of highly respected members of our community. The articles combine research and history of the field's development and the scientist's opinions about future directions. We welcome personal glimpses into the author's scientific life, how ideas were generated and pitfalls along the way. *Perspectives* articles are intended to appeal to the entire geochemical community, not only to experts. They are not reviews or monographs; they go beyond the current state of the art, providing opinions about future directions and impact in the field.

ISSN 2223-7755 (print)
ISSN 2224-2759 (online)
DOI 10.7185/geochempersp.1.3

Principal Editor in charge of this issue
Susan L.S. Stipp
Reviewers
Andrew Putnis, University of Münster, Germany
Eric H. Oelkers, CNRS Toulouse, France

Cover Layout **Pouliot Guay Graphistes**
Typesetter **Info 1000 Mots**
Printer **J.B. Deschamps**

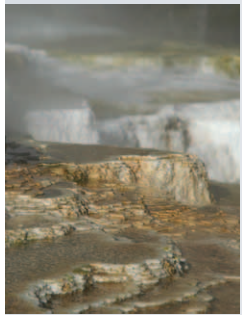

ABOUT THE COVER
Travertine terraces and terracettes growing at a rate of centimetres per year at Canary spring, Mammoth, Yellowstone National Park.
Photo: Dag K. Dysthe, PGP

CONTENTS

DEDICATION

We dedicate this volume to the memory of Ivan Th. Rosenqvist (1916-1994), a truly cross disciplinary Norwegian geochemist. He was sentenced to death for espionage against the Nazis in 1942 and wrote most of his PhD on augen gneisses and granitisation in the Oppdal area (Southern Norway) while on "death row" during 18 months in solitary isolation, before being pardoned and sent to Sachsenhausen in 1944.

Ivan Th. Rosenqvist (1916-1994)

Rosenqvist was a communist and was forced to leave the Norwegian Defense Research Establishment in 1950 because of his political views. He was also highly controversial in the 70s and 80s for his science based, but politically "incorrect", views on the effects of acid rain on Norwegian lakes. Although he was often used as an external consultant by public and private organisations because of his expertise on a broad range of topics relevant for engineering projects, including the properties of clays, he saw this activity as part of his duty as a university professor and refused to accept private income for it.

Although we don't share all of his political views, we certainly believe that Ivan Rosenqvist was an example to follow as a person who was willing and able to extend his science to other disciplines whenever he felt that this was necessary to make his research relevant for society.

The moment one gives close attention to any thing, even a blade of grass, it becomes a mysterious, awesome, indescribably magnificent world in itself.

Henry Miller

PREFACE

The authors of this volume share a common interest in the patterns of the Earth and what these patterns can tell us about how the Earth works. Thus, we are particularly interested in patterns that emerge spontaneously during some geological processes, rather than patterns that are dictated by a pre-existing template or natural heterogeneity formed or controlled by factors external to the system of interest. We are tempted to suggest that the group of geoscientists, who tend to favour natural heterogeneity as the source of most natural patterns, ignores the fact that these heterogeneities must be derived from somewhere and that this somewhere might be a more interesting place than the simple linear world dominated by small causes and dull effects. Moreover, we believe that by studying emergent patterns, we broaden the scope of geoscience from a strictly disciplinary domain, to a more integrated part of natural science where cross disciplinary links must be made to connect causes and effects in a meaningful and precise way.

Geochemistry was born as a new science when Victor Goldschmidt (1911) applied thermodynamics to understand the distribution of minerals in the contact aureoles around the intrusives in the Oslo Rift. More recently, *geomicrobiology* has become a rapidly growing scientific discipline in its own right. Chemical reactions in geosystems at temperatures below the boiling temperature of water are often controlled by microorganisms and microorganisms are too dependent on interactions with Earth materials to explain such processes without this new branch of natural science. It is neither a branch of geoscience nor of biology *but both*.

The conceptual framework that exists within traditional geochemistry must be expanded to include among other factors: mechanical processes, a more adequate description of flow processes (both complex flows such as turbulence and flow in/on complex media), effects of surface forces and biological activity, if we are to understand the variety of the patterns and processes generated by the action of reactive fluids on and below the Earth's surface. This dynamic system thinking has in many respects become a new paradigm in Earth Sciences, commonly referred to as *Earth Systems Sciences*. The birth of this paradigm is a consequence of our increasing ability to treat complex natural systems in a quantitative way. It is also a consequence of the increasing demand for Earth science to be able, not only to produce qualitative insights about the Earth's past, but also to provide quantitative predictions about the future of our planet.

In this issue, we describe a number of patterns that emerge from the interactions between reactive fluids and rocks and we discuss their origin. The paper is organised with respect to which processes are involved and how they are coupled to produce emergent patterns, rather than according to which geological system they occur in. This is natural for us because we wish to focus on dynamic processes in geosystems and because we have approached the Earth from quite different angles. Bjørn saw the complexity of the Earth's interior from the perspectives of a petrologist, whereas Øyvind started out as a mathematically inclined palaeontologist fascinated by the patterns of life through geological history. Our meeting point is pattern forming processes, not specific geological systems. An interest in pattern forming processes was also the starting point for our research centre PGP (Physics of Geological Processes), at the University of Oslo, where we have both worked for the past 9 years.

Many Earth scientists have considered pattern formation to be an esoteric interest, a diversion that brings us capriciously from geosystem to geosystem without taking any system particularly seriously and without a serious concern about *the big questions* in Earth sciences. We might also appear to be unconcerned about the *relevance* of our science because important issues such as where to find natural resources and how pollution will spread from a waste dump require focus on *pre-existing* heterogeneities such as fractures, layering, cap rocks, etc, rather than on process related pattern formation and the *emergence of structure and heterogeneities*.

To some extent, such a criticism is justified. In our defence, we argue that we are driven by a curiosity that is naturally more inclined toward understanding how the Earth works than in controlling it or exploiting its resources. Such a curiosity driven approach might not be entirely irresponsible because it is connected to a humbleness and respect for Nature that is essential if sustainable development is ever to become a realistic option. In some sense, we also feel that our process oriented and pattern forming focus brings the Earth sciences closer to us as humans. Today, when society is spending energy at a rate of ~15 TW, corresponding to ~40% of the total heat loss from the Earth's interior and by some measures, moves more solid mass than rivers, there can be no doubt that

humans *are* a major geological force. Understanding the effects of this human forcing requires a more fundamental insight into geological processes than has often been required to exploit the Earth as an "external" reservoir of energy and resources.

Finally, the pattern forming focus also brings an aesthetic dimension to our science that we find interesting and rewarding and hence motivating. There is truth in beauty.

Bjørn Jamtveit and Øyvind Hammer
Physics of Geological Processes.
University of Oslo.
P.O. 1048 Blindern, N-0316 Oslo, Norway

ACKNOWLEDGEMENTS

For the past 9 years, our work on reactive fluids and associated pattern formation has been supported by a Center of Excellence (CoE) grant from the Norwegian Research Council to PGP. In addition, we have also received support through other grants from the Norwegian Research Council, the Faculty of Mathematics and Natural Science at the University of Oslo and Marie Curie Training Networks (including DISSOLUTION-PRECIP and DELTA-MIN).

During the CoE period, we benefited from interactions with a number of staff and students working full or part time on fluid-rock interactions at PGP, including Paul Meakin, Anders Malthe-Sørenssen, Håkon Austrheim, Dag Dysthe, Jens Feder, Yuri Podladchikov, Francois Renard, Anja Røyne, Joachim Mathiesen, Maya Kobchenko, Henrik Svensen, Espen Jettestuen, Hans Amundsen, Karthik Iyer, Christophe Raufaste, Oliver Plümper, Jörn Hövelmann, and Andreas Beinlich. Among our international partners, Andrew and Christine Putnis (University of Münster) have been valuable collaborators for more than 10 years and their work on coupled dissolution and precipitation processes has influenced our own research path significantly.

We are exceptionally grateful to Principal Editor Susan Stipp for her many contributions to this issue and to Editorial Manager Marie-Aude Hulshoff for continuous support. Reviewers Eric Oelkers, Andrew Putnis and Rob Raiswell provided many valuable suggestions and comments to the manuscript, as did our PGP colleagues Anja Røyne and in particular Paul Meakin.

The water which rises in the mountains
is the blood which keeps the mountain alive.

LEONARDO DA VINCI

SCULPTING OF ROCKS BY REACTIVE FLUIDS

ABSTRACT

Interactions between rocks and reactive fluids produce a plethora of patterns, often visible to the naked eye, both at the Earth's surface and at depth. Patterns arise from the coupling between chemical reactions, transport and sometimes, mechanical processes in systems where fluids and solids are at least initially sufficiently far from thermodynamic equilibrium for non-linear processes to operate. Surprisingly often, similar patterns are formed at different scales under very different conditions in systems with different chemical compositions. For example, many of the patterns formed by growth and dissolution processes mediated by reactive fluids at or near the Earth's surface can also be seen in ice. This independence of details, or *universality*, has inspired us to organise this issue in a way that might appear to be unusual in a geochemistry context, by emphasising the similarities and differences in shapes rather than compositions.

After introducing the principles of pattern formation and reviewing the reaction path approach to reactive transport modelling, which requires a full and explicit account of homogeneous and heterogeneous chemical reactions, we begin a pattern focused discourse with a discussion of simple, surface normal growth. From the spheroidal shapes that result from surface normal growth, we continue

toward the branched and dendritic patterns arising from growth in a diffusive field. Then, the symmetry breaking effects of fluid flow, demonstrated by growth and dissolution processes on free surfaces, are introduced.

The effects of confinement in subsurface environments add another level of complexity because growth is often tightly coupled to dissolution under these conditions and volume changing reactions generate local stresses. Consequently, reactive transport in porous and/or fractured rocks is, in general, coupled with mechanical processes. To avoid the additional challenges of time dependent deformation processes such as creep, only elastic deformation and fracturing are discussed, with a focus on fracturing because many of the most spectacular patterns observed in reactive fluid-rock systems are strongly influenced by fracturing. Deformation that is slowly driven by stresses that are continuously generated by heterogeneous reactions between rocks and fluids often leads to hierarchical fracturing, which divides rock or mineral volumes into successively smaller pieces by smaller and smaller fractures. Hierarchical fracturing occurs during both serpentinisation and spheroidal weathering and it provides first order controls on the evolution of reactive surfaces area and thus overall reaction rates. Then, we explicitly describe how stresses are generated by growth in pores and again point to the lessons that can be learnt by comparing fluid rock systems to the chemically simpler situation represented by the growth of ice in soils or rocks and the similarities between them. The potential implications of reaction driven fracturing for *in situ* carbon sequestration are also emphasised.

Finally, we discuss the significance of the scaling behaviour of patterns and, in particular, the connections between patterns and processes.

Water is fluid, soft and yielding.
But water will wear away rock, which is rigid and cannot yield.
As a rule, whatever is fluid, soft and yielding,
will overcome whatever is rigid and hard.
This is another paradox: what is soft is strong.

LAO-TZU (600 B.C.)

---

1. INTRODUCTION

The morphology of rocks is continuously transformed by the action of water, wind, chemical reactions, mechanical forces and bio-activity. Weathering and erosion carve out exquisite patterns, while chemical and biological processes drive pattern formation via accretion and break down. At large scales, these processes are studied by geomorphologists and at the smallest scales, by material scientists. Geological pattern formation at intermediate scales has received far less attention, although it is primarily at these scales that we observe rocks. Our imaging techniques have a curious gap in the range of scales. At micrometre scale, we have microscopes and at larger scales, a battery of remote sensing techniques. However, at the human scale, rocks are more rarely depicted, described and explained. As a result, we are often unable to answer the most basic of all geological questions: Why does a rock look like it does?

Fluid and solid phase chemistry is, of course, crucial for mesoscale geological pattern formation. However, to form a pattern, chemical constituents have to move, often by diffusive or convective transport in a fluid. Mechanical forces, often considerable, contribute whether material is added or removed. Finally, biological processes can add further complexity. All these players contribute to intricate causal networks with multiple feedbacks and geometric patterns emerge as a result of, but also as a part of, the system. Studying such networks requires a multidisciplinary approach in which geochemistry, solid and fluid mechanics and biology are all brought together to understand how the entire system works.

Perhaps the most striking patterns are formed where rock surfaces interact with flowing water or air. In such places, complex flow, laminar or turbulent, can contribute to the formation of intricate patterns, such as tafoni, travertine terraces, dissolution scallops and rilles. Such interfaces are also prime territory for biota, which are sometimes involved in the formation of shapes such as botryoids and stromatolites.

If space is not available for pattern formation, material has to be replaced or space must be provided by deformation or dissolution. This involves crystal growth in pores, volume changes and the resulting mechanical stresses, which drive ductile and brittle deformation. The changes in geometry and the opening of new conduits accelerate and control fluid flow, driving the processes further. Mechanochemical coupling in the presence of fluids is responsible for most weathering processes and it is also important deeper in the subsurface. One example of potential industrial relevance is natural and artificial geological sequestration of reactive fluids, including serpentinisation and carbonation of mafic and ultramafic rocks.

In this wide ranging and perhaps bewildering field, there are recurrent themes of a more theoretical nature. The study of complex and emergent processes can benefit from systems thinking on a more abstract level, aided by

computer simulation and pattern formation theory, sometimes borrowed from developmental biology. In this overview, we present a number of computer models using a wide range of abstraction levels, from almost purely geometric models to mechanistic models using detailed equations for fundamental processes. These different approaches to modelling are suited for answering different questions – and they are all useful.

1.1 Principles of pattern formation

Patterns in geology and biology raise fundamental questions about how nature works. A naive interpretation of the second law of thermodynamics implies that the world should tend toward homogeneous noise. While this might be the case for the universe as a whole, it is obviously not true at a local scale or for limited time periods. Pattern formation exports structural entropy to other regions or other degrees of freedom. It turns out that this usually happens through only a few basic principles, mainly involving nonlinear feedback mechanisms. Identifying these principles in a geological system is a fruitful way of investigating and understanding geological pattern formation (Hammer, 2009). A more elaborate discussion of the pattern concept is given in the Supplementary Section at the end of this paper.

1.1.1 Positive feedback and lateral inhibition

The fundamental requirement for any pattern to form is *localisation*. There has to be some mechanism that maintains spatial and temporal coherence and stimulates its own growth. For example, a crystal enhances its own growth by providing a growth surface that makes further nucleation redundant and a crack enhances its growth by stress concentration at the crack tip. A city attracts more people the larger it is; a river digs deeper and produces a larger catchment area the larger it is. These are examples of positive feedback processes. They lead to exponential, explosive increase, unless checked by other processes.

Positive feedback is necessary but not sufficient to produce a pattern. A competitive situation, in which the larger or earlier elements of a system win over elements nearby, leading to a pattern of separated units can occur if the elements inhibit growth at a distance (lateral inhibition). Such overdispersed distributions can be detected by standard methods from spatial statistics for detecting deviations from spatial homogeneity, such as Ripley's K analysis (more information in the Supplementary Section and Hammer, 2009).

We have found that many of the self organising geological systems described in this overview can be placed into the powerful paradigm of local amplification and lateral inhibition. Dendrites form through positive feedback by nucleation and lateral inhibition mediated by depletion of the diffusing species that form the dendrites. For travertine terraces, the lateral inhibition is caused

by the reservoir of water that accumulates behind growing rims and drowns upstream rims. For fracturing patterns, the positive feedback consists of stress concentration at the crack tip, while a lateral inhibition loop might be provided by cracks that relieve stress and set up "stress shadows".

Under some conditions, such systems self organise into regular patterns of dots, stripes, waves or other shapes with a more or less constant spacing. It is therefore of interest to identify characteristic wavelengths in these patterns. Self organised, more or less regular patterns are seen in some geological cases, such as dissolution scallops, Liesegang rings and columnar jointing. On the other hand, we have not yet been able to establish whether travertine terraces are regularly spaced or not (Hammer *et al.*, 2010). Another interesting case, which is still unresolved in this respect, is the possible lateral spacing of carbonate concretions in sediments (Fig. 1.1). The possibility that similar self organisation in the vertical direction gives rise to "diagenetic bedding" has been heavily debated and modelled (*e.g.* Böhm *et al.*, 2003). Regular patterns formed by local self enhancement and diffusion of a chemical inhibitor are often referred to as *Turing patterns* (in a broad sense). The extent to which this reaction-diffusion mechanism is important in geological and biological pattern formation is still unknown.

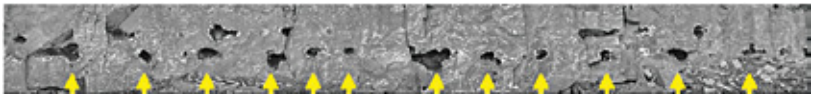

Photo: Øyvind Hammer.

Figure 1.1 Possible metre scale wavelength between carbonate concretions (marked by arrows) along a mudstone bed in the Elnes Formation, Middle Ordovician, Oslo region. In this picture, the carbonate concretions are largely weathered out to form cavities in the surrounding mudstone. Field of view is ca. 10 m.

1.1.2 Travelling fronts and oscillations

Pattern formation by competitive Turing-like mechanisms takes place concurrently over the whole domain. An alternative is sequential pattern formation, in which a morphogenetic zone moves across the domain and leaves a regular pattern behind. To place people with regular spacing in a row (Fig. 1.2), we can either let them all first move into random positions and then move around to adjust the distance to each neighbour (concurrent process) or we can start at one end and measure a fixed distance from one person to the next (sequential process). This distinction has been much debated in biology, where it now has been shown that while some regular patterns are produced concurrently (*e.g.* the distribution of hair follicles), others are made sequentially (*e.g.* the precursors of vertebrae in the vertebrate spine).

Photo: Øyvind Hammer.

Figure 1.2 Self-organised regular spacing of passengers at a metro station in Oslo.

Liesegang banding is a good example of sequential pattern formation in geology (Stern, 1954). This fascinating phenomenon was first studied in detail by Raphael E. Liesegang (1896 and later papers). He dropped a solution of $AgNO_3$ onto a thin sheet of gelatin with $K_2Cr_2O_7$ and observed the development of concentric rings of precipitated $Ag_2Cr_2O_7$. It was later observed that the spacing of the rings followed a geometric series. An intriguing aspect of Liesegang's original paper is that he emphasises the similarity between this phenomenon and biological pattern formation – in fact this seems to have been his reason for carrying out experiments in gels: "Therefore I consider especially the formation of structure in structureless matter and in particular the peculiar rhythmic appearances as important for the developmental mechanics of organisms" (Liesegang, 1896; our translation). This way of thinking predates the work of Turing and later theoretical developmental biologists by fifty years.

Photo: Bjørn Jamtveit.

Figure 1.3 Liesegang banding in rhyolite, Argentina. In this case, the banding is related to oxidation of Fe during post magmatic infiltration in a process similar to that which causes the familiar Liesegang banding in sandstones.

Concentric and parallel stripes reminiscent of Liesegang banding are observed in many geological systems, including agates and cherts, rhyolite (Fig. 1.3), sandstones

and limestones (Fig. 1.4). In sedimentary rocks, the bands typically consist of iron oxides believed to have precipitated as oxygen diffused into regions in which iron was dissolved in pore water (*e.g.* McBride, 2003; Barge *et al*., 2011). A similar banded appearance can occur when a visible rock face intersects undulating primary laminations. In contrast, true diagenetic or weathering related Liesegang bands can cross cut the primary bedding.

The mechanism responsible for Liesegang banding has been heavily debated and the literature is too large to be adequately reviewed here. The most well known model is Ostwald's (1897) supersaturation theory. In this sequential pattern formation model, one reacting species diffuses out from the source into a field containing another reactant. As the diffusion front travels outwards, the pore water becomes supersaturated with respect to the reaction product. When precipitation finally commences, it proceeds so quickly (through the positive feedback loop of nucleation and rapid growth from the supersaturated solutions) that it depletes the field around it, producing a zone of lateral inhibition. As the front continues, the process is repeated, leading to oscillation in time and space. The *delayed response* connected with supersaturation is of fundamental importance in this process. Such delays, and subsequent overcompensation, are responsible for oscillation in many regulatory systems such as predator-prey systems and in engineering challenges such as thermostats and autopilot devices.

Scanned by Øyvind Hammer from the 1808 original.

Figure 1.4 Compartmentalised Liesegang banding formed between cemented fractures in the famous landscape marble (*pietra paesina*) from Tuscany (*cf.* McBride, 2003). This stone was probably first used as decorative table tops by the Medici family. This is a drawing from F. J. Bertuch's *Bilderbuch für Kinder* (Vol. 5, 1808).

Another theory invokes an Ostwald ripening process in which larger particles grow faster than smaller ones (*e.g.* Sultan and Ortoleva, 1993), producing a local positive feedback loop as well as lateral inhibition of smaller nuclei by depletion of reactants.

1.2 Aspects of computer modelling

1.2.1 Why modelling?

The purpose of numerical modelling in the natural sciences, especially geology and biology, is often misunderstood. In engineering, the systems are often relatively well understood, the initial conditions are relatively well defined and the simulations have predictive power. This is not the case for most geological problems where we do not understand the mechanisms. So what is the purpose of modelling based on insufficient knowledge and understanding?

A model is a way to specify and communicate our present understanding of the system. Formulating a numerical model forces us to think about the processes that could be at work and make judgements about which are likely to be the most important. The model is therefore at least a partial cure against fuzzy ideas and futile discussion about definitions. In this respect, modelling is similar to writing down ideas on paper; it is a thinking aid.

The results of modelling establish whether our postulated mechanisms are sufficient to reproduce the most important characteristics of natural patterns and how they are formed. The development of a model is an iterative, experimental process in which processes and parameters are changed and tuned until reasonable agreement with nature is achieved. This process leads to new research questions that can be addressed by field observations or laboratory experiments.

Finally, once we have a reasonable, working model, we have access to a tool providing a degree of control that is unachievable in the laboratory or field. We can use the model to study the effects of varying the parameters or we can switch off specific mechanisms to isolate the dominant processes responsible for pattern formation.

For these reasons, we strongly advocate the use of computer simulation in all areas of geology, in combination with field and laboratory work. This would likely require adjustments to the geology curriculum, with more emphasis on courses in physics, applied and numerical mathematics and computer programming so that geologists would be able to communicate more effectively with modellers.

1.2.2 Abstract and mechanistic modelling

The most important decision when developing a computer (or other) model is to define the level of detail. It might seem that the model should try to address every known process and interaction present in the natural system. However, this is not the most effective way to conduct explorative modelling. Apart from the practical problems of software complexity and insufficient computer power, a full model might not provide improved understanding of the higher level pattern formation processes. If the model captures the full complexity of the system of interest, the results would be no easier to understand than the patterns generated by the system itself. In such cases, highly abstracted and simplified (partly phenomenological) models can be much more informative. Of course, model parameters can be changed at will and observing how this changes the patterns generated by the model is a way to gain a better understanding of how the system works.

The universality of certain patterns, independent of the basic mechanism, implies that although the model reproduces the natural *pattern*, it is difficult to be absolutely certain that the postulated *mechanisms* reflect reality. This can only be investigated by modelling or laboratory experiment at even more fundamental levels.

2. REVIEW & HISTORICAL PERSPECTIVES

Reactive fluids shape the patterns of the Earth at the surface and at depth. In the following sections, we review some of the progress made in this direction, seen from our perspective.

2.1 Growth and dissolution on free surfaces

The literature focusing on three dimensional pattern formation of natural, free mineral surfaces in a fluid is not very extensive, although such patterns are often illustrated in the context of other subjects. The analogous problems in sedimentology, concerning structures such as river channels and sand ripples, have received much more attention. One challenge has been the need to bring together fluid dynamics, chemistry, computational science and field observation in single projects.

Before modern computational fluid dynamics became easily accessible to geologists, important results relevant to limestone precipitation and dissolution mediated by flowing water were obtained by researchers interested in karst phenomena. Rane Curl (1966 and later papers) studied dissolution scallops and flutes by combining theoretical analysis with laboratory experiments on gypsum. He linked hydrodynamic parameters (*Reynolds number*) with surface morphology (characteristic wavelength) through dimensional analysis.

Wolfgang Dreybrodt and his student Dieter Buhmann developed models for limestone dissolution and precipitation under turbulent flow and studied the relationship between reaction rate and flow rate resulting from thinning of a laminar boundary layer (Buhmann and Dreybrodt, 1985). These concepts have been used for modelling pattern formation in cave networks (Gabrovšek and Dreybrodt, 2001).

We discuss travertine terracing in some detail in a later section. When we started working on this fascinating example of natural pattern formation in 2004 after having participated in an expedition to hot springs in Svalbard, about the only previous theoretical work on travertine terracing was an analysis of the growth of a single rim by Wooding (1991). At the time, we did not know that physics professor Nigel Goldenfeld and his colleagues at the University of Illinois at Urbana-Champaign were also starting to work on this phenomenon using similar methods. We were both somewhat surprised and delighted when we saw each other's first publications (Goldenfeld *et al.*, 2006; Hammer *et al.*, 2007).

2.2 The *reaction path* approach to reactive transport

In contrast to the modelling of morphological changes caused by reactive transport on a free surface, reactive transport in porous media has a long history. In the following, I (Bjørn) give a somewhat personal review of the evolution of reactive transport modelling with a geochemical focus. The justification for this subjective angle, is that the progress in this type of modelling, the strengths and weaknesses of the models, as well as some of the individuals involved, influenced the direction of my own research to a significant extent. The people who I, as a petrologist, perceived as the most influential in driving geochemical transport modelling forward during the last 50 years are portrayed in Figure 2.1. I have had the pleasure of meeting all of them, except Korzhinskii.

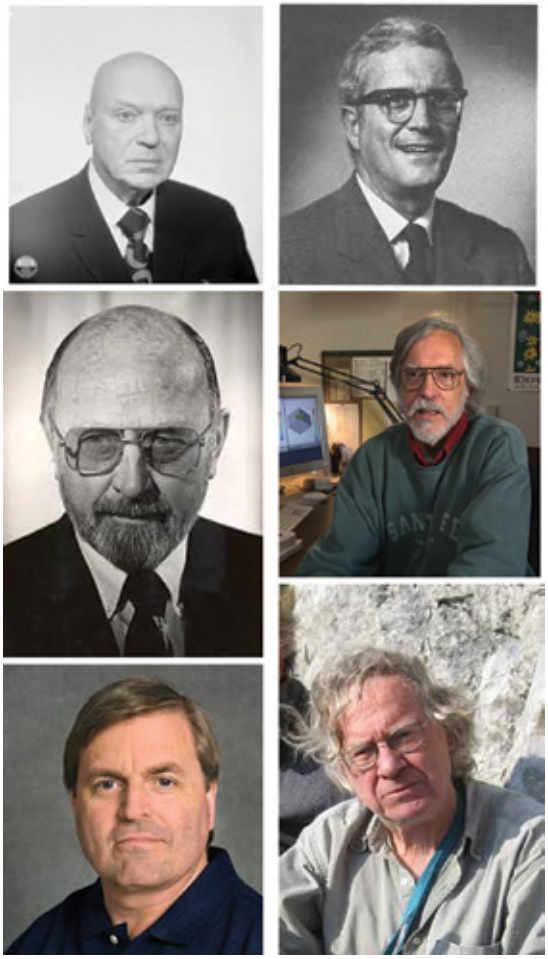

Figure 2.1 Geochemical transport modelling's *Hall of Fame* (seen from a petrologist's perspective). Dimitrii Korzhinskii (upper left), Jim Thompson (upper right), Hal Helgeson (middle left), Peter Lichtner (middle right), Carl Steefel (lower left) and Ray Fletcher (lower right).

Goldschmidt (1911) introduced equilibrium thermodynamics and the application of the Gibbs phase rule to explain the distribution of minerals in contact aureoles around intrusive bodies in the Oslo region, thereby introducing the basic concepts of the new science discipline *geochemistry*. In the late 50s, Korzhinskii and Thomson (Korzhinskii,

1957; Thompson, 1959) analysed systems that were open to mass transport and introduced the concepts "local equilibrium" and "perfectly mobile" components. A new phase rule that separated components into "inert" and "mobile", was introduced to deal with metasomatic systems. This work was later criticised by Weill and Fyfe (1964) who claimed that: "The Korzhinskii phase rule is a statement of the Gibbs phase rule for a special case. The application of it to a system of metasomatic zones is unsound since the concept of perfectly mobile components breaks down in such a system. The derivation by Thompson of a similar phase rule applicable to such metasomatic systems recognises but does not surmount the fact that the system is not in equilibrium".

The last sentence is relevant and important because it reflects the fact that an observed sequence of metasomatic zones is *path (history) dependent*. This was recognised by Hal Helgeson who in his seminal 1968 paper on *Irreversible reactions in geochemical processes involving minerals and aqueous solutions* wrote: "Because the compositional changes resulting from a geochemical process are path dependent functions, they cannot be evaluated by considering only the initial and final states of the system. To predict the mass transfer involved in such a process requires knowledge of (or assumptions about) relative reaction rates and all possible metastable and stable partial equilibrium states that might arise. Because the final observed state may not constitute a stable equilibrium state, and because the system may be partly or completely open with respect to one or more of its components, the alternate paths through which a given overall equilibrium state may be achieved are of particular interest in chemical petrology" (Helgeson, 1968). This insight, followed up by an incredible amount of work by Helgeson and collaborators at the University of California, Berkeley, including compilation of thermodynamic data for rock forming minerals and aqueous solutions, built an essential basis for modern process focused geochemistry. This was the cradle of the "SUPCRT generation (Johnson *et al.*, 1992) of scientists that today runs geochemical models across the world".

In the 1970s, the rates of heterogeneous reactions were poorly known. Thus, a proper kinetic description of these irreversible reactions was often beyond our reach. As a response, more general approaches were suggested, including the introduction of nonequilibirum thermodynamics (Fisher, 1973; 1978). According to the theory of linear nonequilibrium thermodynamics, fluxes (*e.g.* mass fluxes) are linearly related to the driving forces (such as temperature gradients or chemical potential gradients) and this approach is applicable only to systems sufficiently close to equilibrium. Any application of this theory requires insight into the coefficients that relate fluxes to forces – the Onsager coefficients (Onsager, 1931) and because these transport coefficients were also poorly known; even nonequilibrium thermodynamic theory had little predictive power. However, it was used to analyse observed sequences of metasomatic zoning and rims around reacting mineral grains to constrain the relative values of the transport coefficients (*cf.* Joesten, 1977; Foster, 1981; Nishiyama, 1983). Recently, Abart *et al.* (2012) used a similar approach to constrain not only the sequence of layers but also the microstructure of such reaction rims.

By the mid to late 1980s, a sufficient amount of thermodynamic and kinetic data had accumulated to facilitate reactive transport modelling in multicomponent systems with explicit reaction kinetics. Continuum models were developed by Peter Lichtner and collaborators (Lichtner 1985; 1988) largely following the conceptual framework represented by the *reaction path approach* launched by Helgeson (1968) but now formulated in a way that allowed a fully computational approach to reactive transport modelling in multiphase, multicomponent systems. With this advance, reactive transport modelling reached a new level and it was able to handle chemically complex (nature-like) systems.

This was the stage reached when I (Bjørn) started on my PhD in Oslo with Kurt Bucher in 1987. Doing a field based study on metasomatic zoning in the Oslo rift, I had high hopes that the new transport models would be able to explain my observations. This motivated me to travel to Baltimore and Johns Hopkins University to learn more about transport theory. Sadly, the person who had agreed to supervise me, Hans Eugster, suddenly and unexpectedly died while I was on my way to the US, so my main advisor became the young and promising post doc (and former student of Kurt Bucher) Lukas Baumgartner. At Johns Hopkins, I was very surprised when I recognised how famous Lukas had become without publishing more than a handful of papers (3 to be precise), but I quickly realised that he had unusual skills for a metamorphic geochemist. He was the first geochemist who told me that I needed to be concerned about the physical processes actually taking place in my rocks when interpreting geochemical data.

Following Hopkins, I went on to spend the winter of 1989 in Switzerland (University of Bern) to learn about the quasi stationary state approach to reactive transport modelling from *the* expert himself, Peter Lichtner. My hope was to finally model the metasomatic zones that had developed between carbonate and shale layers during contact metamorphism of the Paleozoic sediments, which I had been examining in detail as part of my PhD research. I had all the modal, compositional and mineralogical information that I could possibly imagine would match the output of the cutting edge modelling tools that I could use in Bern. However, despite all my efforts, and despite all the supervision Peter gave me, I got no useful results. Nothing that came out of the program looked like what I saw in my rocks. This was a major disappointment to me, and with the typical low self esteem of a field based petrologist in the company of hard core theoreticians, I blamed the rocks. They were unsuitable for modelling.

There were several problems with my rocks: The individual layers in the metasomatic sequence contained the wrong set of minerals, and often too many minerals, the interfaces between the different layers were often far from sharp, and finally some of the mineral grains had a highly variable composition. The garnets even showed oscillatory zoning, which seemed inconsistent with the local equilibrium assumption, and even inconsistent with the linear relation between fluxes and forces that was a requirement for applying linear nonequilibrium thermodynamics. At this stage, it became very clear that Lukas Baumgartner was absolutely right: I had to think about the physics of metamorphism as well as the

chemistry. Geochemistry and classical petrology had simply not yet evolved to the stage at which it could explain what I could see in my rocks. Inspired by popular science books on chaos, fractals and natural pattern formation (notably James Gleick's *Chaos: Making a New Science* published in 1987), I then decided to seek help outside my own discipline and approached Paul Meakin, Jens Feder, Torstein Jøssang and others who worked on such topics in the *Cooperative Phenomena* group at the Department of Physics in Oslo. Eventually, this collaboration lead to the formation of our cross disciplinary research centre PGP (Physics of Geological Processes) which began in 2003.

I was obviously not the first to realise that reactive transport during metamorphism often occurred in the nonlinear regime of non-equilibrium processes, where emergent patterns can arise by coupling between processes operating at a variety of temporal and spatial scales. Already in the 1981, the *Reviews in Mineralogy* volume on *Kinetics of Geochemical Processes* published by the Mineralogical Society of America (MSA), Fisher and Lasaga (1981) allocated an entire section of their chapter to *Irreversible thermodynamics, chemical reactions and pattern formation in petrology*. They focused on how coupled diffusion and reaction could produce banded precipitation (the so called Liesegang bands) and referred to models presented in the chemistry literature (*cf.* Stern, 1954; Nicolis *et al*., 1978). During the same period, Peter Ortoleva and collaborators provided a number of models to explain emergent patterns of geochemical relevance, including: oscillatory zoning of crystals (Haase *et al*., 1980), metamorphic layering in stressed rocks (Ortoleva *et al*., 1982), evenly spaced dissolution seams (stylolites) (Merino *et al*., 1983) and patterns emerging from the reactive infiltration instability (albeit in two dimensions, Chadam *et al*., 1986). Much of this was presented in two seminal papers on geochemical self organisation (Ortoleva *et al*., 1987a; b).

At this stage, emergent pattern formation by growth and dissolution processes was a very hot topic in the physics literature and the reactive-infiltration instability was approached using both modelling and experimental approaches. Of particular geochemical relevance was the flow channeling experiments of Daccord (1987) and Daccord and LeNormand (1987) which might not, even today, have been fully explored in terms of their relevance for geomorphic patterns such as karsts.

From 1990 onwards, geochemical modelling became more focused on instabilities and emergent patterns. Carl Steefel became a key player in this activity and introduced finite difference methods to analyse instabilities driven by reaction effects on permeability in systems with variable contributions from advective transport and reaction kinetics (Steefel and Lasaga, 1992; 1994). In 1996, another *MSA Review* volume (Lichtner *et al*., 1996) specifically addressed *Reactive Transport in Porous Media*. In addition to presenting the advances in modelling techniques (Steefel and MacQuarrie, 1996, with references therein), this volume made it clear that the entire market for reactive transport modelling had expanded significantly and penetrated into disciplines outside hard-core geochemistry. Not only did the database now include properties of organic compounds, new

models had been developed that also accounted for biological activity. These models attempted to include the chemistry of life (Rittmann and VanBriesen, 1996) and also introduced simplistic models for physical processes associated with biological activity, such as "biological diffusion" which was included to account for biological mixing or bioturbation (Van Cappelen and Gaillard, 1996).

Simultaneously, and partly motivated by an interest in channelised melt migration in the mantle and partly by experiments reported in the chemical engineering literature (*cf.* Bekri *et al*., 1995; Hoefner and Fogler, 1988), Einat Aharonov, Peter Kelemen and collaborators investigated the reactive infiltration instability in 3D, both through physical experiments (Kelemen *et al*., 1995) and modelling (Aharonov *et al*., 1997). This was to our knowledge the first 3D model and it included precipitation in the pores and clogging effects as well as channeling by dissolution. Conceptually, it was in many respects a natural extension of Steefel *et al*. (1994). Aharonov, Kelemen and coworkers were probably also the first to examine possible mechanical effects on such reactive transport systems, by investigating the mechanical stability of channel formation by linear stability methods (Aharonov *et al*., 1995).

During the last decade, the increased capacity of computers, increased access and ease of use, and a parallel development of software has enabled reactive transport modelling to grow into a major industry. Computer programs such as the TOUGH family (and its many varieties TOUGH2, iTOUGH2 etc) that was developed by Karsten Pruess and others at the Lawrence Berkeley National Laboratory (LBNL) have been used to perform highly sophisticated simulations for multiphase, multicomponent, non-isothermal flows in fractured porous media. TOUGH and similar codes have been applied to a variety of problems including transport of radionuclides in the vicinity of radioactive waste repositories and geological CO_2 sequestration. During this period, a variety of approaches had also been undertaken to couple macroscopic reactive transport to grain scale processes (*cf.* Lichtner and Kang, 2007). However, it is beyond the scope of this contribution to cover all of these developments. Steefel *et al*. (2005) and Steefel and Maher (2009) review these topics.

Despite all the advances made in reactive transport modelling during the last 2 to 3 decades, some fundamental components are still lacking. A serious deficiency for modelling reactive transport in rocks with moderate to low porosity, is that the current models do not account for changes in the rock microstructure and in particular the evolution of the pore space. The evolution of the pore space provides first order controls on both the transport properties of the rock and on the surface area available for reaction. A broad pore size distribution could also provide an internal drive for local mass transfer between the pores as well as for stress generation and porosity generation by microfracturing.

Recently, however, there have been several attempts to approach these issues. The effects of pore size on mineral solubility were incorporated into a reactive transport model by Emmanuel and Berkowitz (2007) and applied to quartz precipitation in sandstone by Emmanuel *et al*. (2010). Navarre-Sitchler *et al*. (2009;

2011) on the other hand characterised the pore space, reactive surface area and transport properties during basalt weathering by X-ray microtomography (μCT, also known as XMT), diffusion experiments and numerical modelling. However, mechanical forces were not included in any of these models. Everything was driven by the pore fluid super or undersaturation and chemical potential gradients. There was no change in the pore structure driven by physical forces. We shall return to pore space evolution in Chapter 8.

The first attempts to couple mechanical forces to a reactive transport model of the reaction path type with the chemical reactions explicitly included were made by Ray Fletcher and coworkers (Fletcher and Merino, 2001; Fletcher *et al*., 2006). Fletcher *et al*. (2006) address the problem of spheroidal weathering, where weathering reactions cause expansion and generation of elastic stress that ultimately leads to fracturing and the characteristic, surface parallel onion skin spalling that creates the rounded boulders that give this mode of weathering its name. Because each spalling event brings the external fluid into contact with fresh rock, the progress of this process runs linearly with time, rather than suffering from "diffusional death" because of an increasing distance between the external fluid reservoir and fresh rock. In our opinion, this work, along with some of our own work presented in Chapter 6, is a very important step toward understanding the coupling of chemical and physical processes, which is imperative if reactive transport models are going to be successfully applied to fluid driven changes in metamorphic and magmatic rocks. However, before we elaborate on reactive transport and associated patterns in porous rocks, let us look at growth and dissolution of free mineral surfaces.

3. FREE SURFACE GROWTH IN STAGNANT FLUIDS

Rock and crystal surfaces growing freely into a body of a standing fluid such as a water filled vug can form a number of different morphologies. One of the main controls on shape is whether growth is reaction limited or limited by a diffusive field in the aqueous phase.

3.1 Simple surface normal growth

The simplest possible growth system is that of continuous, homogeneous, isotropic growth at a free surface, with no time varying boundary conditions or interactions with external or internal fields. This is of course an abstraction, not likely to be found in nature. In such a system, the patterns would be completely determined by the initial shape. However, perhaps surprisingly, even this trivial growth model does not preserve shape because the growth is not isometric. As illustrated in Figure 3.1a, a growing object tends to become less elongated, *i.e.* more equant. If the initial shape has concave features, the growth front eventually collides with itself, leading to reduced surface roughness with time (Fig. 3.1b). Shape preserving (isometric) growth of nonequant objects can therefore not be considered a simple "null model" and it requires carefully regulated variation in growth rates and growth directions along the surface. One mechanism for such isometric growth is to force the growth increments to conform to a crystal lattice (Fig. 3.1c).

The concept of growth increments that preserve the shape of the object was important to the classical mathematicians. Such shape preserving increments were called *gnomons*. In Heron's Definitions (1st century AD, sometimes ascribed to Diophantus, 3rd century AD), a gnomon is defined as "that which, when added to anything, number or figure, makes the whole similar to that to which it is added" (Heron in Heiberg, 1912, def. 58, p. 45). This is a generalisation of Euclid's earlier definition, which only applied to parallelograms.

If there is no stochastic (random) component, and for a simple surface that can be described by an elevation, h, above a plane, we can describe the system by a purely geometric surface normal growth (SNG) model (Jettestuen *et al.*, 2006):

$$\frac{\partial h}{\partial t} = k\sqrt{1+|\nabla h|^2}. \tag{3.1}$$

Here, k represents a growth velocity constant, t, time and ∇h, the slope of the surface. The purpose of this equation is simply to describe the vertical growth rate as a function of slope and the growth rate in the direction normal to the surface (Fig. 3.2).

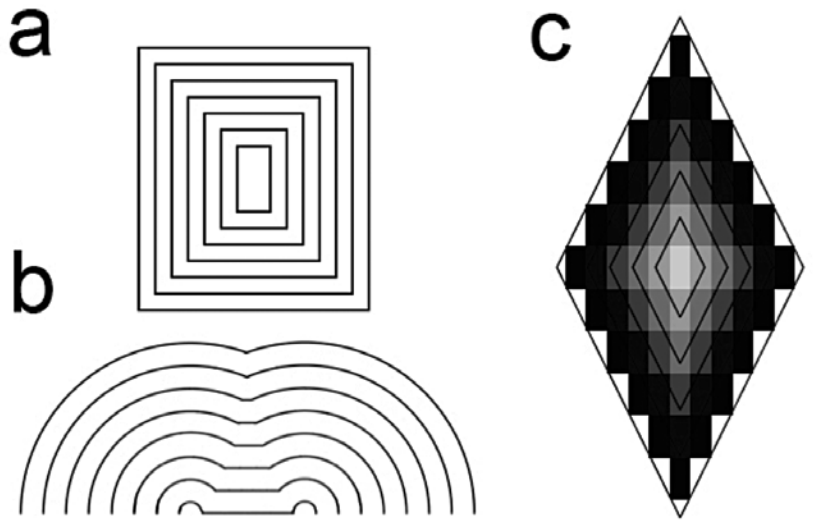

Figure 3.1 Evolution of an initially elongated object (centre) during three different growth processes. a) The object becomes progressively more quadratic even when growing at the same rate on all sides. b) Surface normal growth leads to merging of two botryoids. c) Isometric growth on an anisotropic lattice.

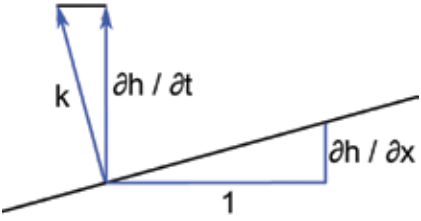

Figure 3.2 Given a surface normal growth rate, k, the growth rate, $\partial h/\partial t$, in the vertical direction can be determined for any slope, $\partial h/\partial x$, using equation (3.1).

A slight generalisation is to relax the requirement of continuous homogeneity but still require statistically stationary growth. In the Eden model (Eden, 1961), growth proceeds by random filling unoccupied sites on the interface. In contrast with the continuous SNG model, this is a discrete particle model. The Eden model was developed to simulate two dimensional growth of cell colonies but can also be applicable to geological systems. It produces a rough surface but the growth is nearly normal to the surface on average.

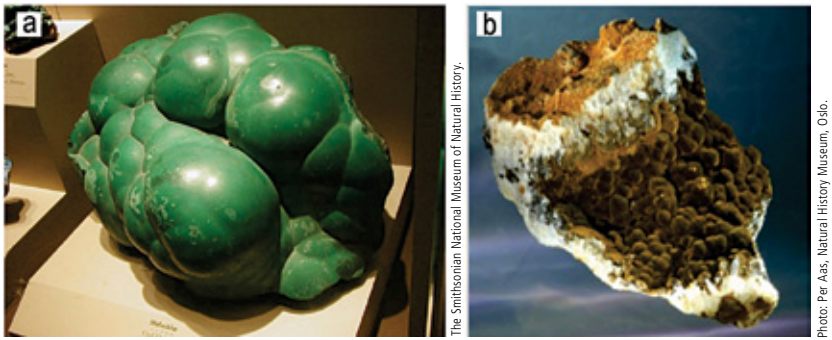

Figure 3.3 a) Smooth malachite spheres formed by surface normal growth. b) Botryoidal growth in goethite from Oppdal, Norway (each botryoid is *ca*. 1 cm across).

3.1.1 Botryoids: surface normal growth in a noisy environment

Starting with a rough surface, the SNG model produces spheroidal shapes that coarsen with time to produce geometries similar to that shown in Figure 3.3a. Such shapes are often referred to as botryoidal or "like a bunch of grapes" (Greek). However, in natural botryoidal growth, the surface is often rough during the entire growth process and small spheres are continuously nucleated, as well as consumed by the larger ones (Fig. 3.3b). This means that the growth is not homogeneous and time invariant but influenced by external events triggering nucleation. This is obviously a very common situation in systems subject to variable fluid flow and advective transport and in botryoidal growth in which biological processes play a significant role.

In their study of growth of rough surfaces, Jettestuen *et al*. (2006) enforced nucleation events at random locations and times, leading to natural looking botryoidal growth patterns (Fig. 3.4). If the growth has not proceeded too far, obliterating previous botryoids, it is possible to simulate the process in reverse in order to reconstruct the timing and spatial distribution of nucleation events (Jettestuen *et al*., 2006).

Interestingly, the SNG model not only produces natural looking botryoidal surfaces, it also produces feathery internal microstructures very similar to what is observed in cross sections of natural botryoidal aggregates (Fig. 3.5). Very similar patterns, in terms of both surface morphology and microstructures, can be observed in biological systems with surface directed growth directed towards the sunlight (Fig. 3.6). The implication is that these kinds of patterns are rather universal and they are not dependent on the details of the growth process (*cf.* Katzav *et al*., 2006). As we see below, the symmetry of the patterns can be broken by various flow processes and the coupling between growth and flow can produce a new level of complexity across many scales in length and time.

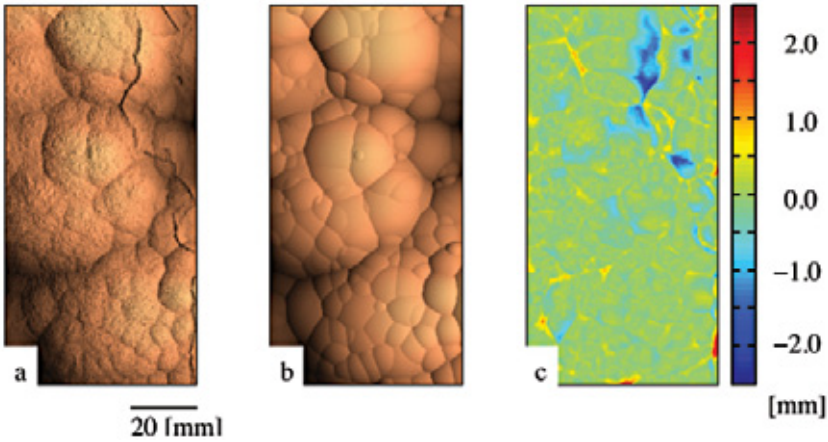

Figure 3.4 a) Natural surface of Ca-Mg carbonate. b) Morphology produced by a surface normal growth model fitted to the natural surface by a cusp network detection method. c) The difference between the natural surface and the modelled surface (from Jettestuen *et al.*, 2006, with permission from Elsevier).

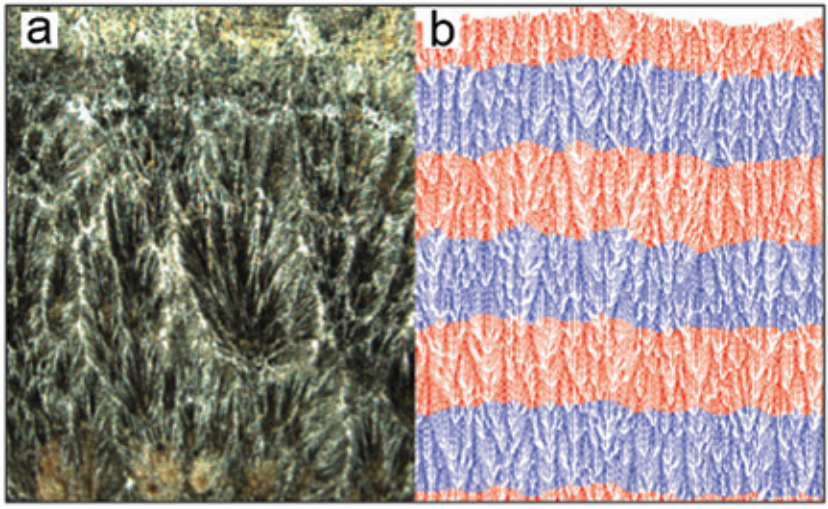

Figure 3.5 a) Microstructure produced by surface normal growth of the Ca-Mg carbonate seen in Figure 3.4a; field of view 2.5 mm. b). Modelled microstructure derived from a SNG model with continuous addition of nucleation sites. The various line segments visualise the local growth directions. Red and blue colours indicate different stages in the growth process and the red-blue interfaces mark the surfaces produced by the various growth stages (modified from Jettestuen *et al.*, 2006).

Picture courtesy of Paul Ward (Coolantarctica.com) and Martin Mach (http://www.baertierchen.de).

Figure 3.6 Moss pillows (left) and moss (Polytrichum) microstructure (right) formed by surface directed growth.

3.1.2 Stromatolites: surface normal growth with sedimentation

Stromatolites are laminated, convex, sometimes branching sedimentary structures that are particularly common in Precambrian rocks but they also form today (Fig. 3.7). They are usually taken as evidence for microbial activity but Grotzinger and Rothman (1996) showed that similar morphologies can also form through abiotic processes. They added three extra terms to Eq. (3.1): a constant term, v, for growth in the vertical direction by deposition of suspended sediment; a diffusive term, $\nabla^2 h$, simulating smoothing of the surface by various processes; and a random noise term, η, that varies with time, t, and position, x:

$$\frac{\partial h}{\partial t} = v + \nabla^2 h + k\sqrt{1+|\nabla h|^2} + \eta(x,t). \tag{3.2}$$

The resulting patterns and their significance for understanding stromatolites are discussed by Grotzinger and Knoll (1999), observing that while the effects of organisms might well affect the system, and could enhance stromatolite growth simply because the biofilm provides a sticky surface, abiotic processes are *sufficient* to explain the emergence of this nontrivial morphology. This also implies that interpretation of variation in stromatolite morphology in terms of evolution or ecology is hazardous.

3.2 Growth in a diffusive field

The growth systems considered so far respond to external influences in a more or less trivial manner. They are unable to self organise or to produce their own ordered patterns. Such *"deus ex machina"* systems are not creative and cannot be considered true pattern forming systems.

Photo courtesy: Viaje Jet (viajejet.com).

Figure 3.7 Stromatolites from Shark Bay, Australia. The ripple marks in the sand provide scale.

Pattern formation generally requires feedback processes that can act at a distance. We first consider diffusion limited, normal growth of a free surface in a fluid. In the simplest case, the precipitation rate depends on a single species diffusing in the fluid. In a continuum model, we can describe this by two coupled differential equations, one for the moving boundary (surface normal growth) with height, h, according to Eq. (3.1) and one for the diffusion of a species with concentration, $C(\mathbf{x})$, in solution, where $\mathbf{x}$ represents position:

$$\frac{\partial h}{\partial t} = f\left(c(\boldsymbol{x})\right)\sqrt{1+|\nabla h|^2} \text{ and} \tag{3.3}$$

$$\frac{\partial c}{\partial t} = D\nabla^2 c \text{ (away from the surface).} \tag{3.4}$$

The function, f, describes the reaction kinetics. In the simplest case of first-order reaction, it has the form: $f = kc(\boldsymbol{x})$. At the solid-liquid interface, the boundary conditions for Eq. (3.4) include removal of c from solution through precipitation. While the coupling from c to h is evident from these equations (*i.e.* surface growth is controlled by the diffusive field), there is also a strong coupling in

the other direction, from *h* to *c*, mediated by the change in geometric boundary conditions for diffusion as the surface grows. This two way interaction produces a feedback system.

It is here assumed that growth is slow compared with diffusion; otherwise an additional velocity term would have to be added. This general formulation covers both reaction limited and diffusion limited growth. These two regimes can both exist at different times and different spatial positions in the system, depending on local concentration and geometry.

A discrete analogue of the continuum model for growth in a diffusive field is known as the diffusion limited aggregate (DLA) model (*e.g.* Meakin, 1998). In DLA simulations, particles are introduced in the fluid far away from the solid interface. The particles migrate by Brownian motion, as in a diffusive process, and stick to the surface on collision (there are computational shortcuts that reduce the need for long Brownian migration pathways for the particles).

Whether simulated with a (possibly discretised) continuum model or a DLA model, growth in a diffusive field gives rise to a *fingering instability* producing a highly branched surface (*cf.* Fig. 3.8). This is because any protrusion tends to extend the surface toward areas in which the concentration of the precipitation limiting dissolved species is high. Further back from actively growing areas, concentrations are lower and precipitation rates are reduced.

Surface energy effects can lead to smoothing of the surface. The combination of roughening and smoothing processes can then lead to the emergence of fingers within a narrow frequency band (*i.e.* with a characteristic wavelength). This is known as the *Mullins-Sekerka instability* (Mullins and Sekerka, 1963).

Figure 3.8 Dendritic growth patterns (from F. J. Bertuch's *Bilderbuch für Kinder*, vol. 5, 1808).

While diffusion limited growth leads to roughening of the interface, diffusion limited dissolution conversely leads to smoothing. In an irregular, fluid filled cavity, dissolution preferentially affects protrusions that reach into areas where the concentration of the dissolved species is low. Eventually this leads to a spherical geometry.

3.2.1 Dendrites

Geological dendrites are tree like branching structures that could have formed by precipitation in a diffusive field (Chopard *et al*., 1991). In geology, the most familiar examples form in very thin fissures between beds in sedimentary rocks, giving a nearly two dimensional geometry (Fig. 3.8). The precipitate often is a manganese bearing phase. In principle, such dendrites can also form in 3D but this is more rarely observed. Examples include native copper and silver, and agate inclusions.

The similarity between dendrites and branching plants is not coincidental but arises from a similar pattern formation process. In both systems, growth is mainly localised at the tips of branches, while growth further back is inhibited by the tip. This inhibition is mediated by a depletion of the solute concentration field in the case of dendrites and by an inhibitory chemical signal transmitted from the tip (the meristem) in the case of plants. It should be mentioned that similar structures can form from the displacement of a high viscosity fluid by a low viscosity fluid, leading to viscous fingering. Garcia-Ruiz *et al.* (1994) explained manganese dendrites by this model.

Perhaps the dendritic growth structures that are best known to the layman (at least to a Norwegian) are the intricate patterns of snowflakes. In contrast to the apparently almost randomly branched structures seen in Figure 3.8, snowflakes have a distinct hexagonal symmetry (see Libbrecht, 2010 to learn more about "The secret life of a snowflake"). In this case, the dendritic pattern is clearly not dictated by a diffusion limited growth process alone but also by the symmetry of the ice lattice. The rates of particle attachment and detachment depend on the surface orientation and curvature, and this, coupled with solute diffusion in the surrounding fluid, controls the dendritic growth process. A similar argument applies to the geometry of the silver dendrites seen in Figure 3.9, where the angle of 90° between the various branches of the dendrite is dictated by the cubic symmetry of native silver.

Photo: Per Aas, Natural History Museum, Oslo.

Figure 3.9 Dendritic growth in native silver, Sachsen, Germany.

4. FREE SURFACE GROWTH AND DISSOLUTION UNDER FLOW

As fluids flow more quickly, advective transport begins to dominate over diffusive transport and a transition from diffusion limited precipitation and dissolution to an advection dominated regime occurs. This transition is often quantified by the dimensionless *Peclet* number, which is a measure of the relative importance of advective and diffusive transport over a characteristic distance such as the overall size of the system or the typical size of a feature of interest. It is the ratio between the fluid velocity and the diffusion coefficient, multiplied by the characteristic length. Peclet numbers much larger than unity imply advection dominated transport. Reactive transport under moderate to high velocity, large conduit or open channel flow can give rise to extremely rich and complex patterns in *e.g.* hydrothermal, karst and travertine systems, in glacial and volcanic settings, and in any systems involving weathering, erosion and deposition by the agents of water or wind. Indeed, reactive, advective, open flow is at least partly responsible for most of the abiotic geometry seen on the surface of the Earth. Again, these systems can be classified in a sequence of increasing complexity.

4.1 Steady, unidirectional flow, ballistic models

The simplest possible flow model is that of unidirectional advection with constant velocity. Such a model is of course unrealistic because it does not include the modification of flow by obstructing objects but it can be a useful abstraction. The ballistic deposition model is a discrete particle model of growth under unidirectional flow (Meakin, 1998).

The dominating feature of these models is that growth occurs predominantly in the direction against the flow, where the concentration gradients are steepest. The introduction of a directional external field breaks the perfect, spherical symmetry of simple or diffusion controlled, surface normal growth (Fig. 4.1a). These patterns are in many respects similar to step patterns in natural travertines or geyserites, as can be observed around hot springs (Fig. 4.1b) but these grow away from the fluid source rather than toward the flow.

4.2 Stokes, laminar and shallow water flow

The most general equations for fluid flow are the Navier-Stokes equations for compressible fluids. This set of equations can, in principle, be used to model flow of any complexity. However, for many geological problems, it is not necessary to include the full set of terms. For water, we can assume that the fluid is incompressible and for the case of very low velocities, high viscosities, or flow in very small systems, such as small pore or crack networks in rocks, we can furthermore assume that the inertial forces are small compared with viscous forces. Under these circumstances, the incompressible Stokes equations:

$$\nabla p = \mu \nabla^2 \mathbf{v} + \mathbf{f}$$
$$\nabla \bullet \mathbf{v} = 0 \qquad (4.1)$$

can be used instead of the nonlinear Navier-Stokes equations. Here, p represents the pressure (scalar), $\mathbf{v}$, the velocity (vector field), μ, the dynamic viscosity and $\mathbf{f}$, the applied force per unit volume. The first equation describes the relationship between the pressure gradient and the viscous forces, while the second (zero divergence) ensures that the rate of transport into a control volume is equal to the rate of transport out of it so that mass is conserved.

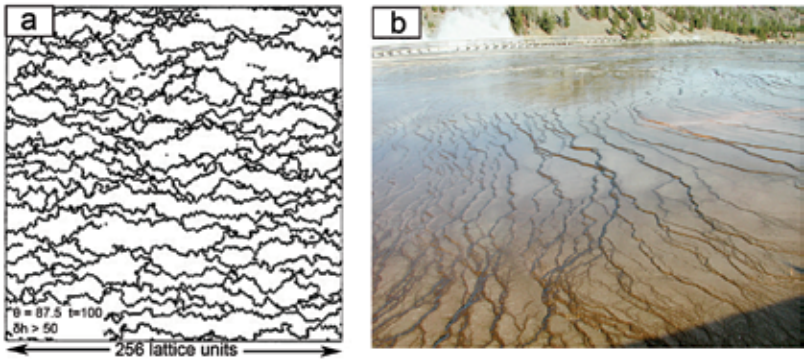

Figure 4.1 a) Top view of a three dimensional simulation of ballistic deposition onto an initially flat surface with an oblique angle of incidence, producing anastomosing step edges (from Meakin and Krug, 1990, with permission from the European Physical Society). b) Geyserite steps around Grand Prismatic spring, Yellowstone National Park. Geyserite is a form of opaline silica often found around hot springs and geysers. The fence and trees in the background provide scale.

Water is the driver of nature.

LEONARDO DA VINCI (1452-1519), *Thoughts on Art and Life*

For faster flow or in larger flow domains, the Stokes equations become inaccurate. It is then necessary to reintroduce the terms for conservation of momentum included in the Navier-Stokes equations. If thermal gradients are important, an energy conservation equation is also needed. For relatively low

velocities, flow is laminar or nearly so, meaning that there is limited flow separation and eddies are large and simple. Under such conditions, the numerical methods for approximating the solution to the Navier-Stokes equations are relatively simple and accurate. However, accurate simulation of highly turbulent (high Reynolds number) flow is still very challenging.

Photo: Dag K. Dysthe, PGP.

Figure 4.2 Travertine terraces at Mammoth hot springs, Yellowstone National Park, Wyoming, USA. The fenced footpath near the upper left corner provides scale.

4.3 Travertine terraces

Travertine terraces (rimstone) are spectacular, often intricate structures formed when calcium carbonate (calcite and also often aragonite) precipitates under running water (Fig. 4.2). Travertine terraces and other deposition patterns form over a wide range of scales from millimetres to tens of metres, in diverse settings, such as hydrothermal springs, cold mountain streams and limestone caves.

Travertine terracing is an excellent example of a complex system that develops self organised patterns with numerous positive and negative feedback paths. The emergence of patterns in such systems is not trivial and intuition often fails us. Our group and the group of Nigel Goldenfeld at the University of Illinois at Urbana-Champaign have studied travertine terracing in detail using a fruitful combination of field observation, laboratory experiments and computer modelling (Jettestuen *et al.*, 2006; Goldenfeld *et al.*, 2006; Veysey and Goldenfeld 2008; Hammer *et al.*, 2007; 2008; 2010). A particularly interesting aspect of this work was the way in which we attacked the problem at many different levels of abstraction, in order to answer several types of questions.

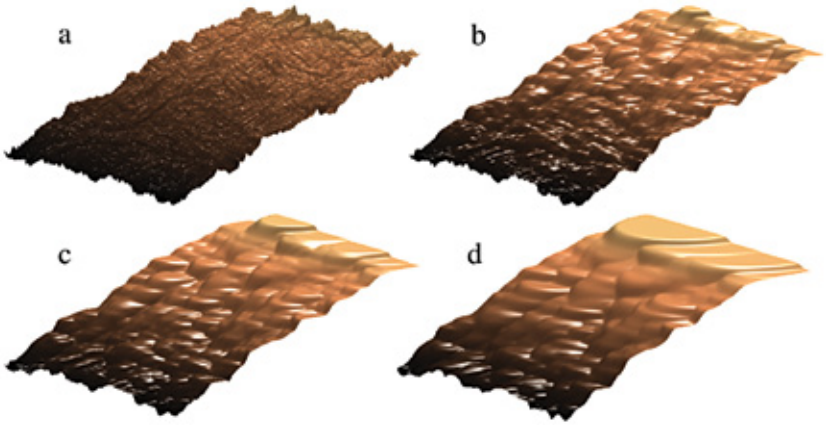

Figure 4.3 Four stages in the development of terraces from the simulations of Jettestuen *et al.* (2006). Terrace patterns emerge when growth is proportional to the local slope (from Jettestuen *et al.*, 2006, with permission from Elsevier).

From a purely geometric perspective, terrace patterns can be produced by a surface normal growth model based on the assumption that the growth rate is proportional to the local slope (Fig. 4.3; Jettestuen *et al.*, 2006). Clearly, there can be no pattern formation if the initial slope is perfectly flat and smooth because the growth rate is then constant across the surface. In such simulations we therefore usually start with a slightly rough surface. Variations in the surface height grow in response to positive feedbacks, while negative feedbacks regulate the system. In this case, any small protuberance increases in the downstream direction, where the slope is high, while flat tops stop growing and remain level.

So far the model is geometric and abstract, and it remains to connect it to mechanisms operating in nature. The morphology emerging in these simulations resembles the small scallops that form on near vertical, travertine walls covered by a thin layer of flowing water. The flow velocity is, to a first approximation, proportional to slope. These results therefore indicate a relationship between flow velocity and precipitation rate. This relationship has indeed been observed and quantified in field studies by many authors. The simulation can be made more realistic by modelling the fluid flow over the surface using the Navier-Stokes equations and specifying a linear relationship between local flow rate and the surface-normal growth rate (we have not yet explored the mechanism for this relationship). A simplification of the Navier-Stokes equations is provided by using the shallow water approximation, where flow is averaged over depth. We found that this results in a morphology that is more reminiscent of larger terraces on less steep slopes (Hammer *et al.*, 2007). The model reproduces several peculiarities of travertine terrace growth observed in nature, such as downslope migration of steps, coarsening by merging and drowning of upstream steps and stretching of

dams in the downslope direction. Goldenfeld *et al.* (2006) and Veysey and Goldenfeld (2008) developed a somewhat similar model, with further simplification of the flow (using a discrete model for Stokes flow) but including several other processes such as surface tension and simplified chemistry and heat transport. These simulations also assumed a relationship between flow velocity and precipitation rate, producing very realistic terrace patterns.

Our simulations (Hammer *et al.*, 2007) demonstrated that a simple flow/precipitation relation is sufficient to explain terracing and its dynamics. This is certainly not a trivial result and could not have been easily achieved by observation or laboratory experiments alone because it is not possible to reduce the real system to such bare essentials. A large number of confounding effects, including biological processes, make it almost impossible to isolate the interactions responsible for the pattern formation. However, the model was still not mechanistic, in the sense that the flow/precipitation rate relationship was simply imposed, without fully understanding the cause of this relationship. This lack of attention to detail, which might seem unconventional, was intentional, as discussed in Section 1.2.2.

The overall reaction for the precipitation of $CaCO_3$ under normal (not hyperalkaline) conditions can be written in a highly simplified manner as:

$$Ca^{2+} + 2HCO_3^- \Leftrightarrow CO_2 + CaCO_3 + H_2O. \quad (4.2)$$

By this reaction, carbonate precipitation produces CO_2, which can be removed from solution by degassing. This might seem counter intuitive but calcium bicarbonate is much more soluble than calcium carbonate and CO_2 degassing can drive the conversion of bicarbonate to carbonate. This observation was the basis for traditional ideas about travertine terracing, involving enhanced degassing at terrace edges. At edges, water is shallower, giving a higher surface to volume ratio and therefore faster degassing. The shallow depth also requires higher flow velocity to maintain the flux, possibly explaining the velocity/precipitation rate correlation. In addition, degassing is enhanced by strong agitation at step edges. Enhanced degassing caused by pressure drop, following Bernoulli's principle (Venturi effect), has also been suggested but is unlikely, considering the small velocity gradients in this system.

In order to identify the dominating mechanism, we developed a detailed model with as little abstraction as possible (Hammer *et al.*, 2008). The model simulated free surface fluid flow over a small obstruction, in a 2D vertical section, using the full Navier-Stokes equations without turbulence modelling. The solution chemistry was modelled, with all relevant reaction kinetics involving CO_2, carbonate, bicarbonate, calcium and pH. All species were transported by advection and diffusion. Carbonate precipitation and degassing were derived from local concentrations. The model was successfully validated by comparison with a laboratory experiment using the same geometry and water composition, in

which the precipitation rate was mapped using an optical technique. As expected, the precipitation rate was higher in regions of faster flow over the obstruction (Fig. 4.4).

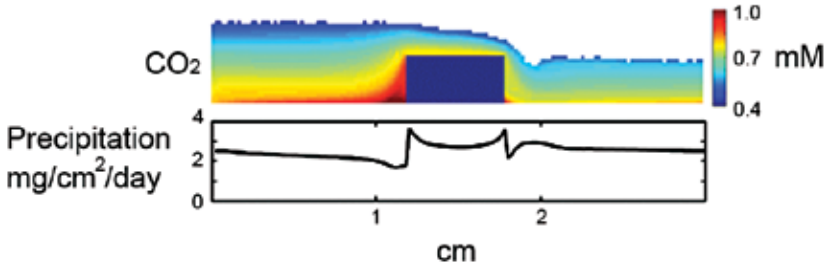

Figure 4.4 2D simulation of free surface water flow (left to right) over a rectangular obstruction, coupled with aqueous carbonate chemistry, degassing and calcite precipitation on the solid-water interface. Colours show CO_2 concentrations in mM (from Hammer *et al.*, 2008, with permission from Elsevier).

The purpose of this detailed modelling was twofold. First it confirmed that we had understood and included the basic processes responsible for the spatial distribution of precipitation rates. Second, the model provided an experimental system which we could use to study the effects of these processes in isolation. Most importantly, we were able to switch off the variation in degassing completely, without noticeable effects on the distribution of precipitation. This demonstrated that while degassing is necessary to drive the precipitation on larger scales, local variation in degassing by hydrodynamics does not contribute to pattern formation, at least for small scale travertine terracing. The reason is that complex advection and mixing prevents degassing patterns at the air-water interface from reaching the water-solid interface where precipitation occurs.

We now believe that instead of degassing, the mechanism responsible for the velocity/precipitation correlation in this particular system is concentration gradients through the water column that are compressed when water is forced through a region of shallower water. This provides an immediate, local effect at the water-solid interface, accelerating precipitation there. Even this quite detailed model relies on empirical relationships that are not explained by fundamental principles. In particular, the rate law for precipitation is still insufficiently known and remains an important source of uncertainty. In principle, even more detailed simulations could be used to address the microscopic details of carbonate precipitation, *e.g.* using molecular dynamics. However, because of computational complexity, such a simulation would have to focus on a tiny region of the solid-fluid interface and could not answer questions about the larger scale emergent properties such as our simulations were able to do.

4.4 Stalactites

For the laminar, thin film water flow on the surface of a stalactite, it is possible to give analytical equations for the film thickness, h, and the water velocity, u_0, at the water-air interface. Using the Stokes flow formulation, and inserting relevant physical constants (viscosity and acceleration of gravity), Short *et al.* (2005) derived the simple equations:

$$h \approx 11\mu\text{m}\left(\frac{Q}{R\sin\theta}\right)^{1/3} \text{ and} \tag{4.3}$$

$$u_0 = 0.060\,\text{cm/s}\left(\frac{Q^2\sin\theta}{R^2}\right)^{1/3}, \tag{4.4}$$

where Q represents the volumetric flux of water in cm^3/h, R, denotes the radius of the stalactite in cm and θ, the angle of the stalactite surface with respect to the horizontal. Under usual conditions for stalactite formation, the film thickness is on the order of a few tens of micrometres and the velocity is less than a few mm/s. The flow velocity deeper in the film is assumed to follow a parabolic profile toward zero velocity at the solid-liquid interface (no slip boundary). Coupling these relationships to the carbonate precipitation system, it is possible to deduce an analytical expression for the growth velocity normal to the surface. Over time, this leads asymptotically to a stalactite shape described using rescaled values, z' and r', that represent the vertical coordinate, z, and the local radius, r, (see Short *et al.*, 2005, for additional details):

$$z'(r') \approx \frac{3}{4}(r')^{4/3} - (r')^{2/3} - \frac{1}{3}\ln r' + \text{constant}. \tag{4.5}$$

This analysis does not include effects that could lead to the smaller scale instabilities with a characteristic wavelength (ripples or rings) that are commonly observed on stalactites (Fig. 4.5). These instabilities presumably originate from a process in which local protrusions induce their own growth, *e.g.* by enhanced degassing, but short wavelength features are suppressed by surface energy or transport effects (*i.e.* a Mullins-Sekerka-like instability).

4.5 Stagnation and flow in combination

In travertine terrace systems, the water flow rate is often very slow in the deeper pools between terrace edges. In such cases, surface normal or diffusion limited growth is observed within the pools (Fig. 4.6a). In other cases, surface normal growth of "cave pearls" (Fig. 4.6b) takes place in dry or almost dry pools, where dripping water causes precipitation of carbonate minerals evenly over a surface.

Cave pearls often nucleate on a sand grain. The forces acting on cave pearls by flowing water can prevent them from sticking together and growing into botryoidal aggregates, which are also common.

Photo: George Chakonas, Northern Illinois University.

Figure 4.5 Single stalactite with clearly visible surface ripples. Field of view: ~50 cm.

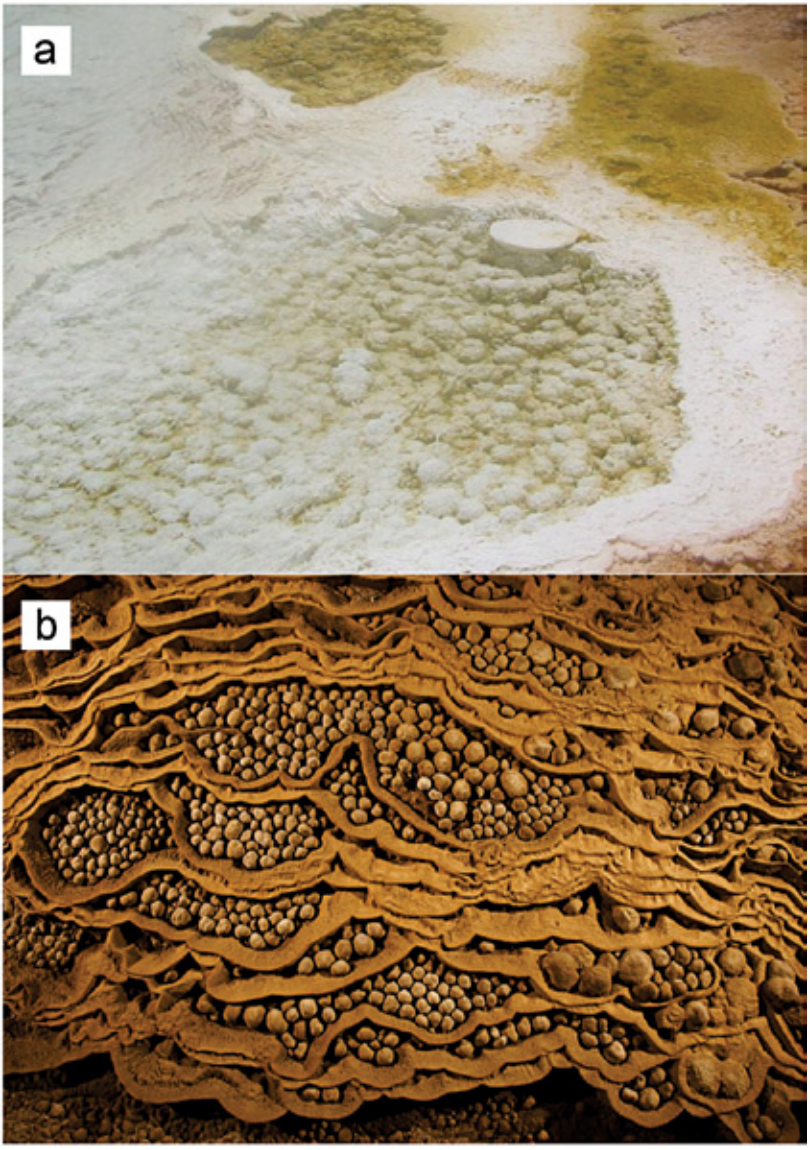

Photo: Bjørn Jamvelt.

Photo: Carsten Peter, National Geographic Magazine.

Figure 4.6 a) Botryoidal growth of calcite in the deeper water pools of the travertine terraces at Mammoth Hot Springs, Yellowstone National Park. Field of view ~1 metre. b) Rare cave pearls (each 1-2 cm across) fill dried out terrace pools near the Garden of Edam in Hang Son Doong.

4.6 Biomineralisation in moving fluids

Many species of colonial corals have branching, dendritic morphologies reminiscent of those seen in DLA (diffusion limited aggregation) simulations. The branches tend to be space or plane filling but are self avoiding (Fig. 4.7). Jaap Kaandorp and his coworkers (*e.g.* 2003; 2005) have made extensive experimental, field and simulation studies on the biology and fluid dynamics of coral growth, demonstrating that the availability of nutrients (specifically inorganic carbon, Kaandorp *et al.*, 2005) in water surrounding the colony can explain the branching.

A coral colony is a self organising system, growing in response to external gradients set up by diffusion and advection but also itself modifying fluid flow and nutrient distribution that depend on its changing morphology. Applying such knowledge to fossil organisms, it might be possible to estimate environmental parameters such as the intensity and prevailing direction of currents and waves (*e.g.* Hammer, 1998).

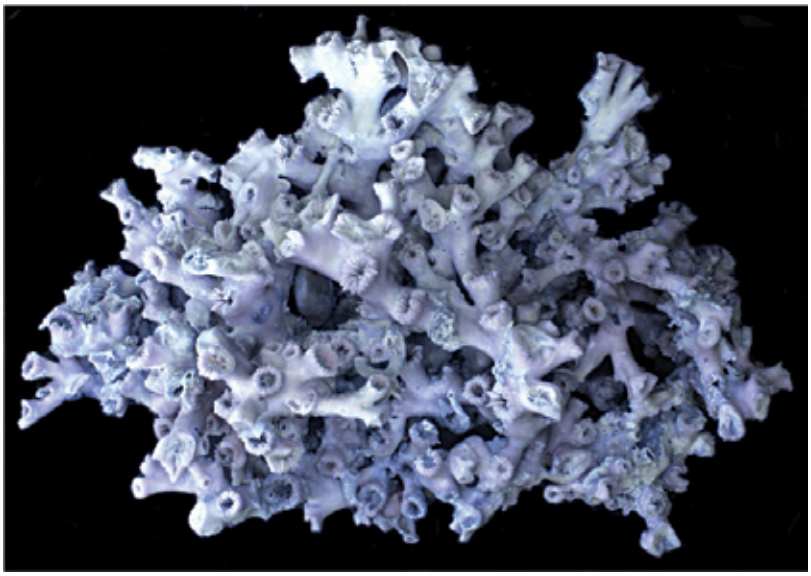

Photo: Øyvind Hammer.

Figure 4.7 *Lophelia pertusa*, a cold water coral from the base of the Holocene, Drammenselva, Norway. Field of view ~20 cm.

4.7 Surface karst morphology

Some of the most beautiful landscapes on Earth result from limestone dissolution over a wide range of scales (Fig. 4.8). Karst landforms are a central theme in traditional Chinese art (Fig. 4.9), where they can appear so bizarre that Western critics often viewed them as artistic fantasies. In fact, they are usually depicted fairly realistically. Undoubtedly, these dissolution processes can be strongly influenced by pre-existing rock features, such as joints that focus fluid flow, giving rise to blocky "clints" separated by deep "grikes" (Fig. 4.8). Of special interest to us are pattern formation processes taking place in more homogeneous rocks, often at smaller scales (Fig. 4.10). The extensive karst nomenclature reflects the richness of these phenomena (*e.g.* dolines, rillenkarren, meanderkarren, rundkarren, poljes, swallets, flutes, scallops, pans, runnels, uvalas and avens).

Photo courtesy: Angus McIntyre (raingod.com).

Figure 4.8 Karst landscape in limestones seen from the summit of Yueliang Shan, near Yangshuo.

Figure 4.9 Tang dynasty painting of karst landscape by Dong Yuan (*ca.* 934-962 AD).

Dissolution of limestone at near neutral pH can be described in a simplified manner by the reverse reaction of Eq. (4.2). Dissolution therefore consumes CO_2, which can be supplied from the atmosphere. Exactly the same considerations about gas transport apply to dissolution as precipitation, just in the opposite direction. In particular, we expect a correlation between flow velocity and dissolution rate and this is what is observed. This correlation is reminiscent of the well known correlation between flow velocity and erosion rate in stream channels, usually leading to localised channelling patterns. Consequently, typical dissolution patterns in limestone produce channels in the downslope direction such as the rills (karren) observed in Figure 4.10.

Photo: Mauro Pau, PGP.

Figure 4.10 Rillenkarren, Oliena, Sardinia, Italy, with an apparent characteristic wavelength. The area is about 2.5 m across.

Hammer (2008) suggested a simplified parameter space diagram for growth and dissolution under flow, such as that shown in Figure 4.11, in this case in the context of karst and travertines. When the flow rate is low, or growth is not strongly dependent on flow rate, botryoidal growth dominates. This is the situation in the stagnant, deeper areas of travertine pools. The upper part of the diagram represents the precipitation regime, where growth rate increases with flow rate, leading to terraced morphologies. The lower part of the diagram is the dissolution (karst) regime, where fast flow on steep slopes is typically associated with straight channel morphology (rillenkarren), while meandering channels usually arise from low flow rates on more horizontal ground.

There are clearly other parameters that contribute to controlling pattern formation in such systems. These include the effects of scale, considering that meanders also form at large absolute flow velocities if the channel cross section is large. Furthermore, this parameter space is not meant to cover sedimentary and erosive patterns in general, without modification. Although straight channels, meanders and even terraces also form in fluvial systems, other morphologies such as braided rivers, alluvial fans and levees demonstrate that additional mechanisms must be included.

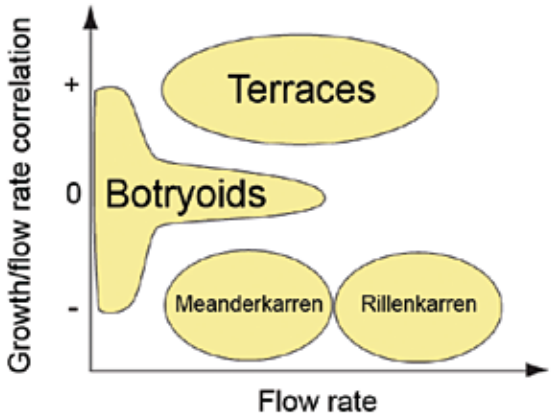

Figure 4.11 A suggested parameter space for growth and dissolution under flow (modified from Hammer, 2008).

4.8 Caves and collapse

Limestone caves can form some of the largest and most spectacular dissolution structures in nature. The Cave of Swallows (Spanish: Sotano de las Golondrinas) in Mexico is a spectacular example (Fig. 4.12a). It is the largest known cave shaft in the world with a depth of about 330 m and an internal room of approximately 300 by 135 m (Fig. 4.12b). The dissolution process itself and the growth of the cavity can to some extent be modelled using geochemistry coupled with simple flow calculations. Gabrovšek and Dreybrodt (2001) simulated the emergence (speleogenesis) of networks of narrow corridors and shafts in fractured limestone in this way.

As a cavity grows, at some point the roof becomes too large to support itself, and it collapses. Such caves are often envisaged as menacing *bubbles in the Earth*, slowly ascending as the roof crumbles and the floor rises by the deposition of rubble, leaving behind a *breccia pipe*. When the bubble reaches the surface it turns into a collapse doline – an abyss that can swallow cars and houses. To model such phenomena requires coupling between dissolution and rock mechanics, typically with linear elasticity equations for deformation and some yield criterion for fracturing. Fracturing and collapse are difficult to handle with continuum modelling. Methods such as discrete element modelling (described later in this article) or discrete deformation analysis are useful.

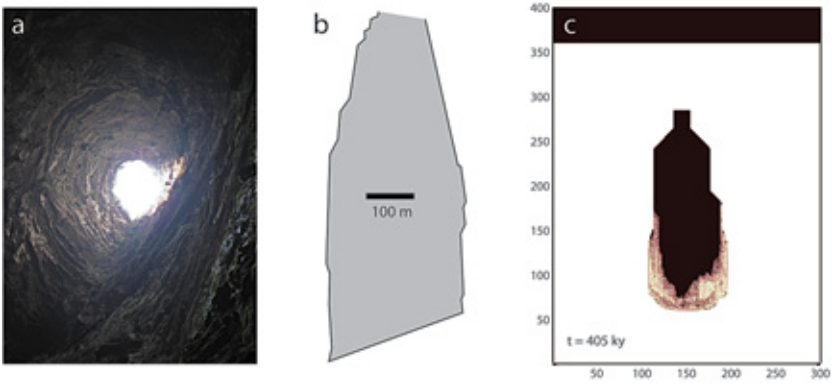

Figure 4.12 a) Sotano de las Golondrinas, seen from within. b) Simplified profile of the Sotano de las Golondrinas collapse doline. c) Simulation of karst pipe formation. Limestone is shown in white, air or water in black and collapse material in pink. Axes are length in metres. The simulated karst pipe is shown 405,000 years after initiation (from Hammer *et al.*, in prep.).

For rock mechanical modelling it is essential to take into account structural inhomogeneities and anisotropies. Limestones are typically bedded on scales ranging from centimetres to metres. A simplifying abstraction (not fully accurate) is to consider only the strata that are not supported below and subject them to a lithostatic load from above. As a further simplification, these strata can be modelled as thin plates or, in the case of a 2D simulation, as beams. When stresses in these beams exceed a yield criterion, they break and produce rubble that falls to the floor of the cavity. Dissolution is assumed to proceed constantly, normal to the surface of both the intact walls and the collapse rubble.

Figure 4.12c shows one stage in such a simulation, just after two large collapse events that have produced upwards propagating pipes formed by an avalanche of successive collapse of overlying strata. Overhangs with straight, diagonal slopes form because this shape minimises the overhang (and therefore stress) of individual limestone benches. The overall morphology of the pipe is very similar to classical sinkholes such as the Sotano de las Golondrinas seen in Figures 4.12a and b.

The subterranean courses of waters, like those existing between the air and the Earth, are those which unceasingly wear away and deepen the beds of their currents.

LEONARDO DA VINCI (1452-1519), *Thoughts on Art and Life*

Such straight sloped roofs form as a result of the discrete, horizontal limestone strata forming a so called *corbel*, a *false arch* or *relieving triangle* (Fig. 4.13). In this geometry, not all tensile stresses are transformed into tangential, compressional forces. In more homogeneous rocks, other geometries are expected to form, generally with curved shapes that provide stability by directing forces downwards and outwards (*true arch*).

Photo courtesy : Clark Anderson/ Aquaimages.

Figure 4.13 Mayan Corbel arches in Belize. A corbel vault is a construction method that uses the architectural technique of corbelling to span a space or void in a structure. The corbelled vault is a technique to support the superstructure of a building's roof.

4.9 Turbulent flow and boundary layers

At larger scales and flow velocities, flow becomes turbulent, unsteady and chaotic. The Reynolds number is often used to characterise the flow regime. The Reynolds number is defined as the ratio between velocity and kinematic viscosity (about 10^{-6} m^2/s for water), multiplied by the length scale. This length scale is a matter of definition for different geometries. For flow in a pipe with circular cross section, we can use the pipe diameter as the length scale. The transition from laminar to turbulent flow happens for Reynolds numbers somewhere between 2000 and 4000, unless the wall is exceptionally smooth. This means that for water flow in pipes of less than 1 cm diameter, the flow velocity has to exceed 20 cm/s before we need to consider turbulence.

In principle, the Navier-Stokes equations are necessary to simulate turbulent flow but become extremely difficult to handle numerically because of eddies cascading down to scales too small to resolve with our computer models. In some cases, it is possible to resolve turbulent flow by direct numerical simulation using the Navier-Stokes equations. This requires very fine grids and enormous computer resources. An alternative approach is to attempt to decompose the flow field into a time averaged (steady) velocity field and additional fields that describe the turbulent motion using derived quantities such as eddy viscosity. Codes are now available for fluid dynamic simulation using a variety of different turbulence models (*e.g.* OpenFOAM and Fluent) but they are computationally intensive and typically require specification of nontrivial model parameters, numerical parameters and empirical relationships, especially at boundaries.

In many geological applications, the most important consequence of turbulent flow is that it enhances the mixing and transport of dissolved species by many orders of magnitude. Near the walls of the conduit however, turbulence is subdued because of friction and reduced velocity. This gives rise to a laminar boundary layer. Typically, the transport of dissolved species to and from a reacting surface is limited by diffusion through this boundary layer. Beyond this layer, in the turbulent core, mixing is almost total and instantaneous in comparison with the rate of purely diffusive mixing. Because the boundary layer thickness decreases with increasing overall flow velocity, this leads to progressively faster dissolution and precipitation rates under more rapid, turbulent flow (Buhmann and Dreybrodt, 1985). This provides an additional mechanism for the correlation between velocity and precipitation rate in the travertine terrace system, at least at larger scales where turbulence is important.

Photo courtesy: David Drew, Trinity College, Dublin.

Figure 4.14 Scallops on the walls of the Polldubh Cave in the Burren, Western Ireland.

4.10 Dissolution scallops

A particularly enigmatic pattern formation process during dissolution of rock (and melting of ice) under turbulent flow is the scalloping observed on cave walls (Fig. 4.14; Curl, 1966; Goodchild and Ford, 1971; Blumberg and Curl, 1974; Villien *et al*., 2005; Meakin and Jamtveit, 2010). Scallops have a characteristic size (wavelength) that depends inversely on flow velocity. As dissolution proceeds, the scallops migrate both normal to the wall, as the whole surface recedes, and in the direction of flow, while maintaining their shape and spacing. This shape stability requires a carefully controlled dissolution rate profile, that itself depends on the shape of the scallop and the resulting hydrodynamics. This self organisation of a stable but migrating pattern under such chaotic and unstable conditions is fascinating. While Bird *et al.* (2009) carried out 3D fluid dynamics simulation of flow over scallops, and Hammer *et al.* (2012) coupled a 2D turbulence model to a dissolution model and partly reproduced the dissolution profile required for shape stability (Fig. 4.15), the full natural pattern formation process has not yet been reproduced by computer simulation. This highlights the complexity and limited knowledge about reactive, turbulent flow coupled with dissolution or precipitation.

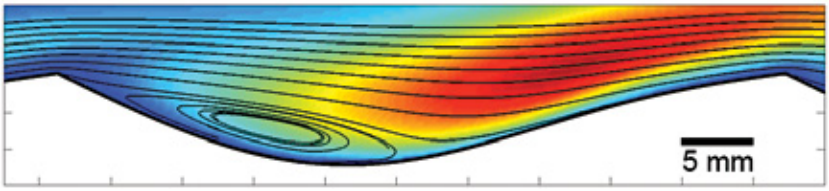

Figure 4.15 Flow over dissolution scallops (from left to right) simulated by computational fluid dynamics techniques (k-ε turbulence modelling). The time averaged velocity field is shown as streamlines, while the eddy viscosity (turbulence) is indicated by the colour scale, where red is maximum and blue, minimum value. Flute wavelength is 5.1 cm (from Hammer *et al*., 2012, with permission from the National Speleological Society, www.caves.org).

4.11 Patterns controlled by air flow

Interactions between rocks and fluids can involve not only water but also air. A particularly interesting case is the phenomenon of *tafoni*, which are intricate weathering patterns formed by growth and coalescence of deep cavities on rock surfaces. Tafoni formation (at smaller scales known as honeycomb weathering, Fig. 4.16) has been studied extensively and it is generally believed that growth of salt crystals plays an important role (Bradley *et al*., 1978; McBride and Picard, 2004).

Huinink *et al*. (2004) presented an informative simulation of the growth of a single tafone cavity. They used a simple 2D model with a wet zone inside the rock, in which water flowed according to Darcy's equation for unsaturated flow (with a saturation dependent permeability and pressure) in a porous medium. Closer to the rock-air interface, there was a dry zone, where water vapour was modelled by the diffusion equation. The complex motion of water vapour in air inside the cavity was abstracted using a diffusion equation with a high diffusivity. The simulation was run in alternating steps of drying and wetting. Interestingly, the model indicated that in the regime of long drying periods, more salt is deposited inside the sheltered cavity, where the rate of drying is lower than outside. Consequently, salt weathering is enhanced inside the cavity. This mechanism provides the positive feedback loop necessary for localisation and growth of tafoni.

Photo: Bjørn Jamtveit.

Figure 4.16 Honeycomb weathering of a gravestone, Whitby, England.

4.12 The role of biology

Microorganisms are present on most wet rock surfaces and many of us have had unfortunate experiences with the slippery biofilm that rapidly grows on immersed rocks. However, the role that microorganisms play in pattern formation is often uncertain. They can influence pattern formation but they do not necessarily change the nature of the pattern formation process and the mere presence of microorganisms does not imply that they exert a controlling influence over dissolution and/or precipitation. The interface between warm water and rocks provides a particularly favourable environment for microorganisms and they are abundant in the travertine hot springs illustrated in Figure 4.2. However, the strikingly large scale (one to tens of metre scale) travertine terraces shown in Figure 4.2 and the smaller scale morphologies can be explained without biological processes. Biofilm is also present during the formation of many cave speleothems and geyserite terraces and other patterns formed in wet environments. In all of these cases, it is common to find the mineralised remains of microorganisms entombed in the mineral deposits but it is also clear that the gross morphology can be explained by abiotic mechanisms alone. Consequently, the relative importance of biotic and abiotic processes remains undetermined and opinions vary greatly. In the case of travertine terraces, where growth is controlled by CO_2

degassing, the presence of a biofilm on the travertine water interface has little or no effect on the fluid dynamics, water chemistry or the transport of dissolved substances in the water.

In most biofilms, the diffusion coefficients of ions and small molecules are at least 10% of the diffusion coefficient in water and often substantially greater (Stewart, 2003). Therefore, biofilms have little effect on the transport of ions and small molecules to and from the rock surface unless the thickness of the biofilm is comparable with or larger than the thickness of the boundary layer and precipitation or dissolution is controlled by diffusion across the boundary layer. Consequently, microorganisms can be mere bystanders during pattern formation. Of course, microorganisms *can* play a critical role by secreting compounds that greatly increase or decrease the rate of precipitation or dissolution by adsorbing strongly on mineral surfaces. Organic material can provide surfaces on which minerals can nucleate and grow and by changing the composition of the fluid in the vicinity of the surface. However, biofilms might only exist on wet rock surfaces because the rock provides a foundation on which a biofilm can form and resist being washed away. In such a case, there might be no reason why the biofilm should have developed the ability to actively control dissolution and precipitation. The formation of patterns that have a striking resemblance to speleothems, travertine and geyserite terraces, scallops, etc. in ice strongly suggest that the formation of these patterns does not depend on biological processes.

4.13 A cold note on universality: bringing it all together

We have a fascination with general principles of pattern formation that are more or less independent of detailed mechanisms. Botryoidal growth in minerals and plants (Figs 3.4 and 4.6) is one example. This does not mean that we are uninterested in those mechanisms; on the contrary, identifying a general principle at work in a particular system can be an important tool for understanding the basic chemistry or physics. The idealised method, as illustrated by our travertine work, can be described as starting with a top down approach, first making hypotheses about overall systems properties, and then identifying processes. Finally, the procedure is reversed by simulating the detailed interactions in order to reconstruct the emergence of the pattern (the bottom up or reductionist phase).

A delightful example of such universality is the emergence of patterns in ice during melting or freezing (*cf.* Meakin and Jamtveit, 2010). These intricate patterns bear an uncanny resemblance to those forming during dissolution (melting) or precipitation (freezing) of limestone. We believe that the general pattern formation principles are the same, involving positive and negative feedbacks between dissolution, precipitation, transport and flow. Considering the detailed mechanisms, there is a curious analogy between the transport of CO_2 in the water phase in the case of carbonate rocks and the transport of heat in the case of ice. The mathematical equations for these two transport processes are more or less the same and similar patterns form as a result.

A few examples illustrate the case. *Ice terraces* (Streitz and Ettema, 2002) form in streams where water flows in a thin film or shallow depth and freezes on top of existing ice (so called *aufeis*). At small scales, such terraces look very similar to travertine microterraces. At larger scales, they form cascades that are almost indistinguishable from those in travertine (Fig. 4.17a). *Icicles* are stalactites, where ripples decorate the surface as for their limestone analogue (Fig. 4.17b and Ueno *et al.*, 2010). Spectacular dissolution scallops form on the walls of melt water tunnels in glaciers, just as in the analogous karst setting, and rillenkarst is a familiar sight on melting glaciers and ice cubes in drinks (Fig. 4.17c).

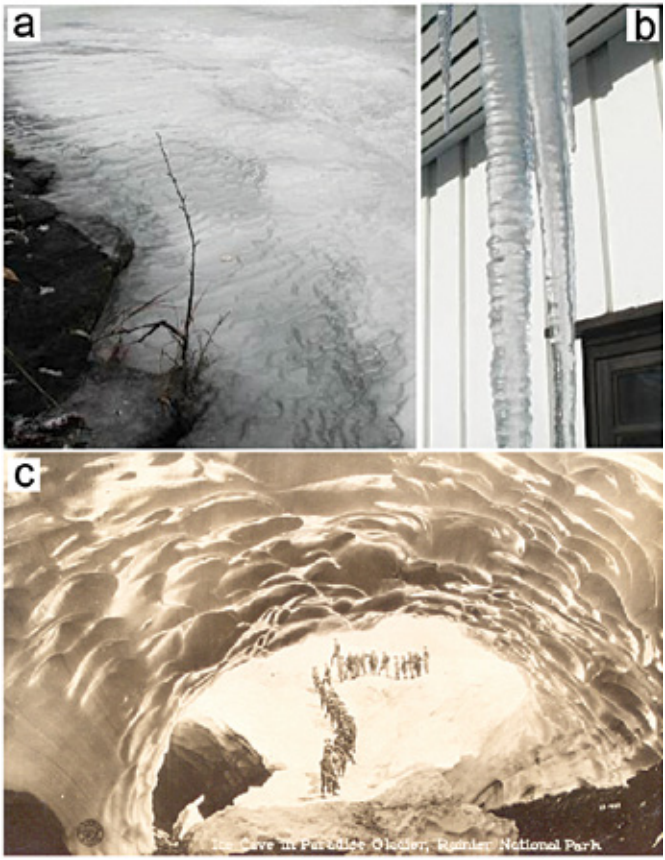

Photos: Øyvind Hammer.

Figure 4.17 a) Ice terraces in a stream in Oslo. b) Rings on icicles. c) Photo from a vintage postcard showing scallops in the roof of the Paradise Glacier, Mount Rainier National Park. In 1978, this set of caves was the longest mapped system of glacier caves in the world but now the caves are completely gone because the glacier has receded.

Water, the vital moisture of the Earthly machine.
LEONARDO DA VINCI (1452-1519), *Thoughts on Art and Life*

5. REPLACEMENT PROCESSES

Reactive fluids can contribute to the production of spectacular patterns upon encountering a variety of geological materials. At the Earth's surface, this can occur by dissolution or precipitation reactions as described above. In more confined environments with less fluids present, precipitation of one mineral often requires local dissolution of another and vice versa. Such *coupled* dissolution-precipitation processes often lead to the replacement of one mineral or rock, by another. Over the last decade, and notably through of the work of Andrew and Christine Putnis and collaborators at the University of Münster, it has become increasingly clear that the evolution of the Earth's crust is to a major extent affected by fluid mediated replacement processes.

Photo from travelrier.com.

Figure 5.1 Roman amphitheatre *pseudomorphically* replaced and reutilised by modern buildings, *Piazza dell' Anfiteatro,* Lucca, Tuscany (Kuroda, 1999).

Replacement processes can create their own set of patterns depending on the details of the transformation processes and the materials involved. Such processes commonly conserve shapes present in the original material by pseudomorphism. This is particularly important for the conservation of *soft matter* patterns such as biological tissues over geological time-scales. A spectacular, man made version of *pseudomorphism* is shown in Figure 5.1.

A prerequisite for completion of a replacement process is that the material to be replaced must be kept in contact with reactive fluids. When replacement occurs at an advancing replacement front, along which the reacting material is converted to the product material, the product material must be penetrated by connected porosity to maintain solute transport pathways between the replacement front and a fluid reservoir. Otherwise, reaction ceases because reactants are depleted, or because the fluid equilibrates with its surroundings. The mechanism of porosity generation is therefore an essential part of any replacement process. This mechanism can differ for materials with different chemical bonding properties but even more importantly, it is fundamentally different for reactions that cause a reduction in solid volume across the front compared to reactions that cause an increase in solid volume.

In a confined environment, the expansion caused by a solid volume increase will inevitably generate stress and thus the entire replacement process becomes dependent not only on coupled chemical reactions and transport processes but also on the mechanical processes that arise as a response to stress generation. Without any mechanical response to the stress, the replacement process must stop when the porosity becomes clogged by the expanding solid.

In the following section, we first describe replacement processes in systems with small or negative volume changes. We subsequently discuss systems in which replacement is associated with swelling, first in unconfined systems and subsequently in confined spaces. At this stage, it is important to recognise that the volume change associated with a mineral replacement is controlled not only by the difference in molar volume between reactant and product but also by possible transport of material into or out of the system during the replacement process.

5.1 Pseudomorphism

Over the last couple of decades, considerable progress has been made toward a better understanding of replacement processes involving isostructural minerals in closed systems with abundant fluid and unconfined solids (*cf.* Putnis, 2009). In such systems, structural information from the dissolving phase is transferred to the precipitating phase during the early stages of reaction and the reactions are often referred to as interface coupled dissolution-precipitation reactions. As outlined by Pollok *et al.* (2011), the key factors controlling the replacement patterns in such systems are the molar volumes and solubilities of the solid phases involved. In general, positive *solid volume* changes lead to the precipitation of a

protective layer of product on the reactant phase so the reaction rate decreases. In many cases, the rate becomes so slow that the reaction is effectively halted. However, a decreasing solid volume change leads to a variety of interesting structures and often to a porous product that does not significantly slow transport rates to and from the reactive interface. Formation of a porous product phase has been studied in a variety of systems, in ionic compounds such as salts, and in more complex solids, such as silicate minerals. Several examples are presented below.

5.1.1 The KBr-KCl system

When a KBr crystal is exposed to a solution saturated with KCl, KBr is replaced by a porous solid solution which is KBr-rich near the centre of the original crystal and KCl-rich near the bulk solution (Fig. 5.2). This reaction and the corresponding solid solution–aqueous solution phase diagram has been described in detail by Putnis and Metzger (2004) and Putnis *et al*. (2005). More recently, the formation of the porous reaction product was studied by *in situ* and *ex situ* experiments by Raufaste *et al*. (2011).

Raufaste *et al*. (2011) addressed two main problems. First, what mechanism generates the observed porosity in the product phase, and second, how is structural information transmitted from the parent to the product phase? The latter question arises because it is commonly observed that during mineral replacement, parents and products are separated by a thin layer of fluid across which the dissolution-reprecipitation process operates. *In situ* observations of the propagating replacement front shows that shortly after the onset of reaction, a surprisingly stable, highly anisotropic and connected pore structure develops, which pervades the product phase, and this maintains contact between the advancing reaction interface and the fluid (Fig. 5.3). The pore space is comprised of a number of 10-100 μm sized cylinders, each containing a stack of saucer shaped cavities oriented parallel to the advancing surface. Growth and dissolution occur at the roofs and floors of such cavities, in such a way that the entire structure propagates into the parent KBr crystal (Fig. 5.3). Why this geometrically complex structure is selected as the way of replacing KBr with a KBr-KCl solid solution is not yet understood.

The transmission of structural information from the original crystal to the product phase takes place before these porous structures form, during the first few minutes of the replacement process, when small (7-10 μm) crystals of KBr-KCl solid solution grow epitaxially on the original KBr surface. Subsequently, the dissolution front evolves from the space between these crystallites and undercuts the contact to the original KBr crystal. However, at this stage, the crystallographic information is already conveyed to the product phase and it keeps a low index surface during the subsequent replacement process.

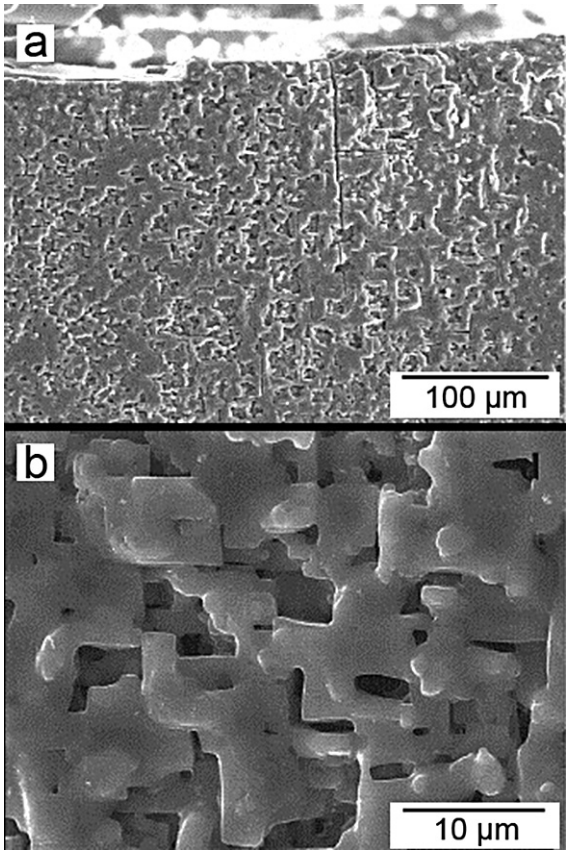

Figure 5.2 Porous KBr-KCl solid solution formed during replacement of pure KBr exposed to a saturated KCl solution (from Putnis and Mezger, 2004, with permission from Elsevier).

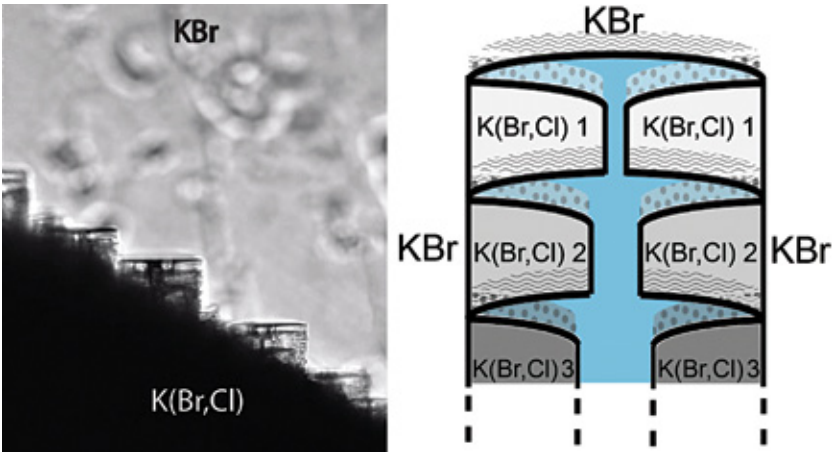

Figure 5.3 Transmitted-light microscopy image (left) of the interface between the original KBr crystal and the porous replacement product, a K(Br,Cl) solid solution. The field of view is ~500 μm. The interface is comprised of cylinders containing a stack of saucer shaped pores (dark) connected by a central pore channel (right) as illustrated on the right. This structure develops a few minutes after the initial KBr crystal is exposed to a KCl saturated aqueous solution and is stable for the remaining replacement history. Propagation of the cylinders into the original crystal takes place by dissolution at the roof of the saucer shaped pores (denoted by wave patterns) coupled with precipitation of a more Cl-rich phase at the floor (dotted pattern). Mass transfer with the bulk external fluid takes place through the central channels (modified from Raufaste *et al*., 2011).

5.1.2 Silicates

Pseudomorphism is common during silicate replacement processes. This is true for both isostructural and other minerals. The term pseudomorphism is used when the products keep the general shape of the parent but it does not imply that a volume for volume replacement has occurred in a strict sense. Shapes can be conserved even with a few percent change in overall volume, which can be very significant in terms of generating stresses in a system confined in a rigid matrix. Secondly, the product phase is often porous so that the volume of the parent mineral can be replaced by a porous material.

Feldspar replacement is one of the most thoroughly studied examples of pseudomorphic replacement where crystallographic orientations are transmitted from parent to product. The importance of dissolution-reprecipitation during feldspar by feldspar replacement has been clear from the early experiments of Orville (1963) and O'Neill and Taylor (1967). However, only more recently, with the help of modern electron microscopy, have the detailed replacement processes become clear (*cf.* Putnis, 2002; 2009). During albitisation, when more Ca-rich

plagioclase is replaced by the almost pure end member albite, the interface between parent and product is very complex and the product phase is invariably porous on a submicrometre scale. This has been observed both for experimentally produced albite (Hövelmann *et al.*, 2010; Norberg *et al.*, 2011) and for natural samples (Engvik *et al.*, 2008).

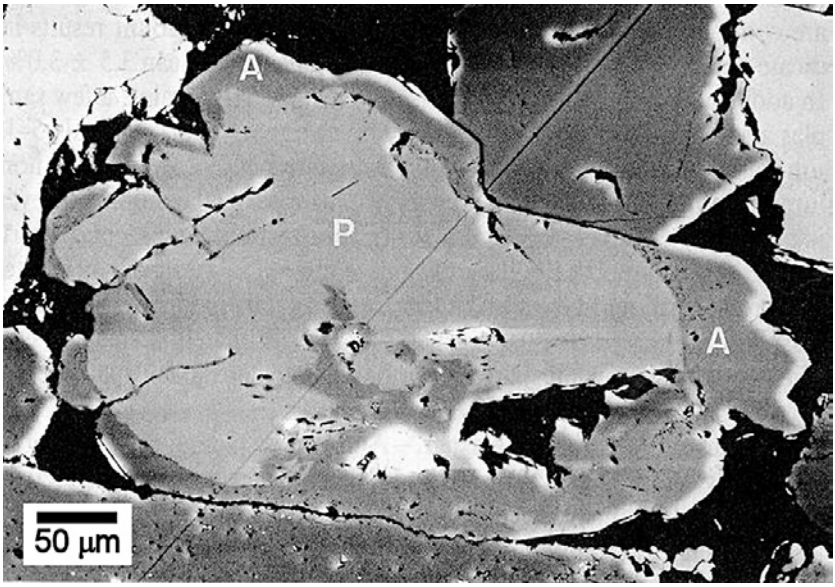

Figure 5.4 Back scattered electron (BSE) image of a plagioclase grain (P) replaced by a porous authigenic albite rim (A) (from Spotl *et al.*, 1993, with permission from the Society of Sedimentary Geology).

Relatively large porosities (several percent) can arise during replacement (Fig. 5.4) although the molar volume differences are small. This underscores the significance of solubility differences in open systems or systems with ample fluid relative to solid. In such systems, porosity forms primarily because more of the parent phase dissolves than product precipitates. Importantly, the rate of these fluid mediated phase transitions is far higher than would be the case if solid diffusion was the rate limiting process. In experiments conducted by Hövelmann *et al.* (2010), 100 µm rims of albite formed on labradorite at 600 °C in just 17 days. Thus, albitisation in natural systems with ample fluids could occur almost *instantaneously* in geologic time, even under medium grade metamorphic conditions.

Olivine is highly reactive at shallow levels in the Earth's crust and olivine replacement is much faster than feldspar replacement. Therefore, the interaction between olivine and water or more complex aqueous fluids is of relevance, not only for evolution of the Earth's crust but probably for the evolution of the

hydrosphere and atmosphere as well. Although the volatilisation processes involved in olivine replacement often lead to significant solid volume changes, it is also quite common to observe pseudomorphic replacement (Delvigne *et al.*, 1979), particularly near the Earth's surface where fluids are abundant and solubility variations have first order effects on the overall mass transfer.

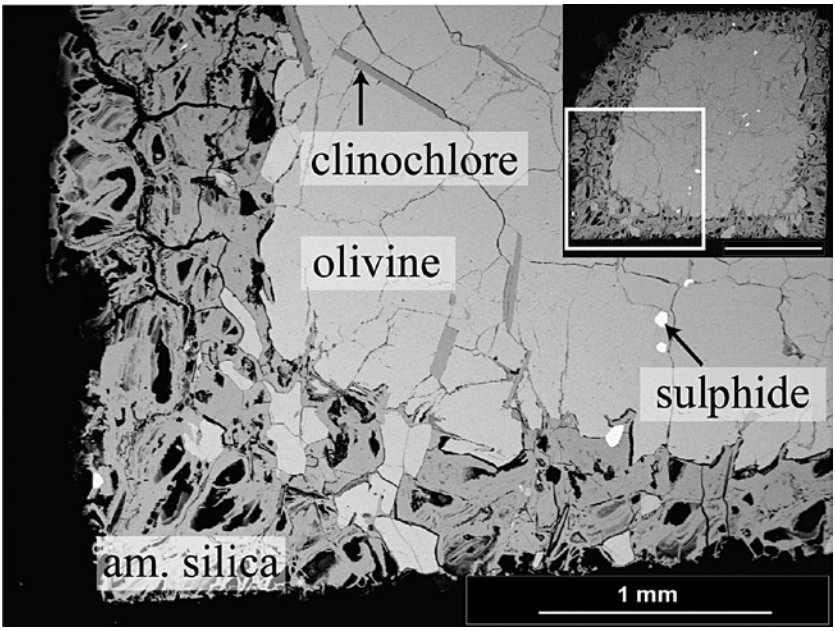

Figure 5.5 BSE image of a cross section through a dunite cube (the entire section shown in the upper right corner) that has been reacted with 3.6 M sulphuric acid solution for 7 days at 90 °C. A highly porous and amorphous silica rim pseudomorphically replaces the original dunite (slightly modified from King *et al.*, 2011).

In a recent experimental study, King *et al.* (2011) demonstrated how millimetre sized olivine crystals could be replaced by pseudomorphs of amorphous silica within a few days at temperatures as low as 60-120°C under extremely acidic conditions. The amorphous product is highly porous (Fig. 5.5), reflecting the effective removal of Mg from the advancing interface during reaction. This is interesting because it has become increasingly clear that serpentinisation of olivine is often associated with the formation of metastable, gel like substances from which serpentine minerals later form and because olivine alteration near the Earth's surface is often associated with extensive loss of Mg and the formation of highly Si enriched products. There is strong textural and geochemical evidence that some jasper deposits, previously thought to be silica rich precipitates on the sea floor, are actually a result of mineral replacement in olivine rich rocks.

Grguric *et al*. (2006) described brown jasper pseudomorphs after olivine from the Agnew-Wiluna Greenstone Belt in Australia and Beinlich *et al*. (2010) showed how entire clasts of variably serpentinised peridotites in the conglomerates of the Devonian Solund Basin in Western Norway are partly or completely replaced by Mg depleted jasper rich layers (Fig. 5.6). Beinlich *et al*. (2010) pointed out that Mg depletion is favoured by an initial low temperature hydration of the olivine bearing assemblage to what has been described as deweylite, a poorly ordered mixture of serpentine and mineraloids with a talc like composition.

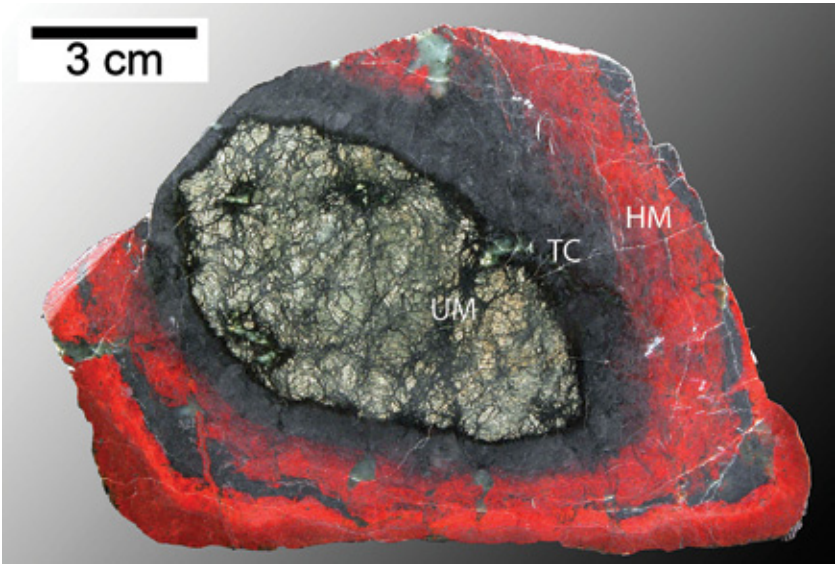

Figure 5.6 Ultramafic clast from Solund (Western Norway) with a green core comprised of serpentine, olivine, deweylite, and chromite. The clast is partly replaced by a talc rich zone (dark grey), followed by a red rim containing abundant haematite. The innermost part of this rim is composed of talc, serpentine, and some carbonate minerals, while the outermost dark red part consists of talc, calcite, quartz and haematite (modified from Beinlich *et al*., 2010).

The significance of the formation of poorly ordered hydrated products of olivine during further alteration has also been pointed out by Hövelmann *et al*. (2011). In their experimental studies of carbonation of partially serpentinised and weathered peridotites, the deweylite component reacted much faster with carbon-bearing fluids than fresh olivine. Thus, they proposed that partly weathered peridotites could in fact be better candidates for *in situ* carbon sequestration by carbonate precipitation than fresh ultramafic rocks (more details in Chapter 9).

5.2 Biological tissue replacement

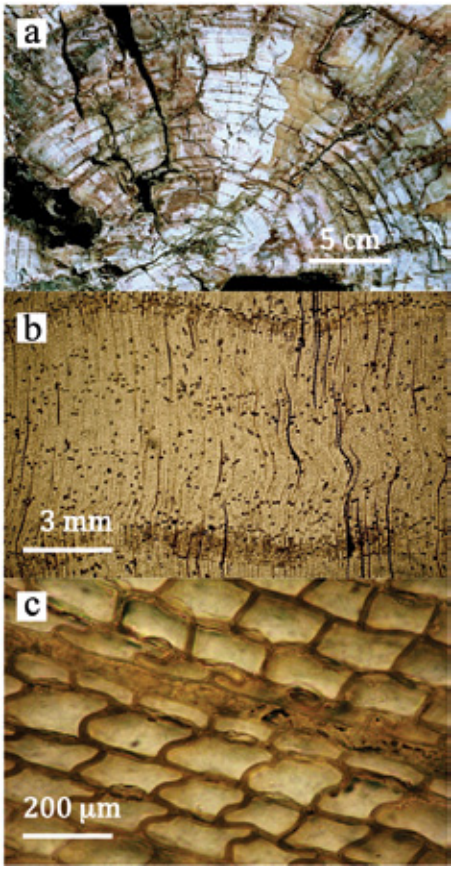

The bulk of the fossil record consists of mineralised "pseudomorphs" of pre-existing biological tissue. Pseudomorphs is in quotation marks, because minerals mainly fill in the original pore space of the tissue, rather than replacing the organic materials in a volume for volume replacement process. Yet, the mineralisation is the result of chemical interactions between an externally derived fluid and either the organic tissue itself or microorganisms present within this tissue. Two major processes are involved during fossilisation of soft tissues: permineralisation and authigenic mineralisation (*cf.* Briggs, 2003).

Permineralisation arises from "permeation of tissue by mineral charged water" (Schopf, 1975) with subsequent mineral precipitation that initially fills in the pore space, but gradually also replaces the tissue in the cell walls. Most examples of permineralisation involve silica and permineralised fossils are known as petrification (Fig. 5.7). In a recent experimental

Figure 5.7 The cellular structure of a silicified conifer from the Miocene (18 Ma) forest of Lesvos, permineralised with opal following burial by pyroclastic deposits. a) A transverse section through the trunk showing at least 25 growth rings. b) Close-up of a transverse section of a conifer from the same locality in transmitted light; the two darker horizontal bands at the bottom and top are latewood (the part of the wood in a growth ring of a tree that is produced later in the growing season), and the light area in between is earlywood. The vertical lines cutting across the growth rings are rays, which form the pathways in a tree connecting the center with the periphery of the trunk. c) A close up of a transverse section in transmitted light with slightly distorted tracheids. All lumina are filled by opal, and cell walls are darkened by brownish Fe oxides (from Ballhaus *et al.*, 2012, with permission from Elsevier).

study, Ballhaus *et al*. (2012) simulated the petrification of trees in volcanic ash. Silica rich solutions (average silica concentration of ~6 mM/l) were prepared by interaction of water with ground obsidian at 100 °C to produce a solution with a pH of ~9.5. During interaction with Douglas fir (*Pseudosuga menzeisii*, a conifer) for 100-300 hours at 80 °C, the pH of the solution falls in response to the release of protons during degradation of the organic material. This decreases silica solubility and drives precipitation of opal. The fact that petrification preserves the fine details of the wood tissue implies that the precipitation rate of silica must be fast compared to the rate of deterioration of the organic cell walls or that the two processes are linked such that the precipitation and degradation occur concurrently. In nature, petrified wood is usually associated with burial in pyroclastic material rich in glass, such as in the famous Petrified Forests in Patagonia (Argentina), Lesvos (Greek) and Arizona.

In contrast to petrification, fossilisation through authigenic mineralisation is the product of decay by bacteria and the generation of steep chemical potential gradients and anaerobic conditions around the decaying tissues (Sagemann *et al*., 1999). The rapid authigenic growth of minerals driven by decay processes occasionally preserves even labile tissues such as muscles, with subcellular details. Common minerals for tissue replacement include phosphates, carbonates and pyrite. The quality of fossil preservation depends on a number of factors including the extent and rate of decay, the nature of microbial activity and the availability of metal forming ions (Briggs, 2003).

5.3 Fracturing assisted replacement

Interface coupled replacement reactions that lead to an increase in the solid volume across the replacement front usually result in the formation of a passivating layer of product phase and very limited reaction progress, unless fresh reactive surface area is continuously produced by fracturing. As is demonstrated in the next section, reaction driven fracturing can arise even in unconfined systems where stresses are generated independent of mechanically rigid walls.

5.3.1 Aragonite to calcite

The aragonite to calcite transition is associated with a molar volume increase of ~8.4%. The transition is so fast in the presence of aqueous fluids that Carlson and Rosenfeld (1981) concluded that preservation of aragonite in high pressure rocks requires that the stability field of calcite is reached at temperatures below 175 °C. Although, this reaction has been studied extensively using a variety of experimental techniques since the early works by Wary and Daniels (1957) and Fyfe and Bischoff (1965), most of these studies were based on reactions with fine powders with very high initial reactive surface area. The inhibiting effect of passivating layers during transformation to calcite would then be minimised. Recently however, Perdikouri *et al.* (2011) studied the partial replacement of

single, millimetre scale, aragonite crystals by calcite at 160-200 °C. Figure 5.8 shows that this phase transition is associated with extensive fracturing of *both* parent and product. This, in addition to the porous nature of the calcite, ensures contact between the fluid and the reactive surface area during reaction. However, Perdikori *et al.* (2011) did observe that, when fracturing caused loss of immediate contact between aragonite and calcite, the reaction rate was reduced although reactive surface area was still available. This underscores the significance of the *coupled* dissolution-precipitation processes at the reacting interface. Fracturing induced separation, between the surface where the precipitates form and the surface where dissolution takes place, can significantly hamper reaction progress.

In explaining the action of water, remember to cite experience first and then reason.

LEONARDO DA VINCI (1452-1519), *Thoughts on Art and Life*

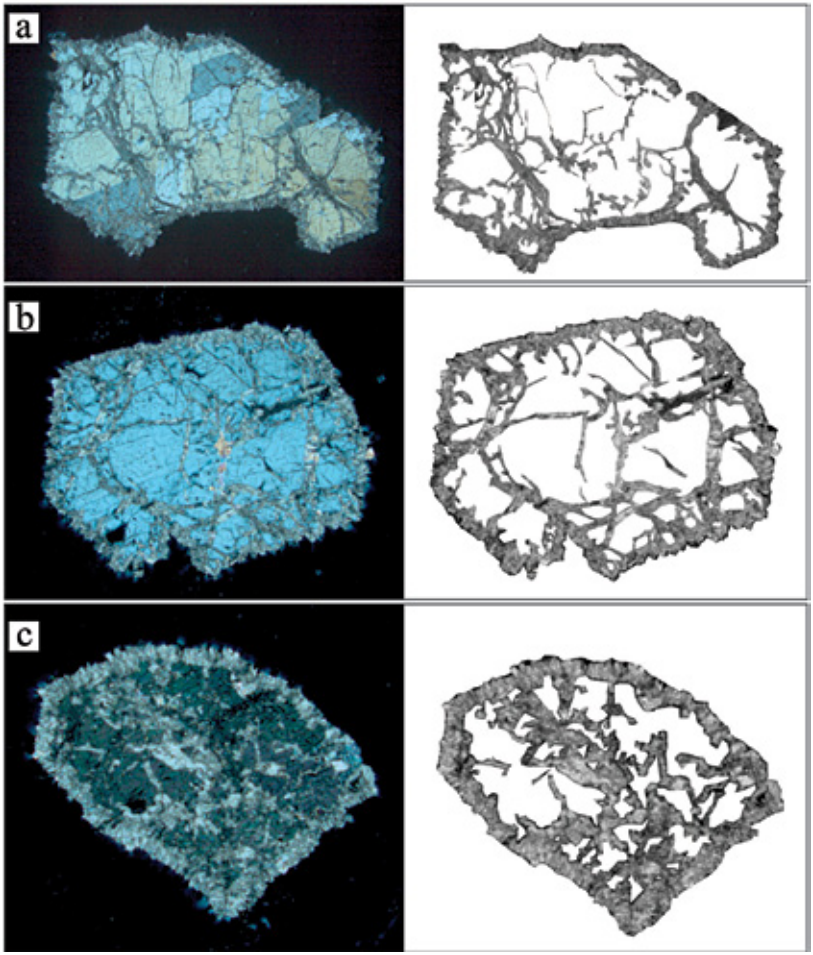

Photomicrographs taken by Christina Perdikouri.

Figure 5.8 Progressive replacement of aragonite by calcite. Right panels show the distribution of calcite in these experiments after a) 5 days, b) 10 days, and c) 14 days. The initial single crystal aragonite fragments are approximately 5x5x1.4 mm and are *unfractured*. The experiments were conducted at 200 °C in a 1 M Na_2CO_3 solution (experimental details are reported by Perdikouri *et al.*, 2011). An evolving network of fractures is driven by the replacement reaction itself.

5.3.2 Leucite to analcime

Another well studied example of reaction driven fracturing during replacement in unconfined environments is the transition from leucite to analcime:

$$KAlSi_2O_6 \text{ (leucite)} + NaCl + H_2O = NaAlSi_2O_6{\cdot}H_2O \text{ (analcime)} + KCl. \quad (5.1)$$

Experiments carried out by Putnis *et al.* (2007) at 150 °C with a 3.5% NaCl solution, demonstrate that this reaction occurs by interface coupled dissolution-reprecipitation. The crystallographic orientation is preserved during the reaction, including a fine scale twinning (Xia *et al.*, 2009).

The *positive* molar volume change of this reaction is about 10% yet the analcime product is porous. In addition, the parent leucite experiences extensive fracturing during the reaction (Fig. 5.9a). As discussed by Jamtveit *et al.* (2009), these fractures evolve in a hierarchical manner whereby fragments of leucite are further subdivided into smaller and smaller pieces. The generation of porosity, including fractures, during phase transitions with an increase in molar volume, implies that the porous product occupies even more space after the reaction than the original parent crystal plus the solid volume expansion of the reaction. Such an expansion would obviously generate local stresses in a confined environment, but as demonstrated by the fracturing observed in this experiment, stresses can even form in unconfined systems. The origin of such stresses is discussed further in Section 7.2.

In nature, leucite is readily replaced by analcime in alkaline volcanic rocks. The replacement process often leads to analcime with a distinct patchy pattern (Fig. 5.9b). This pattern is a natural consequence of the continuous subdivision of the original leucite by reaction driven fracturing. The patches seen within the domain of the original leucite crystal are simply the last unfractured domains of leucite to be replaced by analcime.

5.4 An analogue experiment: plexiglass in acetone

Figure 5.10 shows a particularly spectacular example of fracturing driven by volume increase in an analogue system. The following experiment was carried out by Christophe Raufaste who was a postdoc at PGP in 2008-2009: a thin (0.3 mm thick) plate of plexiglass (PMMA) was confined between two glass plates and placed in contact with acetone along its rim. Swelling was prevented in the third dimension by placing grease between the PMMA and the glass sheets. Acetone and PMMA are miscible at room temperature and dissolution of acetone in the plexiglass caused local swelling near the exposed PMMA surface, fracturing the unswollen plexiglass, which produced new reactive surface area. The swelling took place over a period of several hours, sufficiently slowly to prevent significant temperature perturbations that could contribute to stress perturbations.

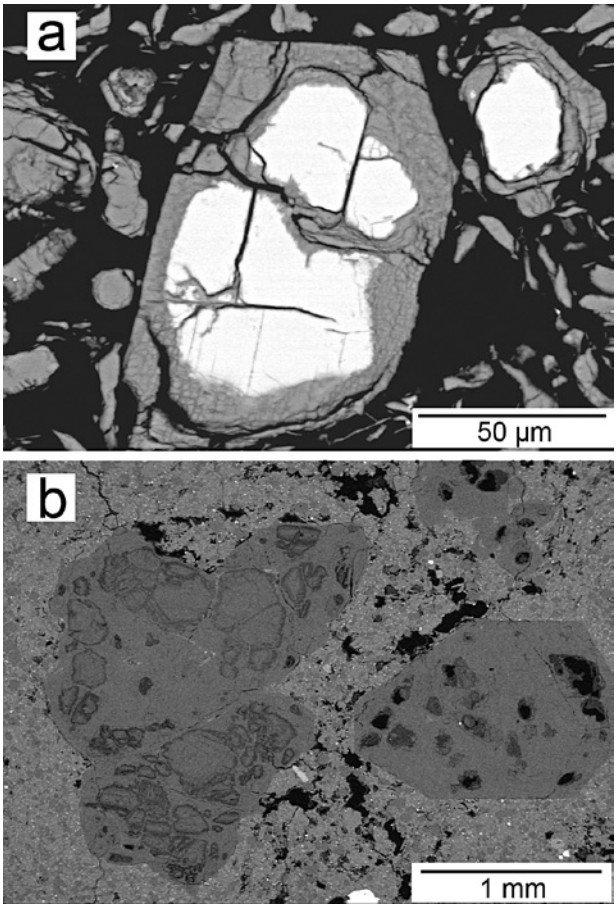

Figure 5.9 a) Back scattered electron (BSE) images of leucite crystals (bright colour) partly replaced by analcime (dark grey) within a period of 4-5 days at temperatures in the range 150-200 °C (from Putnis *et al.*, 2007, with permission from the Mineralogical Society of America). Smaller leucite grains near the fringe of the large one were once part of a single, larger grain. They were isolated from the parent grain by reaction induced fractures (*cf.* Jamtveit *et al.*, 2009). b) Patchy replacement pattern in an analcime pseudomorph after leucite in alkaline lava from Vesuvius, Italy. Darker areas have higher porosity. These are interpreted to be areas of incompletely replaced leucite that formed during an initial replacement process that is similar to that observed in the experiment illustrated in (a). The highly unstable leucite relicts were subsequently also replaced by analcime.

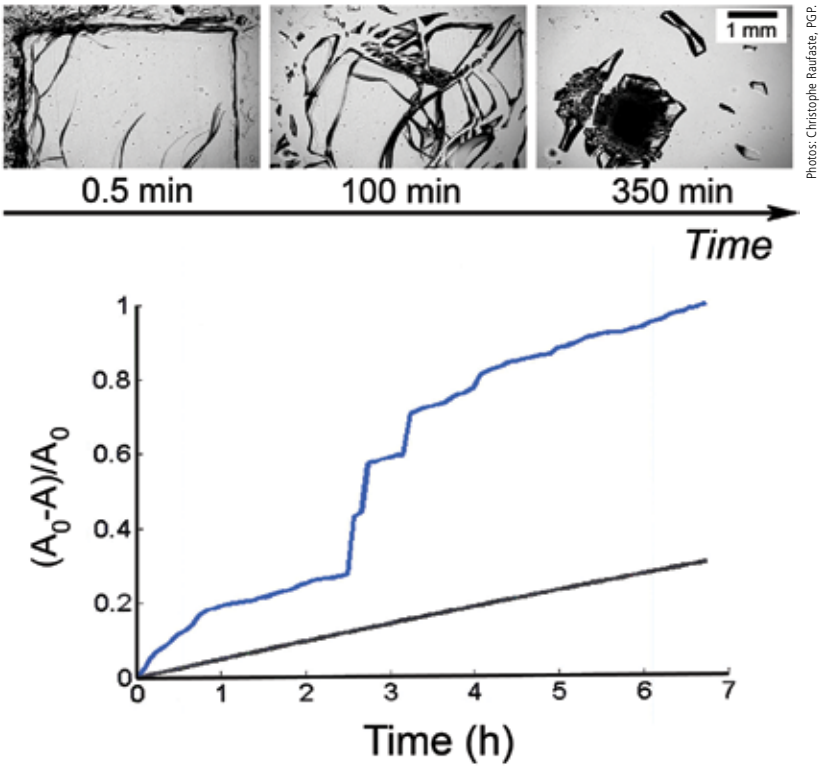

Figure 5.10 (Top) Fragmentation of a 0.30 mm thin plate of plexiglass after exposure to acetone at its margin. The plate is sandwiched between glass sheets that do not allow interaction with acetone at its top and bottom surfaces. A period during which layers spall from the surface is followed by internal fracturing of the main body of the plexiglass plate. In the last (right) panel, the acetone has also gained access to the top and bottom surface of the plexiglass, and the pervasive interaction that follows causes the plexiglass sheet to become completely fragmented. (Bottom) Progress, expressed as fraction of dissolved area (A_0 = initial area and A = remaining area), versus time (blue line). The black line represents the approximately constant, surface reaction controlled rate observed immediately before the onset of fracturing at ~2.5 hours.

The reaction progress versus time (Fig. 5.10) shows a striking acceleration of the dissolution rate when the major fractures start subdividing the PMMA plate into several large subdomains. Such sigmoidal reaction progress versus time curves are characteristic for systems that evolve by reaction driven fracturing and are observed in a number of different systems (*e.g.* Section 6.2).

6. PATTERN FORMATION THROUGH REACTIVE TRANSPORT IN POROUS MEDIA

In the following section, we return to reactive transport modelling (Chapter 2) but with a focus on emergent structures and the role of mechanical processes during fluid-rock interactions. First some of the basic concepts in reactive transport modelling are introduced. For comprehensive accounts of reactive transport modelling in multicomponent systems, the reader is referred to the literature cited in Chapter 2.

6.1 Reactive transport basics

6.1.1 Advection and dispersion

For fluid flow in porous media, it is possible to model flow related transport in the pore networks by direct solution of the Navier-Stokes equations or simplified versions, possibly augmented with a term for surface tension. Such simulations require models of the pore network geometry and typically use special numerical techniques such as the Lattice-Boltzmann method (*cf.* Ferreol and Rothman, 1995; Kang *et al.*, 2010). However, such a highly detailed approach is completely impractical at larger scales and upscaling methods are required (Lichtner and Kang, 2007). Here, we resort to simple phenomenological transport equations with separate terms for the different modes of transport.

Fluid flow in saturated permeable media is driven by imposed pressure gradients and it is usually described by the Darcy equation, which relates the fluid velocity, $\mathbf{v}$, to the pressure gradient, ∇p:

$$\varphi\mathbf{v} = \frac{k}{\mu}\left(-\nabla p + \mathbf{f}\right), \tag{6.1}$$

where, φ, represents porosity, k, permeability, μ, viscosity and $\mathbf{f}$, the external forces per unit volume, such as the effect of gravity. If the advective transport is fast relative to diffusive transport, molecular diffusion can be disregarded; otherwise a diffusion term can be included, as in Eq. (3.4). The effective molecular diffusion coefficient in a free fluid must then be adjusted for the tortuosity of the pore channel network. The fluid flow velocity relative to diffusion is often expressed through the dimensionless Peclet number.

When a fluid containing a solute is driven through a porous medium, the solute concentration field is not simply translated with a small amount of spreading caused by molecular diffusion. Instead, the spreading is much more rapid because fluid volume elements that are initially close to each other could follow different paths with different velocities around obstacles. This produces a separation between the volume elements that increases with increasing time.

Consequently, initially smooth isoconcentration contours become rough (Fig. 6.1) and small regions with high solute concentrations spread. This spreading or dispersion is similar to diffusion and as a first approximation, this effect can be modelled using the diffusion equation but with an effective diffusion coefficient, the dispersion coefficient, which is much larger than the molecular diffusion coefficient (Måløy *et al.*, 1988). We therefore include a diffusive term regardless of the Peclet number but with different interpretations and different coefficients depending on the relative importance of molecular diffusion and hydrodynamic dispersion. It should be noted however, that at high Peclet numbers, where the motion of solutes is determined largely by convection and the dispersion is dominated by local variations in fluid velocity, the dispersion coefficient depends on the flow rate and in fact diverges with increasing Peclet number (Lowe and Frenkel, 1996). On the other hand, flow in narrow channels can retard local turbulence and reduces dispersion compared with a system where flow is less channellised. The latter effect is very important for mixing processes in microfluidic systems (*e.g.* Stroock *et al.*, 2002) and might also be relevant to geological systems with highly anisotropic porosity distribution.

These waters traverse the body of the Earth with infinite ramifications.
LEONARDO DA VINCI (1452-1519), *Notebooks*

The complete, coarse grained, advection-dispersion equation for isotropic and homogeneous porosity and diffusivity, describing the change in concentration, c, of some arbitrary solute then becomes:

$$\varphi \frac{\partial c}{\partial t} = -\varphi c \nabla \bullet \mathbf{v} + \varphi D \nabla^2 c. \qquad (6.2)$$

The first term describes advection, where the velocity can be derived from Eq. (6.1). In the usual case, with hydrodynamic dispersion dominating over molecular diffusion, the second term describes dispersion, where D represents the dispersion coefficient.

This *bulk* equation is valid only at large scales. In particular, for large Peclet numbers (where advective transport dominates over diffusion), it hides the smaller scale variations resulting from incomplete mixing. These errors can be further amplified by reaction terms controlled by the concentrations, leading to large errors in the rates of chemical processes.

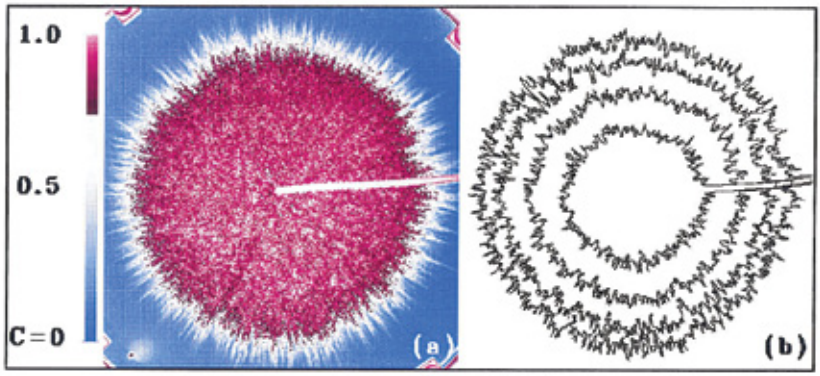

Figure 6.1 The dispersion obtained by injecting glycerol, coloured black by Negrosine, into clear glycerol of the same viscosity and density in a quasi two dimensional porous model. Coloured glycerol is injected at the centre of a monolayer of 1 mm glass beads sandwiched between two plastic sheets and leaves the model at the rim. a) The logarithm of transmitted light intensity, colour coded as shown by the vertical scale in the inset (*i.e.* black=red, colourless=blue). b) Contours show the position of a concentration corresponding to half the injected tracer concentration 36, 77, 122, and 160 seconds following the start of injection. Although the fronts are rough and can be characterised by a fractal dimension of 1.42, the front can, *on average*, be described by a hydrodynamic dispersion coefficient (modified from Måløy *et al.*, 1988).

6.1.2 Reactions

It is not altogether trivial to integrate transport and chemical reaction in one model. Of course we can simply add kinetic reaction terms to Eq. 6.1 and 6.2, which has the advantage of conceptual simplicity. For systems with multiple species, one differential equation is required for each species. However, when all or some of the reactions are very fast compared to transport, we can run into practical problems because the time steps necessary for numerical stability of the reaction terms are much smaller than the time steps required by the transport terms. In such cases, we can assume that the fast reactions equilibrate in each control volume in every time step. Calculating these equilibrium concentrations usually requires the solution of a coupled set of linear or nonlinear equations.

The relative rates of reaction and transport can be quantified by the dimensionless *Damköhler* number, which is the ratio of the characteristic transport time (characteristic length divided by velocity in the case of advection) to the characteristic reaction time. Another difficulty is charge balance. The kinetic and equilibrium equations must always be specified so as to preserve total charge in each control volume. In fact, this is necessary for closure of the equilibrium

equations but if ions are allowed to diffuse at different rates, charge can easily become nonzero in each control volume. Ions might then start to migrate under the influence of electrical forces, which must also be included in the transport terms.

6.1.3 Sharpening of reaction fronts

Visual boundaries in rocks are often extremely sharp (Fig. 6.2). This comes as no surprise if the discontinuity represents the wall of a vein or the boundary of a clast or crystal but if it is caused by a reaction front in a permeable or diffusive medium, then a more gradual transition might be expected. Sharp reaction fronts can be explained by a number of mechanisms.

When a concentration front moves through a permeable medium, the concentration gradient depends on the Peclet number. For pure diffusion or dispersion, an initially abrupt transition in concentration (step function) broadens over time into a sigmoid curve known as the *error function*. Increasing influence by advection and thus a higher Peclet number, results in a sharper profile.

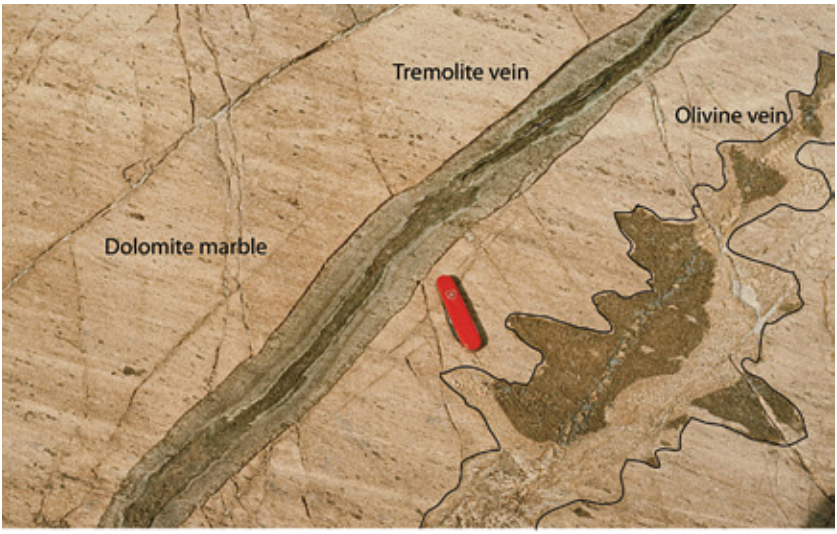

Figure 6.2 Two reaction veins cutting dolomite marble. The symmetric vein to the left contains tremolite and calcite and the vein to the right consists of olivine and calcite. The orientation of the veins is approximately perpendicular to the primary sedimentary bedding. Note the sharp reaction fronts and the contrasting morphology of the fronts. Dark patches on the olivine vein were caused by surface wetness on the outcrop (reaction front is drawn by a black line for clarity). Wall rock dolomite marble contains less than 5% other minerals (slightly modified from Bucher, 1998).

Figure 6.3 shows the results of simple numerical simulation of advective and diffusive transport of a solute with concentration, c, in one dimension, with zero flux boundary conditions:

$$\frac{\partial c}{\partial t} = -vc + D\frac{\partial^2 c}{\partial x^2} \tag{6.3}$$

where, v, represents the fluid velocity, D, the diffusion coefficient and porosity, $\phi = 1$ (pure fluid; *cf.* Eq. 6.2). As discussed above, D could also represent a dispersion coefficient. For a unit characteristic length, the Peclet number becomes $Pe = v/D$. In the simulations, the Peclet number is varied by changing D, keeping v constant. The study of how varying Peclet numbers affect geochemical transport and associated geochemical fronts became very popular in the late 1980s (Bickle and McKenzie, 1987; Baumgartner and Rumble, 1988; Jamtveit *et al.*, 1992).

During reactive flow, the Damköhler number also influences the sharpness of the front (Steefel and Maher, 2009). When reactions are much faster than transport, relative to the characteristic length scale, concentrations approach equilibrium values quickly, leading to steep fronts. Indeed, if the reactions are so fast compared with transport that we can assume local chemical equilibrium in every time step, the Damköhler number is effectively infinite and a completely sharp front separates rocks with different mineralogy. The front is located where the chemical potentials cross a reaction boundary in some phase diagram. However, sluggish reactions require addition of a term to represent kinetic dispersion effects on the transport process and geochemical fronts tend to be broadened. Such effects on isotope fronts were presented soon after the first papers on combined diffusive-advective transport, first by Blattner and Lassey (1989), followed up by important contributions from Bickle (1992), Bowman *et al.* (1994) and others.

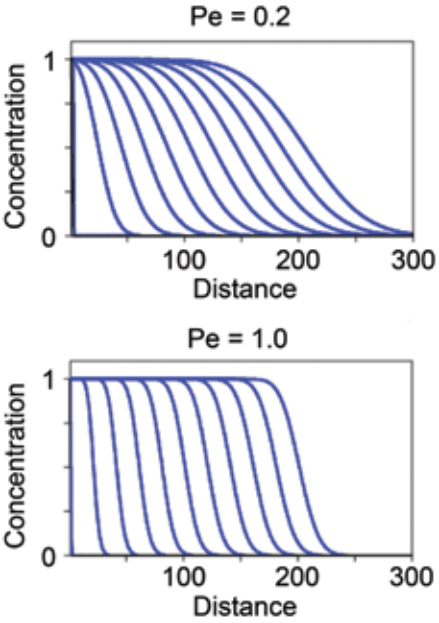

Figure 6.3 An initially abrupt concentration front (step function) travelling from left to right with advection and diffusion but without reaction. The steepness of the front converges quickly to a value that depends on the Peclet number.

Further complications arise when reactions are nonlinear. Sharpening of reaction fronts in biological systems (compartmentalisation) is sometimes explained by *molecular switches* with two discrete steady states. Similar processes are possible in complex geochemical situations involving catalysts and inhibitors (Tompson, 1993). Even more interesting phenomena arise when reactions feed back on transport parameters. This happens when precipitation or dissolution modifies permeability and flow paths, such as in travertine terracing and karst phenomena. When an undersaturated solution infiltrates a porous medium, dissolution increases the permeability, thus enabling faster transport. This can lead to a reactive-infiltration instability, resulting in fingering and dispersion of the reaction front (Ortoleva *et al.*, 1987b; Steefel and Lasaga, 1992; 1994; Aharonov *et al.*, 1997; Steefel *et al.*, 2005; Szymczak and Ladd, 2011). The 3D simulations by Aharonov *et al.* (1997) illustrate the contrasting patterns formed by dissolution and precipitation in a porous medium. With respect to flow, dissolution creates a positive feedback system in which flow opens its own pathways, leading to localisation (focusing of flow) and fingering. In the case of precipitation, flow blocks pathways creating a negative feedback loop, inhibiting localised reaction and leading to a more diffuse distribution of permeability. The parameter space can be compared to that of open channel reactive flow (Section 4.7) where dissolution channelises the flow (*e.g.* rillenkarren) whereas precipitation disperses it (travertine terraces).

The contrasting morphologies of the metasomatic fronts shown in Figure 6.2 were interpreted by Bucher (1998) to reflect a change from reaction kinetic controls for the planar front, to diffusion control for the wavy front. The wavy morphology was ascribed to pre-existing variation in the host rock transport properties. An alternative explanation is that the transport properties are themselves affected by the reactions in a way that creates a reactive transport instability with wavelengths controlled by the coupled reaction-transport processes rather than by the initial layering of the rocks.

6.2 Including mechanical effects by volume changing reactions

Until recently, reactive-transport models presented in the geochemistry literature (*cf.* Lichtner *et al.*, 1996) have ignored mechanical processes that could influence the overall reaction. Changes in solid volume have been directly converted to changes in porosity without any consideration of effects caused by stress. Hence, any negative volume change would produce increased porosity while positive change would reduce porosity. Although it is generally true that a decrease in solid volume will, at least in the absence of compaction, result in increased porosity, the examples shown in Section 5.3 demonstrate that an increase in porosity can also result from reactions that cause expansion. To understand how this arises, we need to couple reactive transport to generation of stress and the associated strain. In the following discussion, we mainly deal with elastic deformation and fracturing to avoid the complications introduced by including time dependent deformation and thus additional time scales.

Several approaches to include mechanical effects are possible. Continuum approaches and analytically tractable 1D models have been presented by Fletcher *et al.* (2006) and Rudge *et al.* (2010), partly inspired by the early work of Yakobson (1991) on fracturing during chemical decomposition of a solid into another solid plus gas (similar to a drying process). Here we describe how a discrete element model (DEM) can be used to treat fracturing in a conceptually simple way. A typical DEM model is illustrated in Figure 6.4 and described in detail by Jamtveit *et al.* (2000) and Malthe-Sørenssen *et al.* (2006). In these models, the solid is represented by discrete elements connected by bonds, which can be described numerically as linear elastic springs or beams, or they can have more complex properties, depending on the application. Each bond has a certain equilibrium length and breaking threshold. The equilibrium bond lengths vary randomly and the distribution of breaking thresholds controls how brittle the solid is. A narrow distribution results in a very brittle solid in which fractures grow rapidly to a large size as soon as they have been nucleated. Stresses can be generated either by subjecting the solid to external forces at its margin or by internal volume changes (positive or negative). In the following, we focus on a volume changing reaction triggered by the infiltration of reactive fluids to a porous rock.

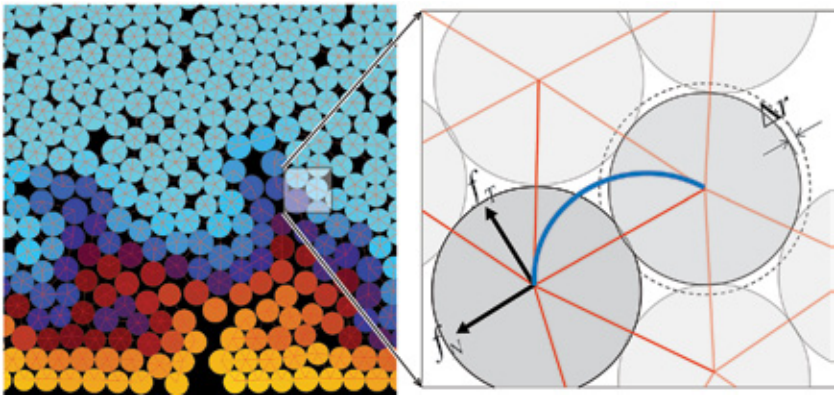

Figure 6.4 Simple DEM model for reactive transport. The solid is comprised of particles connected by elastic *beams* which are removed if their breaking thresholds, which depend on their normal stresses and shear stresses, are exceeded. f_T and f_V are unit vectors used to describe elastic strain in the model. When the solid is exposed to a *fluid* at its lower surface (left), the diffusion of fluid components (for example H_2O) into the solid drive volume changing reactions in the initially unfractured solid. This progress is indicated by the colour scale in the figure (blue: unreacted; yellow: completely reacted). The corresponding volume change is modelled as a change in the size of the particles (represented by Δr in the model). If the elastic stresses generated by the volume change exceed the breaking threshold of the bonds, a fracture nucleates or grows and fast transport takes place in the fracture. In this simple model, infinitely fast transport in the fractures was assumed.

When a volume changing reaction proceeds, the stress in the solid changes and if the local stress in a bond exceeds its breaking threshold, a fracture nucleates. The fracture propagates if the stress is transferred to neighbouring bonds because the initial bond breakage causes one or more of the adjacent bonds to exceed its breaking threshold. Fracturing has two effects. It exposes fresh reactive surface area to the reactive fluid and it generates pathways for fast diffusive or advective transport. The DEM model was initially applied to systems with negative volume changes, such as the eclogitisation of mafic rocks (Jamtveit *et al.*, 2000), but it has also been applied to expanding systems (Jamtveit *et al.*, 2008; 2009). Expanding systems are more challenging because the boundary conditions have large effects on the progress of the expansion process and thus the fracture pattern.

It is also important to recognise that in natural systems at temperatures significantly below melting temperatures, diffusion through solids is an exceedingly slow process. Thus, the rate of reaction (or volume change) in the unfractured solid between fractures is not likely to be controlled by solid state diffusion. In a polycrystalline material, transport can be controlled by diffusion along grain boundaries and stress generating reactions can start there. For individual grains, replacement reactions normally take place by dissolution-reprecipitation (Chapter 5 above), without the formation of a partly reacted and still unfractured product. As demonstrated by Plümper *et al.* (2012) (also Section 7.2 below), stress generation during serpentinisation of individual olivine crystals can be related to roughening of the reactant surface by dissolution controlled pit formation. Associated growth of reaction products within the pits formed during dissolution generates a "wedging" related stress that ultimately leads to the formation of macroscopic fractures. Fluid can then penetrate into the fractures, exposing new reactive surface to the fluid and the cycle is repeated.

6.2.1 Reaction front shape and velocity

The behaviour of a coupled reaction-fracture front for a system, that was undergoing shrinking of solid volume caused by reaction with a fluid supplied from a planar source or fluid generation with a planar fluid sink, was analysed in detail by Malthe-Sørenssen *et al.* (2006). Fluid consuming reactions that lead to a reduction of solid volume are easy to model but relatively unusual in geological systems. However, infiltration driven volume reductions can be seen during CO_2 driven granulitisation of amphibolites (Newton *et al.*, 1980) and during eclogitisation (Jamtveit *et al.*, 2000). However, most volatilisation processes (reactions that consume volatile components such as H_2O and CO_2) are associated with an expansion of solid volume (described later).

Figure 6.5a shows the modelled fracture pattern formed during propagation of a reaction front associated with a reduction in solid volume, using a model similar to that described above. The shape of the reaction front, in terms of average reaction progress with variable distance to the fluid inlet, is shown in Figure 6.5b. Unlike a typical diffusion controlled front, this front moves at

constant velocity and maintains a constant width. This is possible because the transport within the fractures is assumed to be infinitely fast compared to diffusion through the unfractured solid. Under these circumstances, the front velocity, v, is given by $v \approx D/l$, where D represents the diffusion constant of the fluid in the unfractured solid (which controls the local rate of reaction) and l, a critical stable crack length, which depends on material properties and the volume change of the reaction.

A detailed analysis of the parameters controlling the crack length was presented by Rudge *et al.*, 2010. The distance, x, travelled by a diffusion controlled coupled reaction-fracture front at time, t, is thus Dt/l. During the same time interval, a diffusion controlled reaction front without fracturing has travelled a distance $x' \approx (Dt)^{1/2}$. It is easy to show that $x > x'$ *if* $l^2/D > 1$. Hence, for a critical stable crack length comparable to a grain size of 100 μm and a bulk grain boundary diffusion coefficient of 10^{-15} m^2/s, a fracture propagated front would move further than a diffusion front after about 4 months of reaction. However, the propagation distance at which a fracturing propagated front becomes significantly faster than a purely diffusion controlled front is proportional to the square of the critical stable crack length. Thus a critical stable crack length of 10 μm would imply that the coupled reaction fracture front would have moved further than a diffusion front after only 1 or 2 days. Any

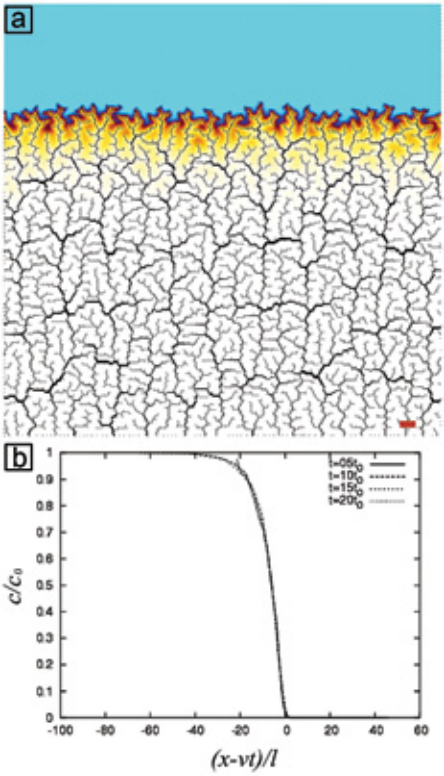

Figure 6.5 a) Fracturing assisted reaction front propagating into an unfractured elastic solid simulated by the model shown in Figure 6.4. The colour scale reflects extent of reaction from unaltered (blue/turquoise) to partly reacted (shades of yellow) and then to completely reacted (white). b) Reaction progress, c/c_0, versus distance, x, minus vt (v=velocity, t=time) rescaled to a characteristic fracture length, l. The coincidence of the reaction front curves for different times indicates that the front does not change width or shape with time and propagates at a constant rate (modified from Malthe-Sørenssen *et al.*, 2006).

stress generating mechanism that operates faster than grain boundary diffusion would reduce the time even further for a fracturing propagated front to overtake a diffusion front.

This model highlights the role of fracturing during the propagation of reaction fronts. However, other mechanisms can enable fracturing to play an even greater role in accelerating infiltration driven reactions. First, a reactive infiltration instability can arise during fracture propagated reactions, when the rock volume is subject to external stresses. Second, in a 2D or 3D situation, where a reacting rock volume of arbitrary shape is exposed to external fluids, microfracturing alone might not be sufficient to relax all reaction produced stresses. In such situations, reaction driven volume changes could lead to macroscopic fracturing which further accelerates the overall reaction progress. These possibilities are examined in the following sections.

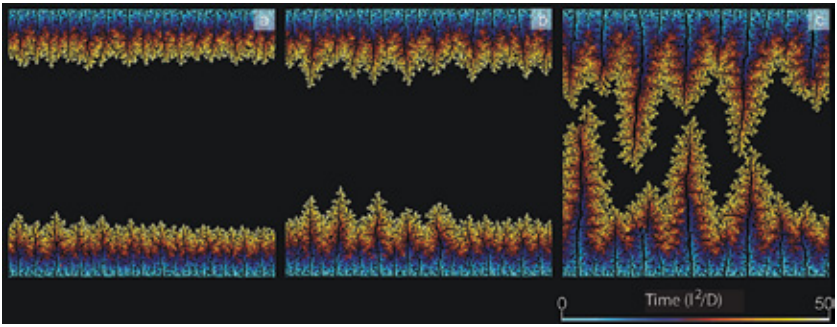

Figure 6.6 Simulated fracture patterns for a system subject to anisotopic external stress, with fluid invasion from the top and bottom surfaces. Initially, only the top and bottom nodes are in contact with the fluid. Nodes are coloured according to the time of fluid exposure with a common time scale at the bottom. Time is measured in units of l^2/D, the reaction time for a single grain, where l represents the critical stable crack length. The effect of increasing the anisotropy in the external stress field, that is, increasing pre-existing stress, s_0, is shown. a) $s_0 = 0$; b) $s_0 = 0.005E$; c) $s_0 = 0.010E$, where E represents Young's modulus. The fingering instability becomes more pronounced as s_0 increases. Even for $s_0 = 0$, the front has some roughness from randomness in the system but here the roughness does not grow with time (modified from Jamtveit *et al.*, 2000).

6.2.2 Instabilities triggered by external stress

An externally imposed stress field can influence reaction driven fracturing in a manner analogous to stress corrosion (*cf.* Jones, 1992). The stress field also influences the direction of fracturing and the stability of a reaction driven fracture front. Figure 6.6 shows simulated fronts for variable anisotropic stress in a model similar to that illustrated in Figure 6.5. Anisotropic stress destabilises a planar

front and macroscopic fracturing propagated fingers start growing parallel to the largest stress axis, *i.e.* with an orientation similar to that of tensile fractures in a nonreactive material.

These kinds of instabilities are probably abundant in natural systems but they can often be hard to distinguish from veins formed by fracturing as a result of tectonic forces. *Tectonically produced* veins usually contain a central fracture with a surrounding metasomatic zone (*cf.* Fig. 6.2). In addition, tectonic fractures often form a conjugate set oriented according to the relevant stress field. *Reaction produced fingering* on the other hand forms by smaller scale fracturing and a central fracture filling vein might not be present. The 3D alteration pattern would be more complex (even in a relatively homogeneous system) than a typical conjugate fracture pattern formed by external stresses. Figure 6.7 shows the pattern of granulitisation of amphibolite facies gneisses in Kerala, Southern India. This is a possible candidate for a pattern controlled by coupled reaction and fracturing influenced by an external stress field. The alteration pattern is complex, yet not random, and the altered fingers or stripes have no central vein. There is also a pronounced control by the original lithological layering and foliation on the alteration pattern and many of the alteration features are finger like or cylindrical rather than planar.

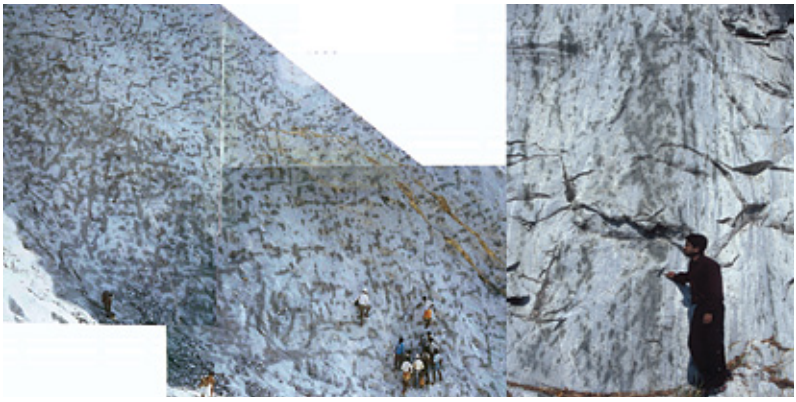

(Left) Photo courtesy of Michael Raith, University of Bonn.
(Right) Photo: Bjørn Jamtveit.

Figure 6.7 Patterns of granulitisation. (Left) In Kottavattom (Kerala, Southern India), where amphibolite facies gneisses have been dehydrated to granulites. The process is probably driven by influx of carbon rich fluids that destabilise the original hydrous minerals (biotite) in the gneiss (Newton *et al.*, 1980; Raith and Srikantappa, 1993). The reaction is associated with a reduction in solid volume and a potential local porosity increase. However, on the outcrop scale, the pattern is somewhat reminiscent of a conjugate fracture set (Raith and Srikantappa, 1993) and not completely random. In this case, the pattern of local reaction and porosity generation by volume reducing reactions might be affected by an external stress field. (Right) Patchy charnockitisation with strong control by the original lithological layering, from the Para Mukku Quarry some 20 km southwest of Kottavattom.

In contrast, a *classical* alteration pattern confined to large scale conjugate fractures is shown in Figure 6.8. In this case, the fractures have a characteristic central vein zone surrounded by an alteration halo or metasomatic zone. Such a pattern would normally be interpreted as infiltration of fluids into a fracture system generated by tectonic stresses and would have no connection to reactive transport instabilities. The formation of the metasomatic zones around the fractures might or might not involve fracturing, but the metasomatic fronts moving away from the main fractures show no evidence for any fingering instabilities.

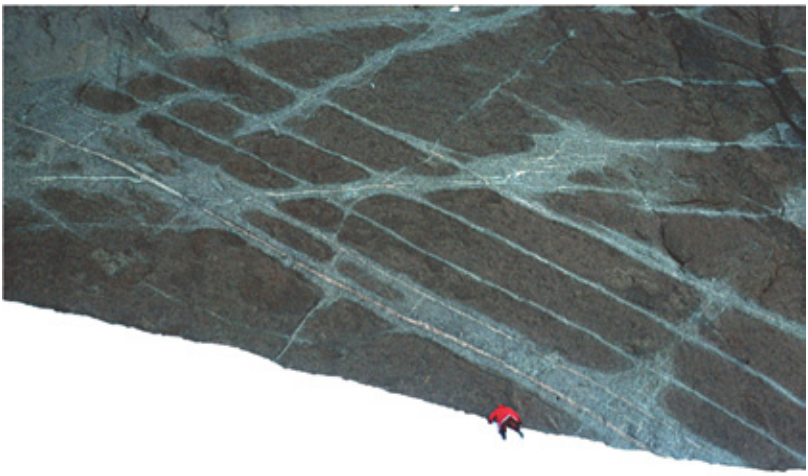

Photo: Håkon Austrheim, PGP.

Figure 6.8 Fracture controlled amphibolitisation of granulites at Trollslottet, Antarctica. The alteration is confined to a conjugate fracture system with a central vein.

6.2.3 Rate controls by hierarchical fracturing

Many natural systems that undergo volatilisation are characterised by fracture patterns that are present over a wide range of scale. This applies to serpentinisation and to weathering, arguably the two most important hydration processes in/on the lithosphere. The complex fracture sequence that takes place during the action of acetone on plexiglass, shown in Figure 5.10, indicates that fracturing driven by volume changing processes can generate highly complex fracture patterns with a variety of fracture lengths and orientations. Before we present natural data and examine the actual fracturing mechanisms in natural systems, we examine an extension of the DEM model presented above, in which the reactive elastic solid is exposed to fluid and stress generating reactions along its entire margin.

It is very nice that the computer understands the problem.
But, I would like to understand it too.

EUGENE WIGNER
(Nobel Laureate in Physics, 1963)

The coupled diffusion-reaction-deformation model used to study shrinkage induced fractures can be modified to include volume expansion reactions. Such a model was used by Røyne *et al.* (2008) to study spheroidal weathering processes. The diffusion-reaction process is described by the following equations:

$$\varphi \frac{\partial c}{\partial t} = D(\varphi)\nabla^2 c_f - Q \text{ and} \tag{6.4}$$

$$\frac{\partial \xi}{dt} = \left(\frac{V_m}{f_0}\right) Q, \tag{6.5}$$

where the rate of consumption of the fluid is $Q = kS\rho f_0 (1 - \xi)\, c_f$. c_f represents the local fluid concentration, ξ, the extent of reaction (ranging from 0 to 1), φ, the porosity, $D(\varphi)$, the diffusion constant, k, a kinetic constant, S, the specific surface area, ρ, the density, f_0, the initial volume fraction of reactive material in the solid, and V_m, the molar volume of the fluid.

Fluid initially enters along the outer boundaries of a block of fresh rock (Fig. 6.9) described using a Neumann boundary condition, which specifies the derivative of the solution to Eq. 6.4 and 6.5 on the boundary of the domain, and diffuses inward. The reaction produces a local volume change proportional to the extent of reaction, x. The local volume change produces a local strain which induces stresses in the elastic rock matrix. Given the stresses induced by the local volume change, the equilibrium configuration of the elastic matrix is found using an over relaxation algorithm. If the elastic stress in an element exceeds the local yield strength of the material, a fracture occurs as described above. If a fracture extends to the outer boundary of a block, fluid infiltrates the fracture and the fracture surfaces become new boundaries for the diffusion-reaction process. In this model, the chemical reaction rate is transport limited, but as a result of the ongoing fracturing process, the bulk reaction rate evolves in a nontrivial way.

The simulation results (Fig. 6.9) show that initially, layer by layer spalling occurs because of expansion near the outer margin of the model domain. This process produces a spheroidal shape by removing sharp corners from the initially rectangular block. The simulation also indicates that corners can be sheared off, resulting in large corner blocks with unaltered cores, something which is also observed in the field (Fig. 7.2, below). Further shells are spalled off as the reaction front continues to penetrate into the block. At the same time, the expanding

boundary generates a tensile stress in the block, which eventually leads to the formation of a tensile fracture that divides the block in two (Fig. 6.9). As fluid penetrates into the newly formed fracture, the diffusion-reaction process proceeds from the surfaces of the two new blocks and the entire cycle is repeated on a smaller scale. Four generations of subdomain formation were observed in the simulations. This domain dividing process results in a hierarchical system of fractures and unfractured blocks. Layer by layer spalling can occur in each generation and sharp corners generated by domain dividing fractures are rounded off by spalling, gradually producing new blocks with spheroidal shape.

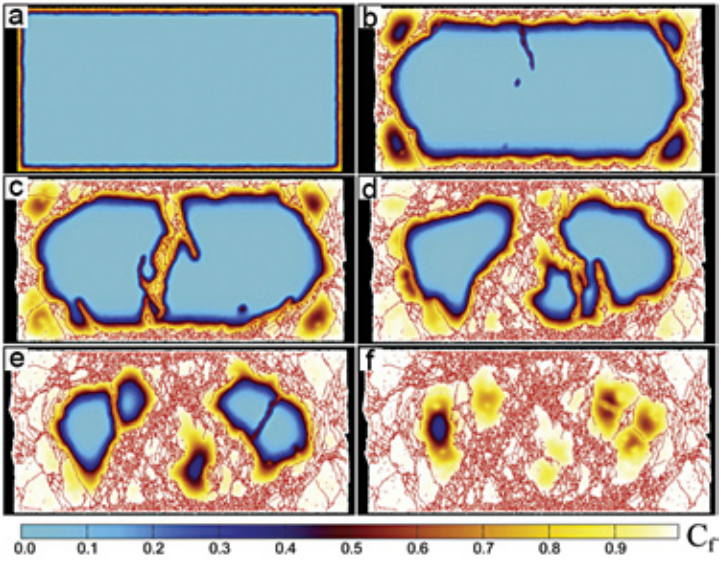

Figure 6.9 Simulation of spalling and hierarchical fracturing. Parts a to f show six successive stages in a simulation of weathering by diffusion-reaction induced volume expansion using a discrete element model coupled to a diffusion-reaction model (from Røyne *et al*., 2008, with permission from Elsevier). Fluid diffuses in from the outer boundaries, reacting with the rock matrix, resulting in a local expansion. Expansion in the *y*-direction is limited by an elastic wall. The colour scale shows the normalised fluid concentration. Fractures are illustrated by red lines. The outer corners are rounded by spalling. Four generations of subdomains are formed and in each generation, a new fracture divides a cell into two smaller cells. The fluid infiltrates the fracture as it becomes connected to the exterior. Therefore the boundary conditions for the reaction-diffusion process change gradually. The outer corners are sheared off early in the process and shear bands associated with the external boundaries are visible in the final fracture pattern.

Implications for reaction rates. Fracturing significantly accelerates the reaction process compared to a purely diffusional processes. Figure 6.10 shows a plot of the extent of reaction, x, for a simulation with fracturing and for the same

simulation with diffusion but without fracturing, as a function of time. For short times, simulations with and without fracturing display nearly identical behaviour. However, from about the time at which the first domain division occurs, the total extent of reaction for the fracturing system starts to increase significantly faster. Eventually, the effect of finite system size limits the growth and both systems tend toward the same asymptotic value (x=1). Comparison of this figure with the experimental results on plexiglass, we see that the same sigmoidal reaction progress curve is obtained: a slow start controlled by diffusion or surface kinetics is followed by acceleration when fracturing commences and finally, size limited deceleration.

Implications for fracture pattern. Reaction driven fracturing, and associated subdivision into subsequently smaller domains seen in Figure 6.9, produces a hierarchical fracture pattern that, in a statistical sense, is similar to many patterns in real systems formed by slowly driven fracturing. Well characterised examples include ice wedge polygons (Lachenbruch, 1963), fracture patterns formed during contraction of lava flows (Aydin and DeGraff, 1988) and fractures formed during a number of replacement processes (Jamtveit *et al.*, 2009). In such patterns fracture angles close to 90 ° and 180 ° (*i.e.* T-junctions) and four sided domains dominate (Bohn *et al.*, 2005). The size distribution of unfractured domains also follows a log normal distribution (Iyer *et al.*, 2008; Plümper *et al.*, 2012).

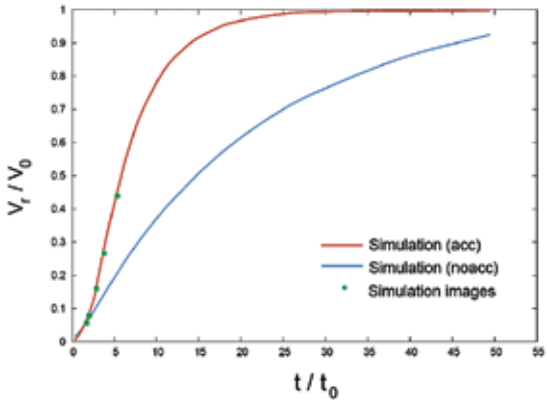

Figure 6.10 Time evolution of reaction progress for the model shown in Figure 6.9. The reacted volume is shown for the case in which the process is accelerated by hierarchical fracturing (Simulation (acc)), i.e. when the system fractures and fluid enters newly generated fractures, and where the system does not fracture and fluid enters only from the initial external boundaries (Simulation (no acc)). The circles along the accelerated simulation curve correspond to the times for the images in Figure 6.9 (modified from Røyne *et al.*, 2008).

7. HIERARCHICAL FRACTURING DURING WEATHERING AND SERPENTINISATION

7.1 Weathering

Weathering processes form a wide range of patterns, many of which are a result of "sculpting of rocks by reactive fluids". Karst and cave morphologies for example, can form by reactive transport (*cf.* Palmer, 2011), often assisted by microbiological interactions (Hose *et al.*, 2000). However, as discussed in Section 4.8, even cave morphologies usually depend on mechanical processes. When it comes to weathering influenced by dissolution and precipitation, emergent patterns are almost invariably affected by the coupling of chemical and physical processes. In discussing the origin of such patterns, we believe that it is useful to make a distinction between weathering of permeable rocks and weathering of rocks with very low porosity and permeability.

Near the Earth's surface, porous rocks weather by processes that include transport of fluids via the pores and weathering can potentially be affected by features such mass redistribution driven by chemical potential gradients associated with a broad range of pore sizes (*i.e.* surface curvatures). However, essentially nonporous rocks are attacked from the outside. In this case, weathering is confined to external surfaces exposed to waters arriving from somewhere else and the weathering front propagates into fresh rock and weathering might depend on porosity producing processes operating near the reacting interface. Spheroidal weathering of many magmatic and metamorphic rocks is a typical example. According to Chapman and Greenfield (1949), "spheroidal weathering is that process by which igneous rocks scale off concentric shells producing rounded boulder like forms". This type of weathering occurs, not only in igneous rocks, but in most rock types and most climates. Dana (1896) was probably the first to recognise that the spheroidal patterns were associated with chemical changes during weathering and despite the many more recent attempts to explain such patterns, Chapman and Greenfield pretty much understood the processes qualitatively from their microscopic observation more than 60 years ago. In their 1949 paper they state: "The current views, held by the best authorities, are that spheroidal weathering results from either of two processes: (1) the swelling and spalling of the exterior surface of angular blocks of rock due to the hydration, carbonation, and oxidation of constituent minerals in the outer surface, or (2) the swelling and spalling of the exterior surface of angular blocks which have been subjected to sudden, intense heating of their exterior by forest fires and bush fires"

Despite this insight, it took 57 years before this qualitative explanation was cast into a quantitative model by Fletcher *et al.* (2006) to explain spheroidal weathering features observed in diorites from Puerto Rico. Fletcher *et al.*'s 1D model assumes that the weathering is driven by diffusion of oxygen into the

fresh diorite. The volume expansion associated with oxidation of ferrous minerals results in a buildup of strain energy in the reacted layer. When the strain energy in a layer equals the fracture surface energy, a surface parallel fracture is expected to form. Oxygen bearing water moves in to the newly formed surface and the process is repeated. A series of parallel spalls form, as is observed, and the model puts constraints on the parameters that control the layer spacing and weathering rate. In subsequent papers, Ray Fletcher, Susan Brantley and collaborators elaborated on how such weathering mechanisms control regolith production and the size distribution of bedrock blocks in weathering profiles (*e.g.* Fletcher and Brantley, 2010; Lebedeva *et al.*, 2010).

In many respects, the chemomechanical model of Fletcher and collaborators from Pennsylvania State University is similar to the models that we have developed at our PGP Research Center, at the University of Oslo (Section 6.2). One main difference however, is that the Penn State models explicitly account for the chemistry and chemical kinetics of the weathering process, while the fracturing process is only accounted for implicitly by its effect on the weathering front propagation rate. The Oslo model explicitly models the fracturing and the resulting fracture patterns but only implicitly accounts for composition changes in terms of a time dependent reaction induced volume change. Both approaches have strengths and weaknesses and which one to choose depends on what problems one wishes to address. Of course, only the time and effort required for code development and computing resources lie in the way of developing a model that treats both the chemistry and the fracturing explicitly.

A general goal in our Oslo group has been to compare, in as much detail as possible, modelling results with what we actually see in the field or the lab, in terms of emergent patterns. In such cases, the fracturing processes must be explicitly accounted for because the fracture pattern determines what an exposure looks like. The fact that spheroidal weathering, with its characteristic structures, occurs in almost all rock types and in most climates, also suggests that the details of chemical composition are not critical in controlling the emergent patterns, although they could control the rate at which rock is converted to saprolite.

Figure 7.1 shows some of the characteristic features of an outcrop displaying spheroidal weathering of a doleritic sill intrusion in Karoo, South Africa. Structures similar to this have been described in many rock types (Blackwelder, 1925; Bisdom, 1967; Ollier, 1971 and others). Usually, the fractures observed in such outcrops were interpreted as having formed prior to the weathering itself because of thermal or tectonically produced stress and it was assumed that ground water or other fluids infiltrated via the fractures and drove the weathering reactions (Ollier, 1971; Turner *et al.*, 2003). Clearly, any pre-existing set of joints would provide first order control on where weathering initiated. However, detailed studies of the outcrops shown in Figure 7.1, as well as of many other outcrops, indicate that fracturing also occurs synchronously with the weathering process. The evidence includes a fracture pattern that strongly resembles the hierarchical

patterns that form during slowly driven volume changes in brittle materials, characterised by a high frequency of T junctions, 4 sided domains and log normal fracture length distribution.

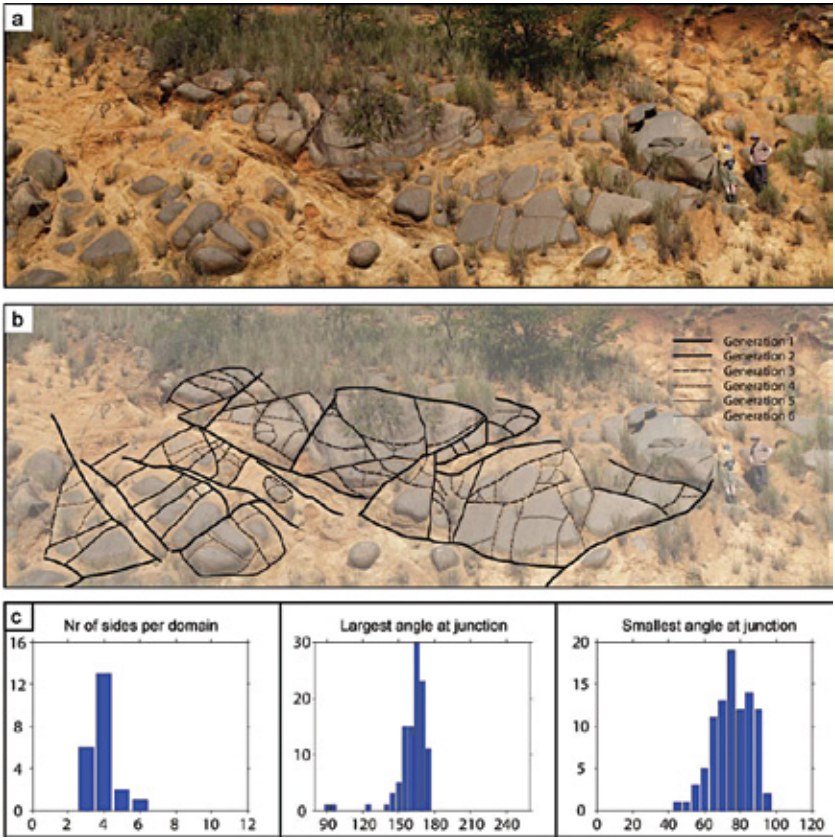

Figure 7.1 a) Spheroidal weathering at Nico Malan Pass, South Africa (S32.50780°, E026.80417°). Field geologists near the right margin of the picture provide scale. b) Outline of hierarchical fractures according to generation following the method of Bohn *et al.* (2005). Long fractures, whose origins are difficult to determine, are labelled as Generation 1. Fractures that join only those of Generation 1 at approximately right angles are labelled Generation 2 and so on until Generation 6. Each higher generation fracture subdivides one domain into two smaller ones, which creates more surface area available for chemical weathering. Part c shows the statistical analysis of the fracture pattern. The number of sides for each domain of the fracture pattern shows clear peaks for the four sided domains, which is characteristic of hierarchical fracture patterns (Bohn *et al.*, 2005). Triple junctions were found to comprise as much as 89.0% of the total junctions in the network. The majority of the large angles at triple junctions are found at around 170 °, indicating that these are T-shaped

junctions consisting of a straight fracture intercepted by a younger fracture. The distribution of the smallest angles at the triple junctions peaks close to 90 °, indicating that new fractures meet old fractures nearly at right angles, which is expected for hierarchical fracture patterns. The distribution includes a small number of very small angles. This is not surprising because, unlike 2D drying patterns, the angles are measured in a 2D cross section through a 3D fracture network. Fractures and domains at the outer edges of the image were excluded from the statistical analysis (modified from Røyne *et al.*, 2008).

Figures 7.2a and b also demonstrate beyond any reasonable doubt that large blocks can become subdivided into smaller blocks after a period of onion skin spalling. This domain dividing process is similar to the evolution of the rectangular domain observed in the numerical experiment displayed in Figure 6.9. After a period of swelling and spalling in the outer layer of a fresh *core stone*, the internal elastic stresses become large enough to crack the entire unit into smaller subdomains that then start their own spheroidal weathering and become rounded. When this process is repeated, the resulting outcrop pattern contains a mixture of variably sized core stones caught in various stages of being rounded and broken up into smaller domains. Therefore, relatively fresh fractures that have not yet had the time to develop a visible set of onion skin spalls are commonly observed (Figs 7.2c, d). This domain dividing process has previously been referred to as twinning (Sarracino and Prasad, 1989) but it does not stop after one generation of twins have been born. It keeps generating successive generations of progressively smaller offspring.

During fieldwork, one often tends to observe what one is looking for. Occasionally, a numerical model produces features that guide observations in the field. During our work with spheroidal weathering, we noted that the numerical model shown in Figure 6.9 often produced fracturing that rounds off the corners of the initially rectangular blocks (because of shear stress in these areas). Going back to the field, we observed that this process also takes place in the natural systems. Figure 7.2f shows such a corner of an originally rectangular block. The traditional view was always that the rounding of the corners occurred by onion skin spalling, which produces wedges that are a little thicker in the corners. Such features are indeed observed (Fig. 7.2e) but in addition, we also observed that some corners contain a fresh core and thus could not have been produced by the usual spalling process. These corners had been chopped off by shear fractures generated by the swelling of the block.

The hierarchical fracturing of core stones is obviously important for the overall rate of spheroidal weathering because it keeps generating new reactive surface area in addition to that exposed by the spalling process alone. In the numerical model presented above, the hierarchical division of unfractured domains, core stones, occurs because the reaction driven expansion along the outer boundary in a 2D or 3D system generates tensile stresses *within* the block, which eventually leads to the formation of a tensile fracture that causes the subdivision. The localisation of fractures in a natural system is however sensitive to details, such as the morphology of the reacting interface. Any roughness or even

curvature change along this interface contributes to perturbations in the elastic stress field and controls the location of fracture nucleation and growth. Field observations indicate that domain dividing fractures often grow from concave areas on the surface of the otherwise convex core stones (Fig. 7.3). Today, we do not know if such concave areas are associated with instabilities arising during front propagation or if they are caused by some heterogeneity of the system. However, whatever their origin, such areas develop into wedges that help break larger core stones to smaller daughters. The role of surface roughness in fracturing is an issue we return to in the next section, on the hydration of olivine.

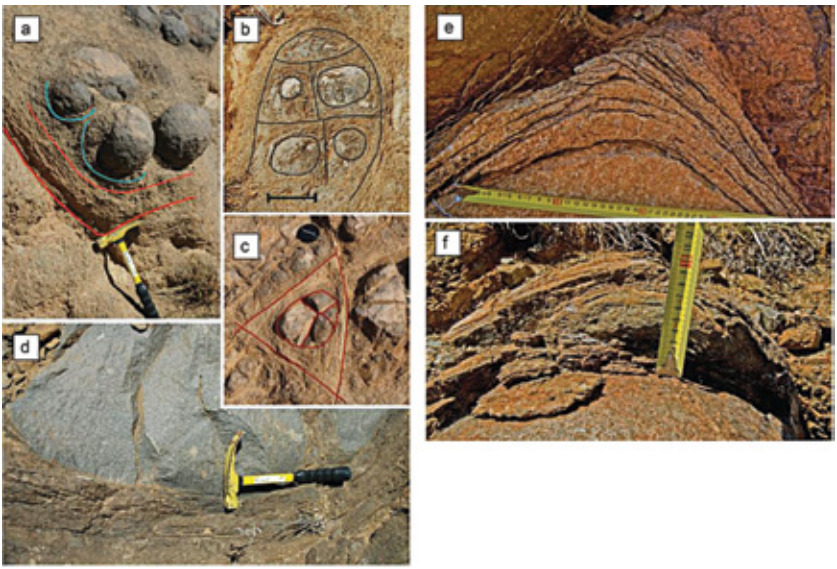

Figure 7.2 Details of the fracture patterns from the road section shown in Figure 7.1. a) A block with an initial right angled corner became progressively rounded until it fractured into four smaller pieces, which were subsequently rounded off by spheroidal weathering. The continuous spheroidal shells of the original block are marked in red. b) The core stone has been subdivided into five angular parts by fracturing. These have subsequently been rounded by a new period of spheroidal weathering. The scale bar shows 10 cm. c) and d) Fresh radial fractures through an unweathered core stone meet the spheroidal shells of the original block. If weathering had progressed further, the individual domains of the freshly fractured block would have become rounded by spheroidal weathering. e) Spalled layers are thicker in the corners, thus spalling tends to round angular corners to form subspherical shapes. f) Corner with less altered core, demonstrating that this region is chopped off by shear fractures that are different from the regular spalls (from Røyne *et al.*, 2008, with permission from Elsevier).

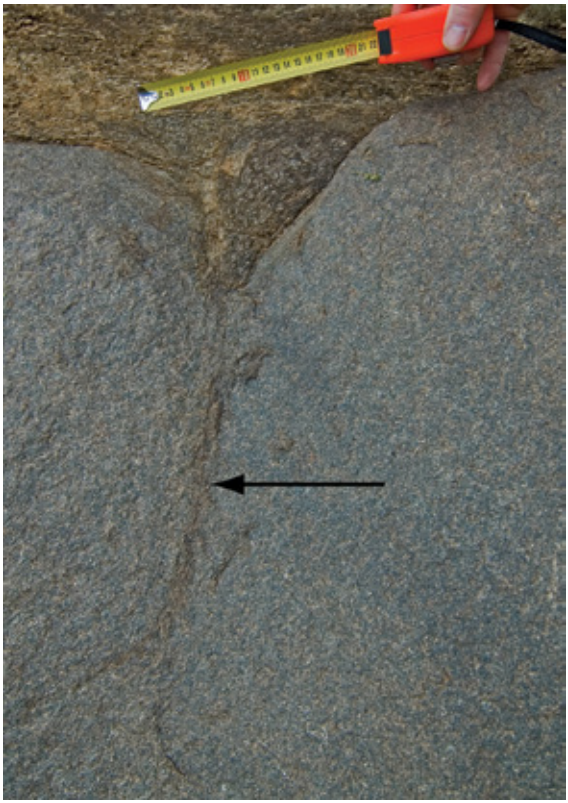

Photo: Bjørn Jamtveit.

Figure 7.3 Incipient fracturing (arrow) of a dolerite core stone, starting from the tip of a wedge shaped weathering zone.

7.2 Serpentinisation

Serpentinisation is probably *the* most important metamorphic hydration process. The reaction of olivine rich, mantle derived peridotite to form serpentinite is associated with a reduction in rock density from ~3.3 g/cm^3 to <2.7 g/cm^3. Hydration of the end member forsterite (Mg-olivine) can be described by the reaction:

$$\underset{\text{forsterite}}{2\,Mg_2SiO_4} + \underset{\text{water}}{3\,H_2O} \Leftrightarrow \underset{\text{serpentine}}{Mg_3Si_2O_5(OH)_4} + \underset{\text{brucite}}{Mg(OH)_2}. \qquad (7.1)$$

In a natural system, the Fe component of the original olivine is at least partly absorbed by a corresponding Fe component in the brucite. Production of iron furthermore contributes to the very important redox reaction that oxidises ferrous

Fe to magnetite (Fe_3O_4) while hydrogen from the water is reduced to H_2 (Peretti *et al.*, 1992; Bach *et al.*, 2006). The hydrogen generated can sustain microbial communities (Takai *et al.*, 2004).

In the presence of carbon, serpentinisation can produce CH_4, which is observed seeping from midoceanic ridges (Charlou *et al.*, 1998). Such an environment, with possible production of abiotic methane and other hydrocarbons, is regarded as the most likely location for the origin of life (Konn *et al.*, 2009; Pons *et al.*, 2011).

Complete serpentinisation in closed systems (except from the introduction of H_2O and/or CO_2) results in a solid volume increase of nearly 50% and causes a pronounced change in rheology (Escartin *et al.*, 2001; Hilairet and Reynard, 2009), seismic properties (Hacker *et al.*, 2003; Bezacier *et al.*, 2010), electrical conductivity (Stesky and Brace, 1973), magnetic properties (Oufi *et al.*, 2002) and porosity. The hydration reaction (Eq. 7.1) also produces considerable heat (≈290 kJ/kg forsterite consumed). Serpentinisation has therefore been suggested as an explanation of observed heat flow anomalies in oceanic basins (Schuiling, 1964; Delescluse and Chamot-Rooke, 2008). Finally, serpentinisation provides significant controls on geochemical subduction zone input (Kendrick *et al.*, 2011).

7.2.1 Fracture patterns

The serpentinisation rate is highest at temperatures close to 300 °C (Martin and Fyfe, 1970). At lower temperatures, slow reactions limit the overall rate, whereas at higher temperatures, the approach to equilibrium decreases the chemical affinity of the hydration reaction. The higher the reaction rate, and the associated rate of rock volume increase relative to the rate of ductile deformation, the more probable it is that serpentinisation will cause fracturing because there is insufficient time for the rock to accommodate the stress of the extra volume generated. Figure 7.4 shows fracture patterns developed in serpentinised peridotes. The characteristic length scales of the fractures vary over more than 5 orders of magnitude from a few metres to less than 10 micrometres.

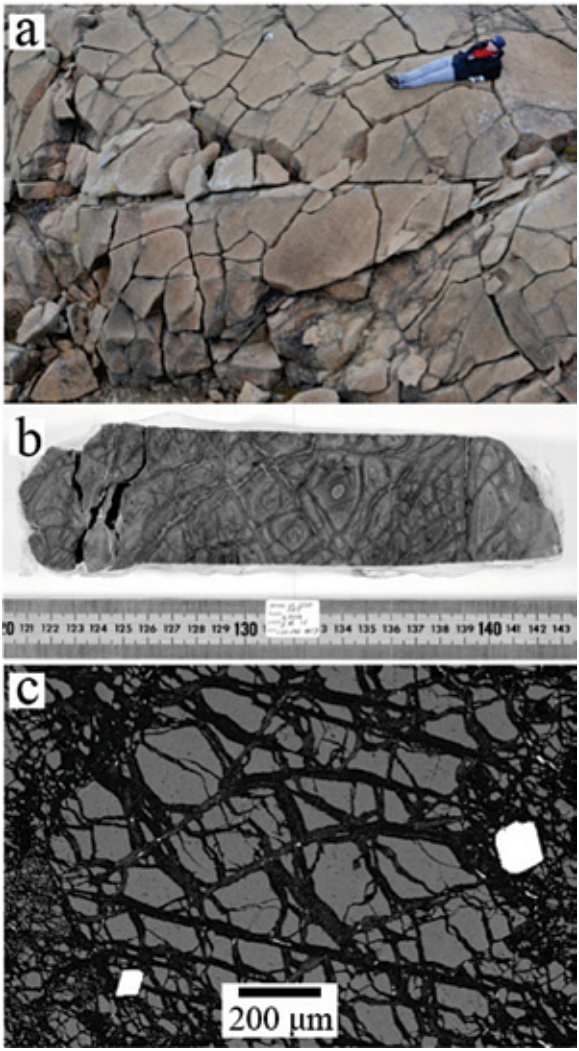

Figure 7.4 Fractures developed in serpentinisation across four orders of magnitude. a) Serpentinised peridotite from the Norwegian Caledonides at Røragen, near Røros (62°33N, 11°48′E) (from Jamtveit and Austrheim, 2010, with permission from *Elements*). b) Tortoise shell texture in a core sample of serpentinised peridotite from the Mid-Atlantic Ridge, Ocean Drilling Program Hole 670A, Sample 109-670A-5R-1 (Agrinier and Cannat, 1997). c) Photomicrograph of mesh texture in a partly serpentinised olivine crystal from the Leka ophiolite complex, Norway. Tiny white streaks and euhedral white crystals are magnetite (from Jamtveit and Austrheim, 2010, with permission from *Elements*).

Although serpentinites are subject to tectonic stresses that can drive fracturing both in the oceanic lithosphere and during their emplacement into a continental setting, there is compelling evidence that fractures over a broad range of scales can also form as a response to the volume change associated with the serpentinisation process. Reaction driven fracturing of olivine crystals during hydration to form brucite and serpentine minerals at 250 °C was recently demonstrated by Okamoto *et al.* (2011) who also demonstrates that the bulk reaction rate increases with time over the duration of the experiments (~1000 hours) and that the fracture pattern developed is similar to the hierarchical patterns described by Jamtveit *et al.* (2009).

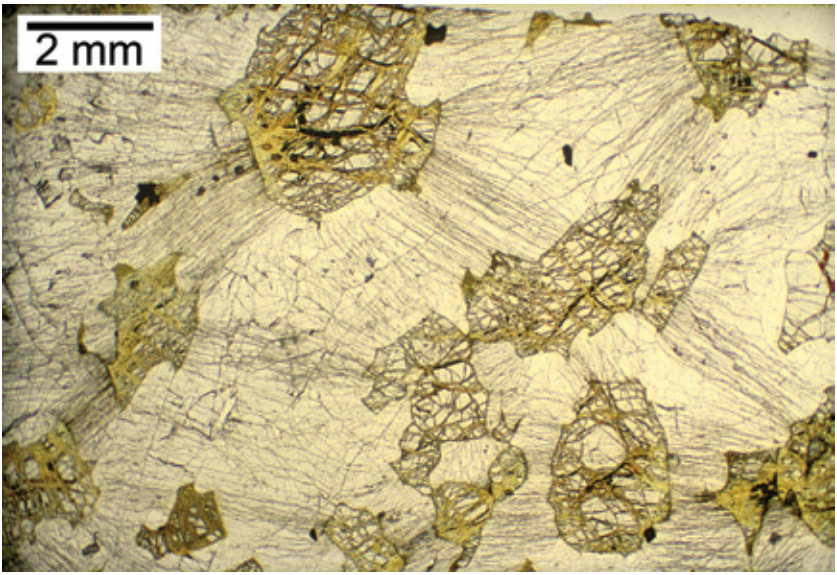

Figure 7.5 Microphotograph of *wagon-wheel* texture in a troctolite from the Duluth Igneous Complex showing partly serpentinised olivine grains in a plagioclase matrix. A dense network of microfractures connects individual olivine crystals. The microfracture network is most extensively developed where the distance between neighbouring olivines is smallest. Small olivine grains in unfractured regions are virtually unaltered (from Jamtveit *et al.*, 2008, with permission from Elsevier).

Other compelling evidence for reaction driven microfracturing during serpentinisation comes from the *wagon-wheel* textures that develop during hydration of olivine crystals in a plagioclase matrix in gabbros (Fig. 7.5). Such microstructures were described by Evans (2004) and presented by Jamtveit *et al.* (2008) as an example of reaction control on permeability production during retrograde metamorphism. Recently, Kelemen and Hirth (2012) provided a detailed mechanical model demonstrating that the formation of densely spaced microfractures

radiating out from the reacting olivine into surrounding plagioclase requires a reaction generated stress of 260-270 MPa. This strongly suggests that reaction driven fracturing is plausible even for depths approaching 10 km.

A field scale illustration of reaction generated stress during serpentinisation comes from the ophiolite complex located on the island of Leka, off the coast of Nord-Trøndelag in Norway. The northwestern part of Leka is comprised of dunites and hartzburgites, locally crosscut by a network of enstatite veins or dykes (Fig. 7.6a). These enstatite dykes range in thickness from less than a centimetre to a couple of metres and constitute only a small fraction of the overall rock volume. They are extensively cut by a fracture system that is always oriented normal to the contact between the dykes and the surrounding dunites. Iyer *et al.* (2008) interpreted these fractures as a response to the expansion of the dunite matrix during serpentinisation. Because these dykes are quasi-2D sheets slowly squeezed between expanding wall rock, they develop a regular hierarchical fracture geometry (Fig. 7.6b) similar to that observed during contraction of ceramic glazing or during drying of paint. Such patterns, dominated by T junctions and 4 sided domains, are largely controlled by the propagation of fractures, rather than by frequent nucleation of new ones, which tend to produce fracture junctions with 60 degree angles (Toga and Alaca, 2006).

7.2.2 Stress generating mechanism

Despite the general understanding that serpentinisation related expansion causes fracturing of the original olivine (O'Hanley, 1992), the actual mechanism of stress generation has not been well understood. Most conceptual ideas have been similar to the weathering model of Fletcher *et al.* (2006) with the initial step being diffusion into fresh rock, then incipient reaction within this diffusion length controlled layer and subsequent fracturing when the accumulated elastic stress is sufficient to generate new surfaces. While this mechanism can apply to polycrystalline rocks, in which diffusion takes place along grain boundaries, it is most probably not adequate for reaction induced fracturing of individual mineral grains during replacement processes. Key arguments against such a model include the exceedingly slow solid state diffusion at temperatures significantly below the melting temperature, the key role of dissolution-reprecipitation processes rather than diffusion during replacement (Chapter 5), as well as recent observation of the nanometre to micrometre scale features involved in serpentinisation and accompanied fracturing of olivine during formation of the characteristic mesh textures of partly serpentinised olivine grains (Plümper *et al.*, 2012).

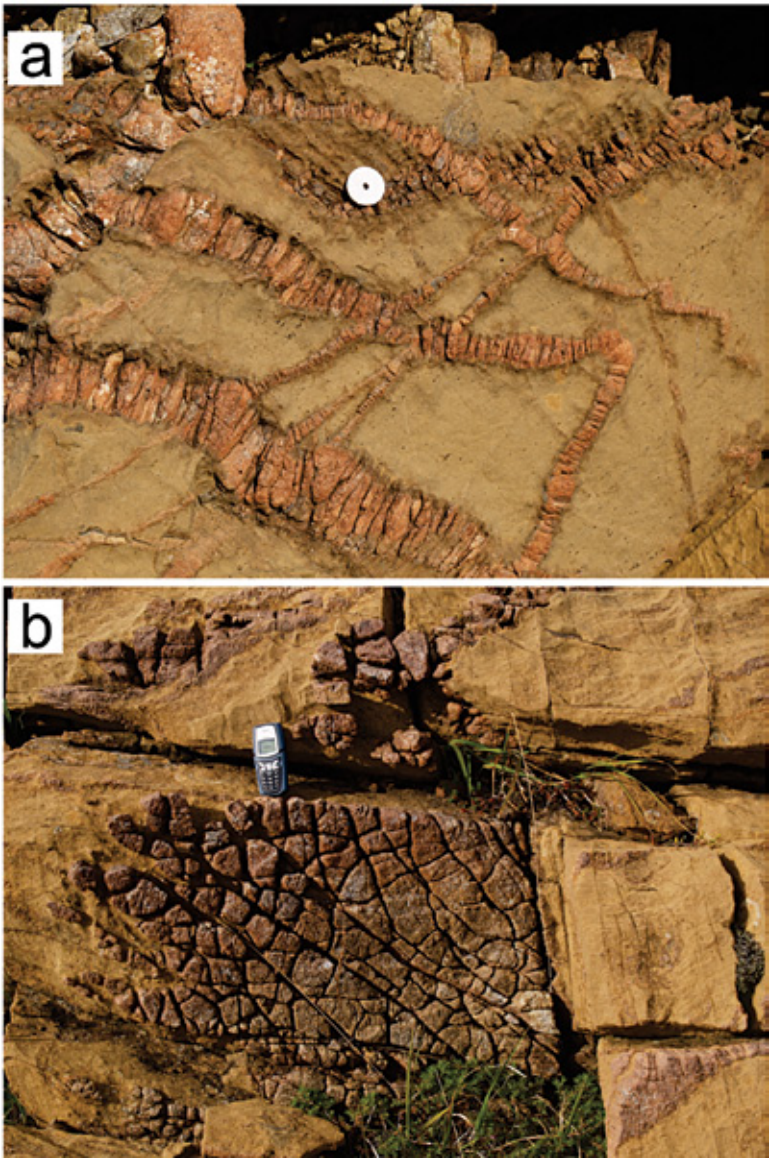

Photos by Kjell Ove Storvik, PGP.

Figure 7.6 a) Crisscrossing orthopyroxenite dykes (red) within dunite (light brown). Both the dunites and the dykes are hydrated. The dykes are extensively fractured with fractures propagating normal to the strike of the dyke. b) Plane view (cross section) of orthopyroxenite dyke (red) broken into polygonal domains.

Figure 7.7 illustrates some of the pertinent features of a partly serpentinised olivine grain. Most importantly, there is no evidence for a partly reacted outer layer of olivine. The interface between olivine and the hydrated product is always sharp, even at the nanometre scale. However, the interface is always rough, with extensive pitting during incipient olivine dissolution (Fig. 7.7a). Furthermore, the material precipitated at the product side of this interface is not crystalline serpentine but a more or less amorphous proto-serpentine layer. Such layers have been described previously by Rumori *et al*. (2004), but the implication of the growth of a low density phase at an olivine surface that develops considerable roughness by dissolution controlled pitting had not been realised. The key issue is that any irregularity at a surface subject to the growth of a low density phase, without loss of material to the outside (and thus swelling), would cause local stress concentration. Figure 7.7b clearly demonstrates that the microfractures, that subdivide the olivine grains to form the mesh texture, emanate from deep etch pits on the olivine surface. Pitting thus prepares the fracturing processes, in a way that has some similarity to the much larger scale spheroidal weathering, in which core stones tend to fracture wherever their generally convex shape is perturbed by concave surfaces (Fig. 7.3).

When fracturing starts, the permeability of the system also increases and when water gains access to fresh fracture surfaces, pits are formed by dissolution, and fracturing repeats itself to produce the observed hierarchical fracture pattern presented by the mesh texture.

7.2.3 The scolecite to tobermorite experiment

Perhaps the most convincing example of the critical role of dissolution controlled pitting on fracture formation during reaction comes from a zeolite system recently studied by Kristina Dunkel and Andrew Putnis at the University of Münster. During exposure of scolecite ($CaAl_2Si_3O_{10}{\cdot}3H_2O$) crystals to a 2 M NaOH solution at 200 °C for 3 days, tobermorite ($Ca_5Si_6O_{16}{\cdot}5H_2O$) partly replaces the scolecite (Fig. 7.8, Putnis *et al*., in prep). During replacement, tobermorite precipitates in dissolution pits formed at the scolecite surface. When these pits develop into wedge shaped cavities and reach a certain depth, they often develop fractures at their tips. These fractures expose fresh reactive surfaces where the process can repeat itself. This is very similar to the olivine to serpentine replacement described above.

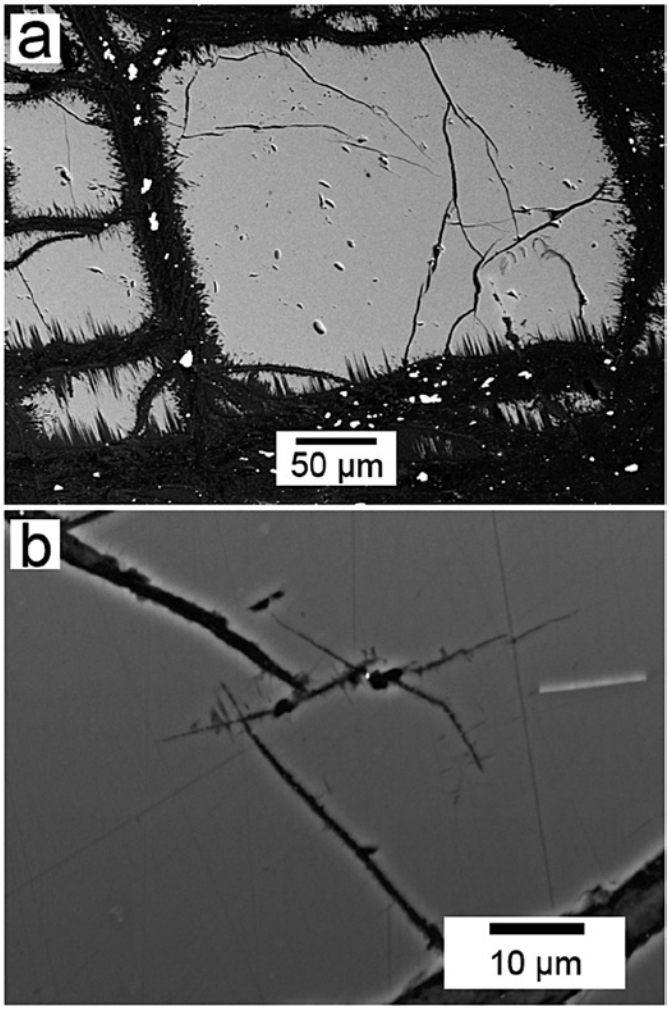

BSE images by Oliver Plümper, PGP.

Figure 7.7 Olivine crystals undergoing serpentinisation. a) Extensive pitting around the olivine periphery. Fractures subdivide the olivine to form the invariably observed mesh texture, starting at the tip of etch pits. b) A new generation of etch pits starting at fractures through olivine crystals. These then develop a new generation of fractures and the process repeats itself to form a hierarchical fracture pattern.

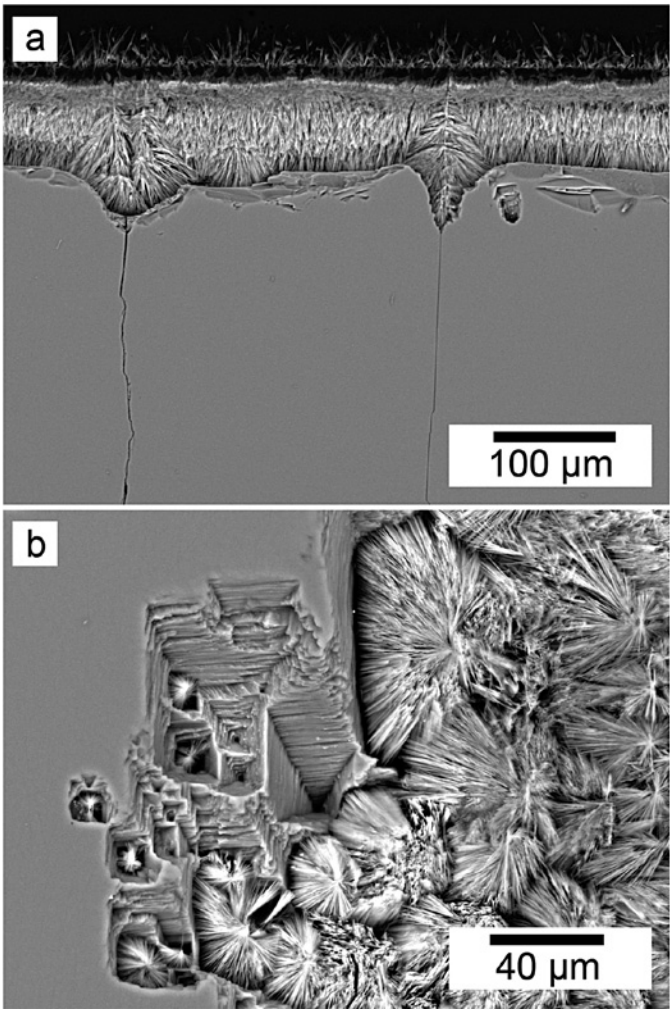

Figure 7.8 Scolecite reacting to form tobermorite. a) Fractures into scolecite emanating from dissolution controlled wedge shaped depressions on the scolecite surface. b) Radial growth of fibrous tobermorite precipitating in etch pits formed on the reacting scolecite surface.

7.2.4 Reaction progress versus time

Recently, Malvoisin *et al*. (2012) reported the first experimental results on serpentinisation of peridotite, where the reaction progress was followed in detail over time by measuring the amount of magnetite produced. Experiments ran for up to 500 days for variable initial grain sizes, allowing the reaction progress to be followed to ~80% conversion to serpentine (chrysotile). The resulting reaction progress versus time curve is shown in Figure 7.9. It can be directly compared with the reaction progress versus time curves obtained by our numerical model of reaction driven hierarchical fracturing (Fig. 6.10) and the plexiglass experiment (Fig. 5.10). Interestingly, the experiments of Malvosin *et al*. (2012) show the same sigmoidal shape predicted by our model. Fracturing of olivine grains is also observed in the serpentinisation experiments and Malvoisin *et al*. (2012) stressed the role of new surface area production by etch pit formation and fracturing. The causal connection between these two processes was proposed by Plümper *et al*. (2012; Fig. 7.7 above) and spectacularly demonstrated by the scolecite to tobermorite experiment of Dunkel and Putnis (Fig. 7.8).

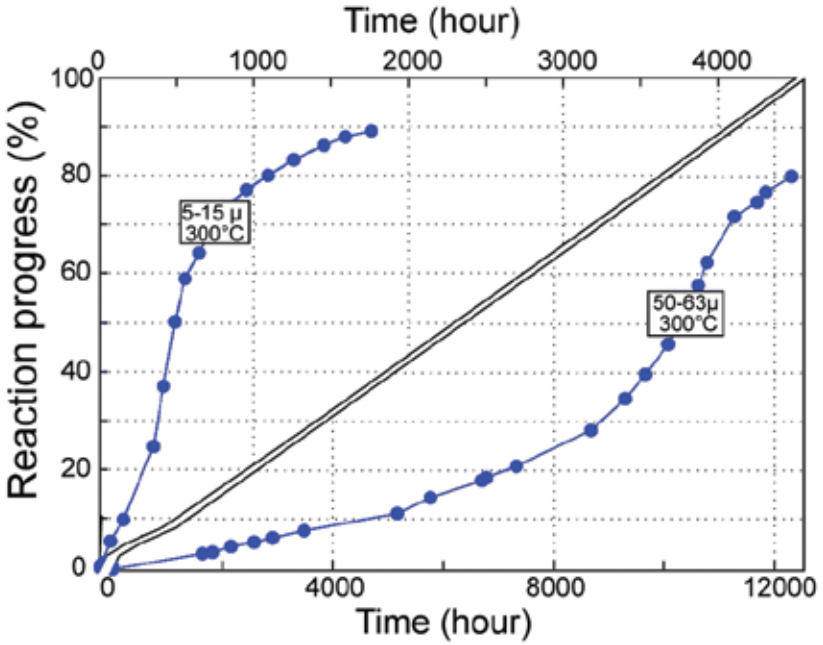

Figure 7.9 Reaction progress versus time for serpentinisation of olivine at 300 °C for two different initial grain sizes (5-15 μm and 50-63 μm). Both curves show the sigmoidal shapes characteristic of a reaction driven increase in surface area where reaction includes such processes as fracturing and dissolution generated etch pit formation (*cf*. Fig. 7.7) (modified from Malvoisin *et al*., 2012).

If you're not part of the solution, then you're part of the precipitate.
STEVE WRIGHT

8. GROWTH IN PORES

Traditional reactive transport modelling (*cf.* Section 2.2) does not couple the chemical and physical processes that influence the evolution of the pore structure during fluid-rock interactions. However, as early as 1853, J. Lavalle noticed that crystals growing from supersaturated solutions were able to push themselves upward. Later Becker and Day (1905) and Taber (1916) demonstrated that growing crystals could lift considerable weight. Correns and Steinborn (1939) subsequently provided the first quantitative expressions for crystallisation pressure as a function of supersaturation (see also the annotated translation by Flatt *et al.*, 2007).

Growing crystals can clearly perform work on their surroundings and thus also generate stresses when growing in the pores of a porous medium. This *force of crystallisation* or *crystallisation pressure* plays a major role during both frost heaving (Taber 1929; 1930; Walder and Hallet, 1985) and weathering of various man made porous materials such as concrete (Espinoze-Marzal and Scherer, 2010 and references therein). Clearly, crystallisation pressure must also be important during weathering of porous rocks and play a potentially important role during reactive transport in general.

Mechanical effects resulting from growth in pores have many similarities with weathering and serpentinisation as described in Chapter 7. However, the source of the force of crystallisation is the supersaturation of a pore filling fluid, rather than the affinity of a heterogeneous reaction that changes the rock volume. Another important difference is that replacement of essentially nonporous rocks or minerals by more stable assemblages takes place near a more or less sharp reaction front, such as the spalling front described for spheroidal weathering above, whereas reactions in porous rocks or minerals can start well inside the fracturing front, thus contributing to fracturing from within.

An important aspect of growth in pores was realised by Correns and Steiborn (1939), who postulated that for a crystal to be able to continue growing after reaching the pore wall, there must be a fluid film between the growing crystal and the wall. Otherwise, transport to the reactive surface would be shut off and growth would cease. This film must be able to sustain the normal load generated between the crystal and the wall as the crystal continues to grow, without being squeezed out. The reason why such a thin film can exist is the

presence of repulsive forces between the growing crystal and the wall in the presence of a fluid film. These include electrostatic interactions and structural forces (mainly hydration forces) in electrolytes and they are commonly referred to as a *disjoining pressure* (*e.g.* De Gennes, 1985). The disjoining pressure also plays a key role in processes such as pressure solution (Robin, 1978) and during freezing and associated frost heaving in soils (below).

The magnitude of the disjoining pressure depends on many factors, including surface charge and electrolyte concentration. For mica systems, disjoining pressures of more than 100 MPa have been measured for films only a few nanometres thick (Alcantar *et al*., 2003; Anzalone *et al*., 2006) but for other systems, there is no repulsion at all. In the halite-quartz-H_2O system, molecular dynamics simulations have recently indicated that the net force between halite and quartz is attractive (because of oppositely charged surfaces). Thus, in contrast to common assumptions, halite growth in the pores of pure quartz sandstone does not exert crystallisation pressure (Webb *et al*., 2011). Damage still occurs, however, because of significantly different thermal expansion coefficients for halite and quartz.

The critical role of the disjoining pressure implies that if chemical treatment of a building stone (for example by surfactants) can reduce the disjoining pressure, it can also decrease the stress generated by salt crystallisation in the pores and thus reduce the risk of damage by salt growth (Espinoza-Marzal and Scherer, 2010).

Provided that the disjoining pressure in a given system is sufficiently high, growth in the pore generates considerable crystallisation pressure on the pore walls. This pressure is decribed by Steiger (2005):

$$\Delta p_c = \frac{RT}{v_n} \ln \Omega - \gamma_{cl} \kappa_{cl} , \qquad (8.1)$$

where Δp_c represents the deviatoric pressure (stress) which is defined as the difference between the pressure on the advancing crystal face and the pressure of the surrounding liquid. For small pores (< 0.1 μm), curvature effects must be taken into account. In Eq. 8.1, γ_{cl} represents the crystal-liquid interfacial energy, κ_{cl}, the local curvature and v_n the molar volume. From Eq. 8.1, it is clear that there are two major factors controlling the force of crystallisation during growth in a pore: curvature effects, which are important for small pores and the local supersaturation state of the solution (Ω).

Finally, it is also important to realise that stresses generated by crystal growth in a pore will not lead to fracturing unless the stress field affects a sufficiently large region of the porous medium to communicate with the flaws that invariably dictate the strength of rocks and building materials, such as concrete (*cf.* Scherer, 1999). In rocks, these defects could be grain boundaries or pre-existing microfractures, often much larger than tens of microns. Thus, growth in very small pores does not cause fracturing individually and it only becomes

important when stress fields generated by growth in a number of pores interact to affect strength controlling flaws. However, when growth occurs in individual pores of sufficient size or shape to trigger fracture propagation, the rate of crack growth is initially slow if the load is exerted slowly by a growing crystal. As demonstrated by Røyne *et al.* (2011), during the early stages of crack formation, crack growth is subcritical (*i.e.* occurring at stresses less than the critical stress intensity factor, Atkinson, 1984) and propagate at a rate controlled by the crack tip kinetics. Subsequently, the crack can grow large enough for critical crack growth to occur and the velocity is then eventually controlled by the crystal growth kinetics. However, the transient period of subcritical crack growth can be very long for systems in which crack tip extension is fast relative to the growth rate. Many (most) natural rock systems that experience fracturing induced by growth in pores probably evolve by subcritical (slow) crack growth.

8.1 Pore size effects

For small particles, surface energy contributes a significant portion of the overall energy. Thus, during crystal growth in small pores, the solid-fluid interfacial energy affects the solubility of the solid and hence the saturation state of the pore fluid (*e.g.* Stumm and Morgan, 1996; Navrotsky *et al.*, 2008). It has also been shown experimentally by Putnis *et al.* (1995) that nucleation is suppressed in finely porous media. Small pores can therefore affect the fluid composition both at equilibrium (*i.e.* fluid-crystal equilibrium within the pore) and nonequilibrium conditions.

In porous rocks containing a significant population of pores with diameters much less that a micrometre or so, nucleation and growth within the pore space depends on factors such as pore size distribution and the spatial distribution of the pores. In general, equilibrium and nonequilibrium effects favour growth in large pores rather than in small pores. This has been observed for halite cemented sandstones (Putnis and Mauthe, 2001), for quartz cementation between stylolites in sandstone (Emmanuel *et al.*, 2010), for gas hydrate (clathrate) growth in sediments (Rempel, 2011) or during precipitation of weathering products in porous andesite (Section 8.3 and Jamtveit *et al.*, 2011).

The pore size effects in reactive transport modelling have recently been investigated by Simon Emmanuel and collaborators (Emmanuel and Berkowitz, 2007; Emmanuel and Ague, 2009; Emmanuel *et al.*, 2010) by adding provision for pore size on the mineral solubility expression. The solubility, S_d, is given by:

$$S_d = S_0 \exp\left(\frac{v_m \gamma \kappa}{RT}\right), \tag{8.2}$$

where S_0 represents the bulk solubility, v_m, the molar volume of the mineral, κ, represents the crystal curvature (the size effect) and, γ, the interfacial energy. The enhanced solubility leads to a size dependent precipitation rate, Q_d, given by:

$$Q_d = KA_d \left(\frac{s}{s_d - 1} \right)^{\beta}, \tag{8.3}$$

where K represents a kinetic rate coefficient, A_d, the area associated with pores of size d, S, the ion activity product and β, the rate order. This rate expression applies to porous systems near equilibrium (Lasaga, 1998). Emmanuel *et al*. (2010) concluded that during quartz precipitation in sandstone, significant pore size effects can be observed for pore widths up to 10 μm. This is surprising because the solubility effects for 10 μm sized pores is <<1% for surface energies on the order of 0.1-1 J/m^2 (Stumm and Morgan, 1996). However, it is consistent with observations for natural sandstones.

Nonequilibrium effects have so far not been considered, although slow nucleation in small pores might well be important, especially in low temperature systems and in systems in which the supersaturation rises quickly, such as when rocks and fluids are brought into contact by a rapid geological process, such as magma emplacement, a fracturing event, seismic activity etc. A possible example of this is presented in Section 8.3. However, we first examine a few other aspects of growth in open porous systems focusing on the growth of ice in soils and rocks.

8.2 The ice analogue

The role of pore scale growth processes in controlling large scale pattern formation in reactive fluid-rock systems is still poorly understood. However, considerable advances have been made in understanding the closely related problem of freezing in porous materials.

Soil heave resulting from freezing is a well known phenomenon that produces a variety of fascinating patterns in periglacial landscapes, including stone circles, polygons, and labyrinths (Williams and Smith, 1991; Kessler and Werner, 2003). Frost cracking of rocks is a closely related process. These processes are conceptually analogous, as has already been recognised by Taber (1950). Everett (1961) noted that most Earth scientists assume that both processes are driven by the volumetric expansion associated with water freezing, even though Taber demonstrated that this notion was false 30 years before Everett's paper (Taber, 1929 and 1930).

There are many ways to show that the classical volume expansion concept is wrong. The most unambiguous way is simply to observe how much ice actually forms in many examples of freezing in a porous medium. Figure 8.1 shows a striking example of large scale pattern formation by subsurface growth of ice lenses that are several metres thick. Clearly, the formation of such structures requires the transport of water toward the location of ice formation (Fukoda, 1983). The mere 9% volume increase during freezing of pore water to ice is insufficient to explain such structures.

Migration of water toward the freezing regions requires the presence of liquid water at subfreezing temperatures, including a continuous fluid film between the growing ice and the matrix material (the source of water). Water migrates down a chemical potential gradient from the source to the growing ice body and a significant disjoining pressure between the ice and the substrate is required to prevent the water film from being forced out of the gap between the ice and the surrounding solids (Gilpin, 1979). Gilpin (1980) equated the disjoining pressure with the heaving pressure developed in slowly freezing soils, which has been experimentally shown to exceed 20 MPa. This is large enough to cause crack propagation in most rocks near the Earth's surface. Based on the conceptual ideas of Taber, Everett, Gilpin and others, Walder and Hallet (1985) presented the first theoretical model that relates frost damage in rocks to fracture mechanics, material parameters, environmental conditions (in particular temperature) and time.

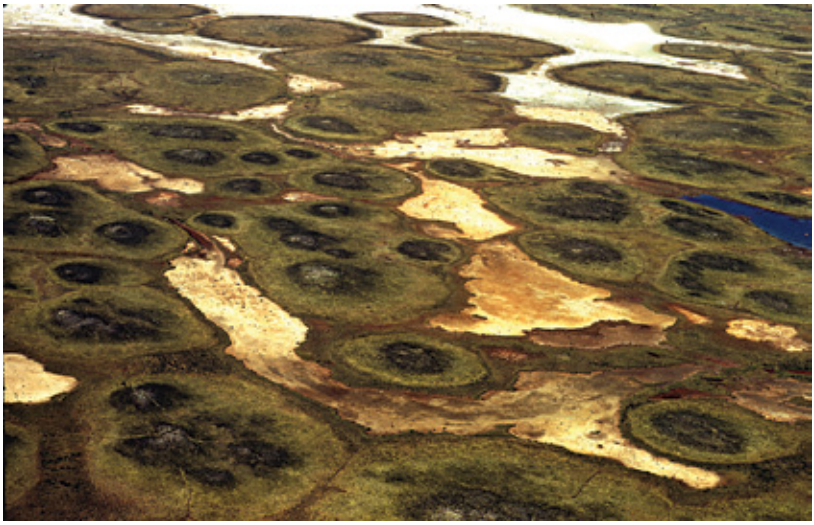

Photo courtesy: William W. Shilts, Prairie Research Institute, Illinois.

Figure 8.1 Aerial view from about 300 m altitude of low, pingo, or palsa like features near the mouth of the Maguse River, Nunavut, Canada. These 4-8 metre diameter, 1-2 metre high mounds are surrounded by seasonally flooded, vegetation free, stony mud and the mounds themselves are composed largely of medium grained sand, which is vegetated by grasses and caribou moss (*Cladonia rangiferina* – a lichen). The mounds are thought to be uplifted by the formation of ice lenses just below the surface. The features are typically decorated by prominent cracks radiating from their centres as a result of expansion of the sediment surface caused by the doming.

Recently, there has been considerable progress in understanding the dynamics of freezing in porous systems, most notably by John Wettlaufer and collaborators at Yale University. The basic mechanisms of premelting (the presence of a liquid film in the solid region of a normal phase diagram) are now

well understood (*cf.* Dash *et al.*, 1995) and so are the forces (sometimes referred to as *cryosuction*) that cause fluid transport through a liquid film to the sites of freezing (Rempel *et al.*, 2004). A key conclusion is that the migration of water through the water film is driven by the same forces that give rise to these films, the repulsive forces between the ice and the solid matrix. The thin film of water still has the properties of a Newtonian fluid (Raviv and Klein, 2002), with an effective viscosity that is not very much larger than the viscosity of bulk water. Thus the transport of water to the sites of freezing can be treated using classical hydrodynamics.

This has the interesting implication that, for a system with sufficiently high disjoining pressures, *growth in pores is not likely to reduce the permeability to negligible values*. Even if the growth does not cause an increase in porosity and permeability because of fracturing, a continuous fluid film could exist between crystals and pore walls. Moreover, this film can have the properties of a bulk fluid causing it to flow under the influence of a pressure gradient.

Several aspects of freezing in porous materials have implications for other solid growth processes in pores. First, systems with a population of small pores experience local transport from the smaller to the larger pores where nucleation and growth takes place at lower supersaturations and this keeps the force of freezing high in the large pores. Second, in an open system, growth in pores generates a force (a chemical potential gradient) that sucks material toward the site of crystallisation on a scale much larger than a few grain diameters.

The first effect is important during salt damage in building materials. Scherer (2004) demonstrated that the maximum pressure generated during pore growth occurs when large crystals grow in large pores with small pore throats. Therefore porous materials that contain pores much less than a micrometre or so in diameter as well as a significant density of larger pores are particularly susceptible to damage by salt growth in the larger pores because the smaller pores provide material to keep supersaturation high in the large pores.

Recently, the same principles have also been used to explain the distribution of gas hydrates in layered sediments. Rempel (2011) presented a model to explain how hydrates accumulate in coarse grained layers, immediately adjacent to hydrate free, fine grained regions with slightly elevated solubility. In a process analogous to the growth of ice lenses, hydrate growth can unload sediment contacts and hydrate nodules and lenses can form. Such features affect the mechanical stability of the sedimentary matrix in which they form.

8.3 Weathering of a porous andesite

In this section, we describe a spectacular example of spheroidal weathering where growth of weathering products in large pores is a key ingredient. It includes a number of emergent patterns, including Liesegang banding, onion skin spallation and hierarchical fracturing. Moreover, this example of spheroidal weathering is

different from the situation commonly described in the literature (*e.g.* Fletcher *et al.*, 2006; Røyne *et al.*, 2008), in which spalling occurs at the outer margins of essentially unweathered impermeable core stones. In this case, weathering products are found throughout *porous* andesitic core stones, and the stresses driving the onion skin fracturing are more adequately described as a consequence of growth within the pores of an open system, rather than the positive volume change associated with heterogeneous weathering reactions taking place at the rims of unaltered andesite.

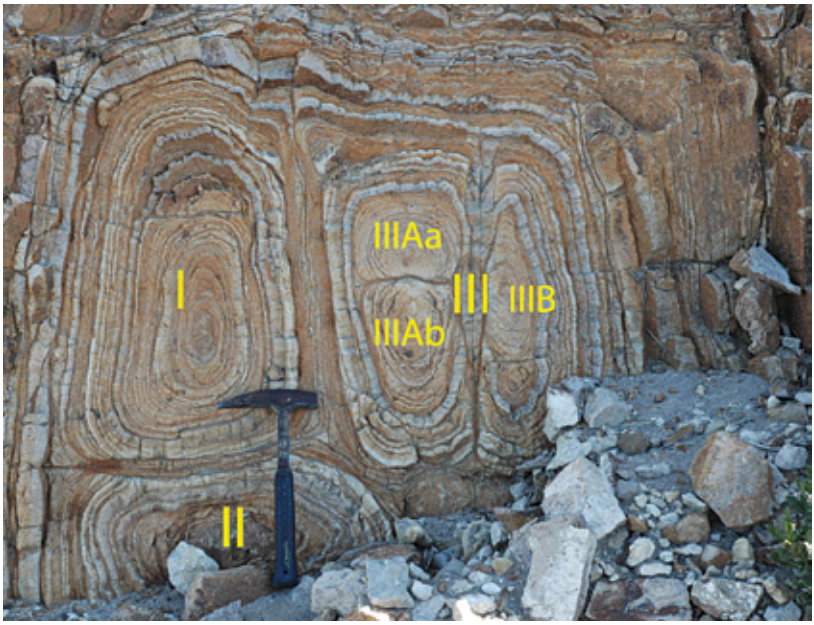

Photo: Bjørn Jamtveit.

Figure 8.2 Andesitic core stone subdivided into smaller domains (I–III) by internal fracturing (details presented in the text). Domain III is further subdivided into IIIA and IIIB, before IIIA split into *twins* IIIAa and IIIAb. The brown coloured striation is a combination of Liesegang bands and onion skin fractures (slightly modified from Jamtveit *et al.*, 2011).

Figure 8.2 shows a block of andesite, originally cut out by perpendicular joints probably formed during thermal contraction of the andesitic sill intrusion of which the block is a part. Porosimetry measurements and X-ray microtomography (μCT) demonstrate that the fresh andesite (not visible in this photo) has a porosity of ~8%. Most of this porosity is represented by pores <10 μm, but 10-20% consists of pores in the 10-300 μm range. The porosity is characterised by a high frequency of narrow pore throats, with a maximum frequency ~20 nm and a maximum value ~200 nm (Fig. 8.3; more details presented in Jamtveit *et al.*, 2011).

With a significant population of large pores surrounded by very narrow pore throats, this rock is expected to be vulnerable to damage caused by growth in the large pores, where the supersaturation is sustained by the large population of small pores with elevated solubility of the weathering products (*cf.* Scherer, 2004).

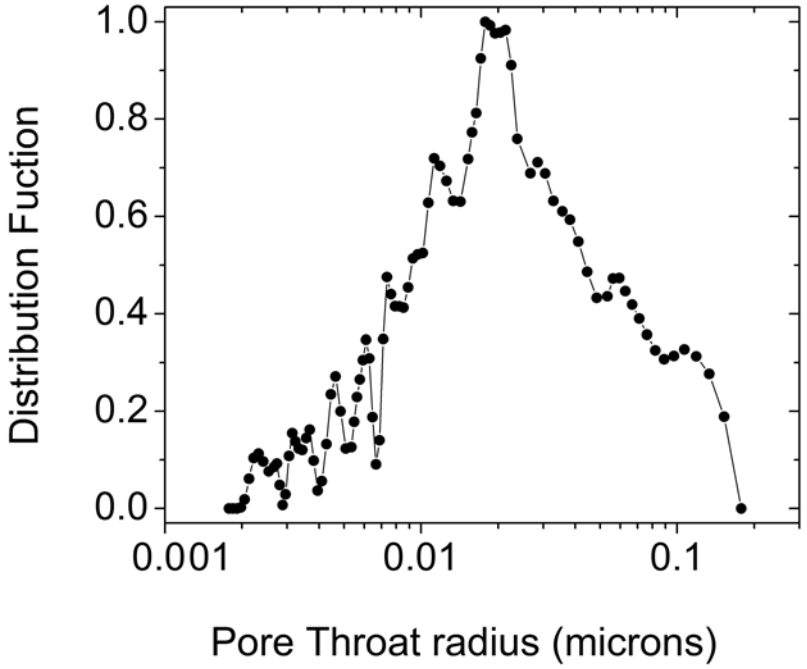

Figure 8.3 Distribution of pore throat radii for the fresh andesites obtained by Hg-porosimetry (modified from Jamtveit *et al.*, 2011).

With exposure to external fluids, the andesite starts to weather and the patterns seen in Figure 8.2 develop. Weathering is associated with the introduction of carbon bearing, oxidising fluids, which drive hydrolysis of the original magmatic plagioclase, amphibole and ilmenite and cause growth of ferrihydrite and carbonate minerals in the pores of the andesite through coupled reactions such as:

$$\text{(i) } Ca_2Fe_5Si_8O_{22}(OH)_2 \text{ (actinolite)} + 14H^+ \Leftrightarrow 2Ca^{2+} + 5Fe^{2+} + 8SiO_2 \text{ (quartz)} + 8H_2O \quad (8.4)$$

$$\text{(ii) } Ca^{2+} + HCO_3^- \Leftrightarrow CaCO_3 \text{ (calcite)} + H^+ \quad (8.5)$$

$$\text{(iii) } 2Fe^{2+} + 1/2O_2 + (3+n)\ H_2O \Leftrightarrow 2FeOOH \cdot nH_2O \text{ (ferrihydrite)} + 4H^+, \quad (8.6)$$

where n is a stoichiometric coefficient accounting for the variable water content in the ferrihydrite. In this case, actinolite is representative of any magmatic mineral consuming protons during hydrolysis. The weathering of ilmenite and plagioclase would, in a similar way, consume protons and produce Ca and Fe ions. Quartz is a weathering product commonly observed in pores along with carbonate and ferrihydrite. The formation of the weathering products (calcite and ferrihydrite) is favoured by the proton consumption and the production of cations (Ca^{2+} and Fe^{2+}) during hydrolysis of the original magmatic minerals. At the same time, proton production during the formation of the weathering products provides a positive feedback to the hydrolysis of the magmatic minerals.

Thus, weathering is an autocatalytic reaction, albeit dependent on an external supply of carbonate ions and oxygen. Once started, the progress of this reaction can only be halted by precipitation in the pore space to either decrease the reactive surface area or to limit the access of externally derived components by clogging the connected pore structure.

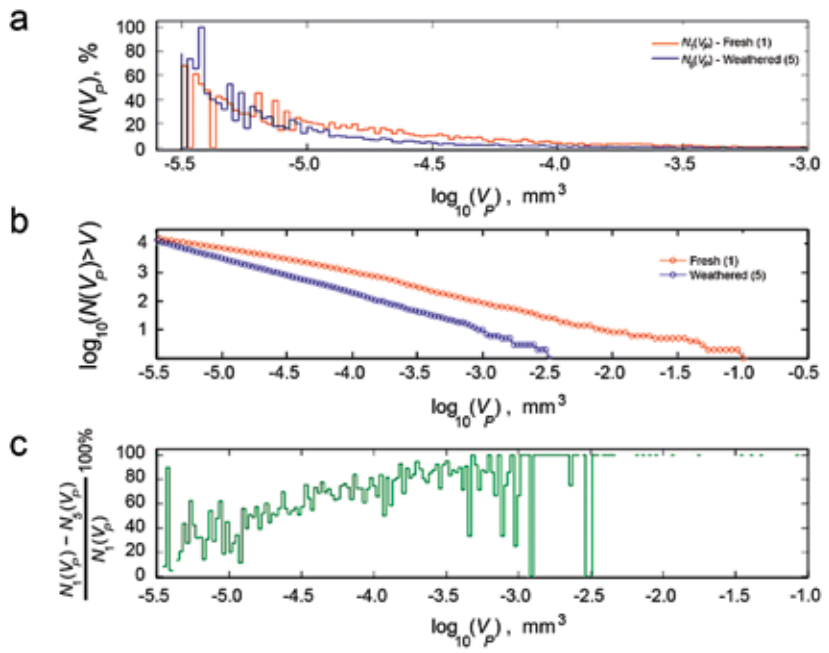

Figure 8.4 a) Pore size distribution; number of pores, $N(V_p)$, as a function of pore size, Vp, for pore size intervals of 0.0226 mm^3 for the fresh and weathered andesite, normalised to the values for the interval with the largest number of pores. b) Cumulative distribution of pore size for the fresh and weathered andesites. c) Degree of pore filling (in %) as a function of pore size. Pore dimensions were obtained from µCT scans (Jamtveit *et al.*, 2011 for details).

Interestingly, the precipitation of weathering products is concentrated in Liesegang bands oriented parallel to the margin of the core stones with a characteristic spacing of 2-5 mm. The current models for the origin of Liesegang banding invoke either a supersaturation-nucleation-depletion process (Ostwald, 1897; Smith, 1984) or a postnucleation, surface tension mediated, competitive, particle growth mechanism (Sultan and Ortoleva, 1993). In this study, supersaturation arises because of the counter diffusion of ions that can form a precipitate, with an external source of carbon and oxygen and internal production of cations (Ca, Fe, Mg). We observe that Liesegang bands are invariably oriented parallel to the macroscopic fractures. It is difficult to see how these features could be explained by a postnucleation redistribution of mass driven by surface tension. Thus, we argue that the observed banding is generated by a supersaturation-nucleation-depletion process. An important implication is that growth in the pores can occur far from equilibrium, from highly supersaturated solutions *whenever nucleation commences*. If this is the case, nucleation can also influence the location of precipitation and because the probability of nucleation scales with the square or cube of the pore size (depending on whether nucleation takes place on the pore surface or in the bulk of the pore), nucleation control also tends to favour precipitation in the largest pores.

Indeed, μCT images show that the large pores (>100 μm) of the andesite become filled by weathering products, while smaller pores (<10 μm) remain open (Fig. 8.4). However, the total porosity (measured by He and Hg injection) remains high. This is because growth in the large pores drives dilation of grain boundaries to form a network of microfractures (Fig. 8.5). Only when stresses are generated in pores that are large enough to affect the strength limiting flaws does growth lead to fracturing (Scherer, 1999). Therefore pores that are located at or near grain boundaries, which represent such flaws, are more prone to cause damage than pores located within the individual mineral grains.

However, microfracturing driven by growth of weathering products is evidently not able to relieve all the stress developed in the core stones. After the formation of 5-10 Liesegang bands, the layer, often referred to as a rindlet, that contains these bands spalls off the core stone and the process is repeated to form the characteristic set of onion skin fractures. Thus, two sets of pattern forming processes operate hand in hand: periodic precipitation of Liesegang bands and periodic spalling of weathered rindlets. Both are driven by the presence of highly supersaturated fluids in the large pores.

This is not the end of the story, however. The volume changes associated with spheroidal weathering also add stress to the central core stone (*cf.* Section 7.1). This applies whether expansion only occurs at the margin of nonporous core stones or also within porous core stones. This stress then ultimately subdivides the core stones into smaller and smaller blocks by hierarchical fracturing producing its own characteristic pattern. It is the combination of these three pattern forming processes that creates the spectacular pattern shown in Figure 8.2.

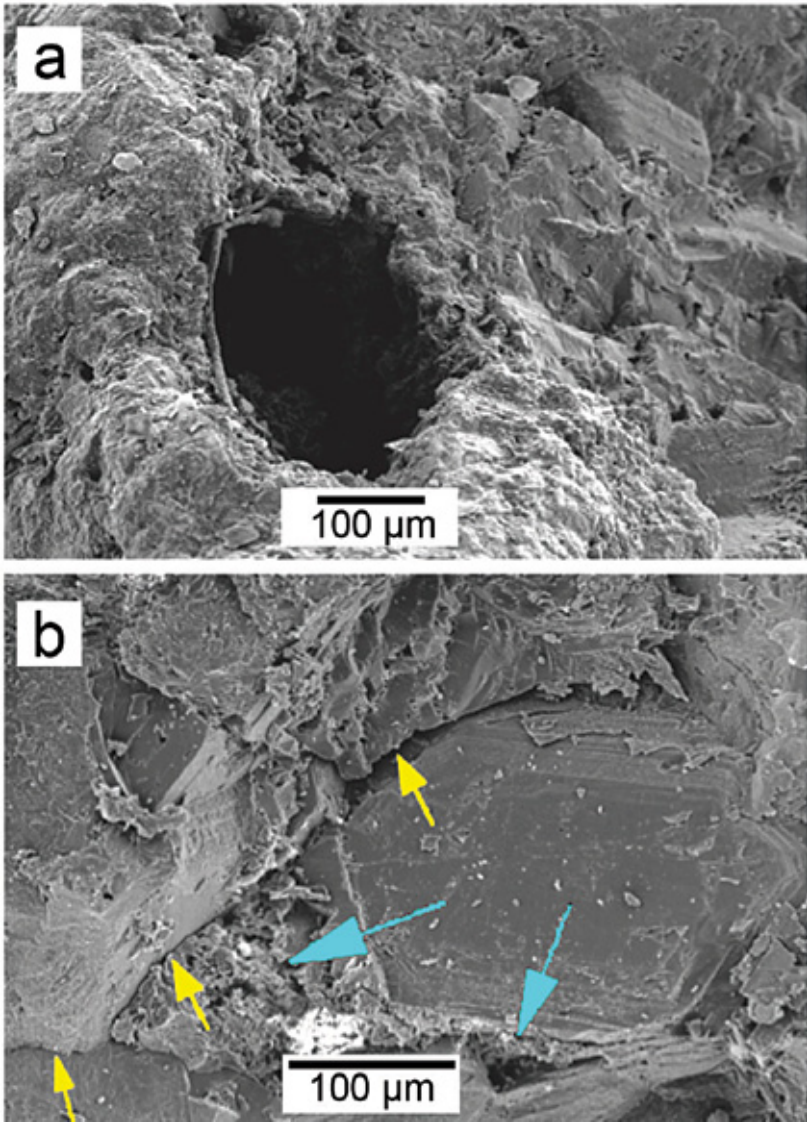

SEM-images: Bjørn Jamtveit.

Figure 8.5 Secondary electron image of the surface of a) fresh and b) weathered andesites. Note the large subspherical pore in *a*. The blue arrows in *b* indicate inferred preexisting pores that are now filled with a fine grained mixture of ferrihydrite and calcite. Yellow arrows indicate microfractures inferred to have formed during growth in the preexisting pores.

9. IN SITU MINERAL CARBONATION OF ULTRAMAFIC ROCKS

Interaction between carbon bearing fluids and silicate minerals in mafic and ultramafic rocks during weathering or low grade metamorphism generally leads to the formation of carbonate minerals. The total consumption of carbon by silicate weathering alone has been estimated to be ~150 Mt/year (Gaillardet *et al.*, 1999; Hartmann *et al.*, 2009), while carbonation of basaltic lavas on the sea floor accounts for ~10 Mt/year (Alt and Teagle, 1999). By comparison, the current anthropogenic carbon emission is about 10 Gt/year.

Natural mineral carbonation is thus a significant component in the global carbon cycle and one might ask if it would be possible to artificially increase this rate to counteract the increasing CO_2 content of the atmosphere resulting from anthropogenic CO_2 emissions. A critical factor is then the rate of interaction between carbon bearing fluids and common rock types. Several authors have pointed out that the mineral that reacts fastest with CO_2 bearing fluids is olivine (Kelemen *et al.*, 2011 with references therein). Olivine rich rocks (peridotite) are common on the sea floor, particularly in association with ultraslow spreading ridges, and Kelemen *et al.* (2011) estimated that the formation of carbonate from peridotites in such settings accounts for the consumption of about 1 Mt of C per year. This is a modest amount on a global scale but given the high reactivity of such rocks and the large volumes of peridotites that have been exposed by tectonic processes around the world, it is still conceivable that such rocks might become important storage sites for carbon (Kelemen and Matter, 2008).

9.1 The Oman example

The largest scale example of peridotite carbonation to be seen on land is the Semail Ohphiolite in Oman, recently described in a series of papers by Peter Kelemen, Jürg Matter and collaborators (Kelemen and Matter, 2008; Matter and Kelemen, 2009; Kelemen *et al.*, 2011). The Semail ophiolite contains magnesite and quartz rocks (listwanite) formed at temperatures that could have reached 200 °C, as well as carbonate veins and surface travertines that are the result of low T (30-60 °C) carbonation processes that have been ongoing for at least the last 50,000 years (Kelemen and Matter, 2008). Kelemen *et al.* (2011) estimated that an average of ~$5x10^4$ tons of carbonate minerals form per year in Oman.

The listwanites comprise extensive outcrops in Oman and appear as breccias, with hierarchical fracture networks that extend to microscopic scales (Fig. 9.1). Kelemen *et al.* (2011) concluded that carbonate growth and fracturing are coeval processes. A network of veins consisting of a cross cutting set of calcite filled fracture apertures, often associated with travertines (*cf.* Section 4.3), is a surface expression of carbonate precipitation (Fig. 9.2). These fractures are interpreted to form by spalling and buckling, in a nearly isotropic stress regime

generated by the subsurface growth of carbonate, *i.e.* by a mechanism analogous to spheroidal weathering (Section 7.1). Carbonate growth is a result of the interaction between alkaline fluids, initially formed by low T interactions between surface waters and peridotites (*cf.* Barnes *et al.*, 1967) and atmospheric CO_2 or ground waters that contain CO_2 derived from the atmosphere.

Interestingly, the travertine terraces developed in Oman (as well as in many other localities where alkaline fluids associated with serpentinisation of peridotites at depth emerge at the surface) are formed by calcite precipitation associated with CO_2 *uptake* from the atmosphere. These are morphologically very similar to travertines formed by hot springs, where carbonate precipitation is driven by a pH increase as CO_2 is *released* to the atmosphere. Thus again, similar patterns form as a result of different chemical pathways.

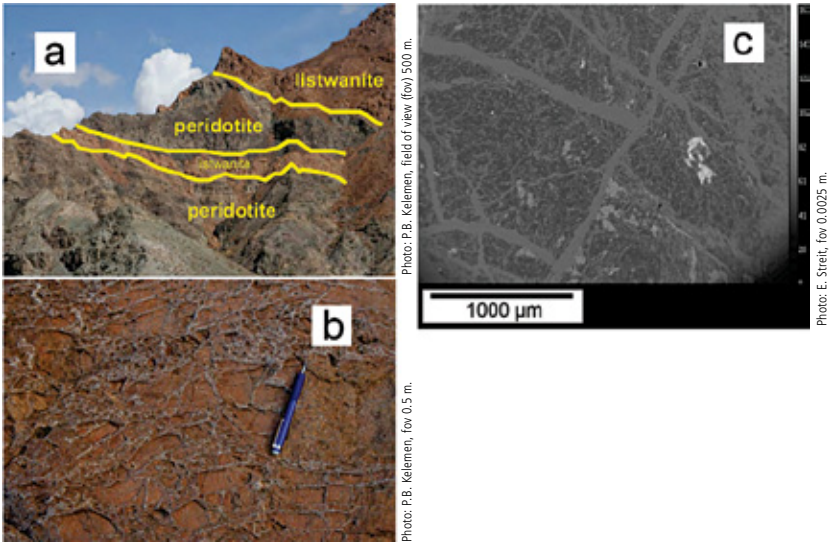

Figure 9.1 Outcrop and thin section scale photographs of listwanites replacing peridotite in the ophiolite massif of northern Oman (modified from Kelemen *et al.*, 2011). *a*) The gently eastward dipping listwanite band is 10 m in true thickness, approximately parallel to banding in partially serpentinised peridotite and an overlying, thicker band of listwanite along a ridge in Oman at approximately 23.37 °N, 58.19 °E. *b*) Typical quartz vein texture in listwanite talus block in the same location. *c*) Backscattered electron (BSE) image of listwanite from the same location. Dark gray indicates magnesite, light gray indicates quartz and white indicates relict chromium spinel.

Photo: Bjørn Jamtveit.

Figure 9.2 Peter Kelemen (centre) and Jürg Matter (upper left) in front of cross cutting carbonate veins within the Semail ophiolite in Oman during the January 2011 Carbon Capture and Sequestration Workshop.

9.1.1 Implications for large scale CO_2 sequestration

The observed fracture networks, that form during listwanite formation and near surface carbonate veining, clearly have implications for the extent of carbonation of these rocks. Without fracturing in concert with carbonation, the solid volume increase and pore filling processes associated with these reactions would decrease flow rates and thus the rate of carbon sequestration. As argued by Kelemen *et al.* (2011), there is every reason to believe that carbonate growth in partly serpentinised peridotites near the surface in Oman would be able to drive fracturing

by a mechanism similar to the serpentinisation driven fracturing first proposed by MacDonald and Fyfe (1985) and confirmed by many subsequent studies, including the recent experiments of Malvoisin *et al*. (2012).

However, in a setting such as the Semail ophiolite in Oman, where surface directed flow is driven by a high evaporation rate, it is likely that the rate of fluid flow, and hence shallow level carbonation, might not be entirely controlled by the permeability of the rocks through which the fluids involved pass. With a high evaporation rate, it is likely that rocks with large initial porosity and permeability become desaturated near the surface. In this case, the fluid flux is controlled by the rate at which water can move along pore walls in the desaturated zone (*cf.* Richards, 1931). For even higher evaporation rates, the connected liquid water network becomes disconnected and fluid transport becomes extremely slow and controlled by transport through the vapour phase. In contrast, fine grained rocks with small pores and narrow pore throats (which in a saturated system would be far less permeable than a rock with high permeability) might, under similar conditions, be able to retain a connected liquid water film because the high curvature of the pores would reduce the equilibrium water pressure to match the far field vapour pressure. For such rocks, the fluid flux toward the surface would be controlled by the permeability of the water *saturated* rock and potentially be much higher than the flux in a coarse grained and porous, but *desaturated*, rock. More than 80 years ago, Taber (1929; 1930) noted that ice growth was more extensive in fine grained materials, such as clays, than in coarser grained sands with a higher permeability. In some sense, the mechanism of near surface fluid migration through low permability rocks in regions of high evaporation rate has striking similarities to water migration during freezing in periglacial regions. In both cases water flows along potential gradients through thin films or small pores in contact with ice or water vapour, which is not at equilibrium with bulk water under the same temperature and pressure conditions, because of the disjoining pressure/capillary effects.

The possible implications for carbonate precipitation in Oman is thus that even if the porosity is significantly reduced because of precipitation in the pores of the partly serpentinised peridotites, this can actually help to maintain a significant surface directed fluid flux rather than shutting it off. If carbonate mineral formation is not limited by a reduction in porosity and permeability, it will be limited by reaction kinetics. Based on current kinetic data, and the simple reactive transport model of Rudge *et al*. (2010) which does account for mechanical effects, Kelemen *et al*. (2011) suggested that by increasing the temperature of carbonation to about 185 °C, elevating the CO_2 concentration in the reacting fluids from that in equilibrium with the partial pressure in the atmosphere (0.00004 bar) to that in equilibrium with 150 bar in seawater, and by inducing a fracture porosity of 1%, a reaction driven fracturing front should be able to propagate into peridotite at a rate approaching 1 metre per day. Although many would regard such rates as utopian fantasy, this raises the possibility of sequestering carbon in peridote at rates that are sufficient for long term geological storage of a significant fraction of the anthropogenic production. It should also be stressed that the heat

required to keep the temperature up during the reaction would be derived from the exothermic carbonation reaction itself once the temperature of a sufficient volume of rock has been raised to about 185 °C to increase the reaction rate and prevent rapid heat loss.

9.2 Serpentinite carbonation at Linnajavri

Despite the high reaction rates obtainable during carbonation of fresh peridodite, a solid volume change of 44% during complete carbonation would still be an obstacle to *in situ* storage of Mt to Gt of carbon as carbonate minerals. Simple 1D models, such as the one presented by Rudge *et al.* (2010), or 2D models such as the one described by Röyne *et al.* (2008), probably do not describe the consequences of swelling at these scales in an adequate way. Storage of 1 GT of CO_2 *per year* (approximately the amount of CO_2 produced by one hundred 1 GW coal fired power plants) would produce an excess volume on the order of 1 km^3 or the volume ejected by a large volcanic eruption (the volume ejected during the May 1980 Mt. St. Helens eruption was ~3 km^3). It is also about one order of magnitude larger than the annual growth of some of the largest mine tailings accumulations in the world, such as the Grasberg mine in Indonesia (the largest gold and third largest copper mine in the world) and it roughly corresponds to the size of the largest open pit mine in Australia, the Kalgoorlie superpit.

It therefore seems reasonable to look for alternatives to olivine rich rocks. The most obvious candidate is serpentinised peridotite, because the carbonation of serpentinite would produce a far smaller excess volume. However, the challenge with serpentinite is that it reacts with CO_2 at a rate that is orders of magnitude slower than olivine under relevant temperature conditions (Gerdemann *et al.*, 2007).

In natural systems however, there are excellent examples of carbonation of serpentinite. Perhaps the most spectacular locality in Scandinavia is the Linnajavri deposit in northern Norway. At Linnajavri, more than 13 Mt of CO_2 has been consumed in the conversion of completely serpentinised peridotite to soapstone comprised mainly of talc and magnesite and locally also to the completely carbonated listwanite (Beinlich *et al.*, 2012). Soapstone formation occurs almost isovolumetrically, preserving the sometimes spectacular structures seen in the serpentinites (Fig. 9.3). Stable isotope data suggest carbonation at around 250 °C, and mass balance calculations indicate a volume change of only about 3% during conversion of serpentinite to soapstone.

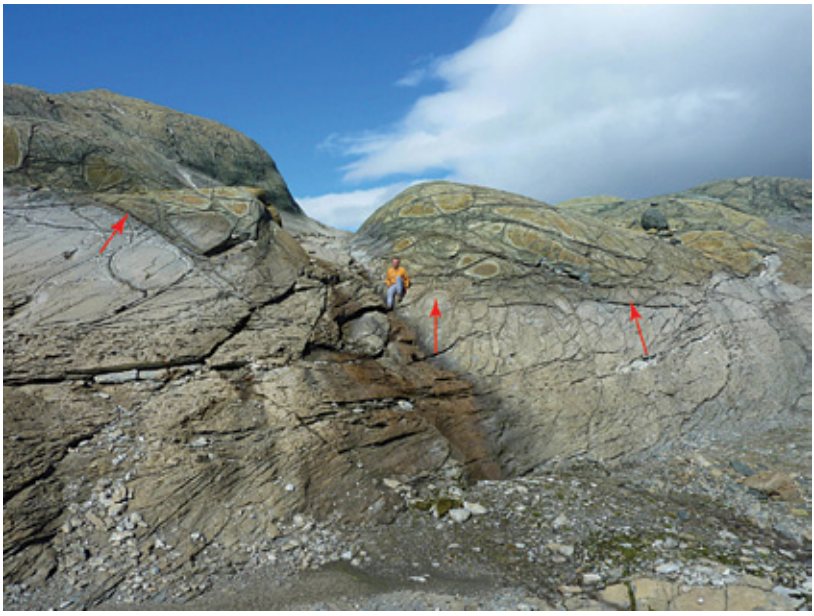

Photo: Oliver Plümper, PGP.

Figure 9.3 Carbonation of serpentinite (top) to form soapstone (bottom) at Linnajavri, Northern Norway. Arrows show approximate position of the front. The structures and extensive fracture network present in the serpentinite are well preserved during the transition to soapstone in a nearly volume for volume replacement process. More details can be found in Beinlich *et al.* (2012).

Another attractive feature of the soapstone formation, which would also be true if the soapstone formed directly from peridotite rather than from serpentinte as in this case, is that the carbon would be sequestered as magnesite rather than calcite. Carbonation would thus be independent of an external supply of Ca, which is usually present in only small amounts in peridotites (depending on the amount of clinopyroxene in the original mantle derived rock). However, a less attractive feature of magnesite formation is its notoriously slow reaction kinetics at ambient temperatures. In a recent paper, Saldi *et al.* (2012) showed that the rate of magnesite formation at the expense of forsterite at temperatures between 100 and 200 °C is probably controlled by the slow rate of magnesite precipitation and not by forsterite dissolution, as is often assumed. In fact, magnesite precipitation is so slow that it would likely also control the rate of magnesite formation at the expense of serpentine.

Photo: Bjørn Jamtveit.

Figure 9.4 Liesegang banding in soapstone blocks pseudomorphically replacing blocks of serpentinite during carbonation process at Linnajavri. The banding is defined by variable quantities of magnesite and talc (the dark layers are magnesite rich). Field of view ~1 metre.

An additional complicating factor is that the rate of magnesite nucleation at similar temperatures is also slow (Giammar *et al.*, 2005; Hanchen *et al.*, 2008). In fact, magnesium carbonate precipitation often does not occur until the saturation state has reached levels at which hydromagnesite ($Mg_5(CO_3)_4(OH)_2{\times}H_2O$) or other mixed carbonate-hydrate phases form.

This implies that carbonation of Mg silicate rich rocks at low (at least from a metamorphic petrologist's point of view) temperatures could in many cases occur under far from equilibrium conditions and conceivably have the potential to create interesting emergent patterns. A possible example is the Liesegang banded precipitation pattern formed during soapstone formation from serpentinite blocks in Linnajavri (Fig. 9.4). In many respects, this is similar to the banded precipitation of weathering products during alteration of the porous andesite shown in Figure 8.2. They both indicate that the precipitation process is hampered by slow nucleation that brings the system into a supersaturation-nucleation-depletion cycle which is known to produce Liesegang banding in a wide range of environments.

9.3 Carbonation of weathered olivine

Olivine carbonation produces a large solid volume increase and serpentine carbonation is slow, so one might ask if there is a Mg silicate with a low density and fast reaction rates, *i.e.* a material that reacts quickly without producing much excess volume. The best candidate would be extensively weathered peridotite. Hydration of peridotite at low temperatures produces a complex mixture of talc and serpentine mineraloids, referred to as dewleyite (Lapham, 1961). Figure 9.5 shows how the mesh texture of a partly serpentinised olivine crystal evolves, as the olivine is first replaced by dewleyite, and then the dewleyite is replaced by calcite.

Høvelmann *et al*. (2011) conducted carbonation experiments on partly weathered peridotite, using a Na-Ca-Cl solution of approximately seawater salinity at 200 °C. The experiments show that dewleyite becomes carbonated much faster than olivine, while serpentine does not react at all. Dewleyite rich weathered peridotite might thus be the optimal rock type for *in situ* mineral carbonation. The problem is obviously the huge volumes of weathered peridotite required to make a difference in terms of *in situ* storage for global quantities of CO_2.

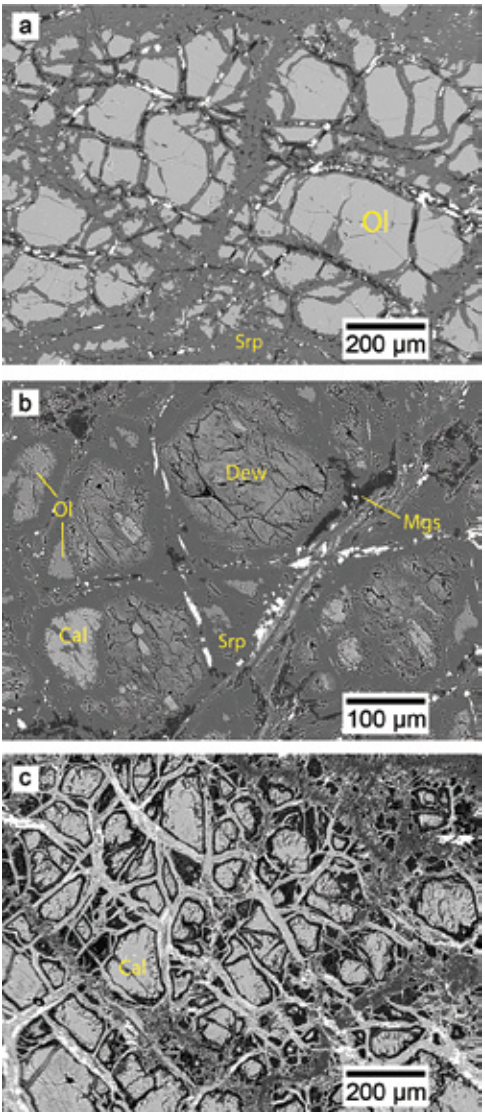

Figure 9.5 Backscattered electron (BSE) images of textures in variably altered peridotite clasts from the Solund basin. a) Partly serpentinised olivine (Ol) displaying a mesh texture. Olivine (Fo_{90}) is veined by serpentine (Srp) and magnesite (dark). The bright phase is magnetite. b) Mesh texture in extensively weathered olivine grain similar to *a*, but with dewleyite (Dew) replacing olivine and with calcite (Cal) as an additional cell filling phase. c) Almost completely carbonated sample, with the original mesh texture intact (modified from Beinlich *et al.*, 2010).

10. PERSPECTIVES

We hope we have convinced the reader that the study of emergent patterns in fluid-rock systems is a fascinating and integral part of Earth sciences. Many emergent patterns can be easily observed with the naked eye in the world around us and fluid-rock interactions might have played a key role in the origin of life itself. Consequently, emergent patterns in fluid-rock systems are of considerable interest to the public at large as well as specialists.

The information contained in these often beautiful products of irreversible processes is, we believe, the key to a more fundamental and quantitative understanding of how the Earth works at our own scale: From micrometres to miles, from seconds to centuries.

We have tried to emphasise that many emerging patterns are insensitive to the details of the system in which they form. Terraces form during coupled flow and precipitation in carbonate systems, during travertine formation but similar structures are also formed by the precipitation of geyserite. Similar terrace patterns can be formed by freezing water in gently sloping creeks. There are other examples of this type of *universality*[1] in pattern formation at the Earth's surface and under more confined conditions in the subsurface.

Many of these patterns have a complexity that reminds us of biological systems and many have been interpreted as such. Botryoidal mineral aggregates with fibrous and branched internal microstructures are reminiscent of some types of moss on several scales. This is obviously not because the detailed growth mechanisms are the same but because growth takes place more or less normal to an external surface where sunlight or dissolved chemical constituents provide critical ingredients for growth and because nucleation occasionally produces new branches in particularly favourable locations on the surface during growth.

These similarities between fundamentally different systems encourage us to believe that it might be possible to understand how the Earth works without having explored and investigated all of it. The similarities suggest that fundamental insights into pattern forming processes in one system can indicate how other systems work – including systems that might be of relevance not only for curiosity driven researchers such as us but to the rest of society as well.

1. In physics, properties of a class of systems, materials or models are said to be universal if they do not depend on details and systems, materials or models that have common properties and are said to belong to the same universality class. For example, the flow of many fluids can be described quite accurately by the Navier-Stokes equation and these fluids are said to belong to the Navier Stokes universality class. Similarly, the thermodynamic properties of materials near second order phase transitions can be described in terms of power laws with corresponding exponents, and materials with the same exponents are considered to belong to the same universality class.

10.1 Challenges across scales

The patterns described in this paper occur on a broad range of scales. Some have a characteristic length scale (such as Figs 1.1 and 4.8), while others show striking similarities across many orders of magnitude in length (such as Figs 3.8 and 7.4). Similar relations apply to time scales. Temporal events can be quasiperiodic, such as fluid expulsion at the *Old Faithful* geyser in Yellowstone or complex and unpredictable, such as earthquakes. It is natural to ask what the various scaling behaviours can tell us about the underlying processes and in particular about the coupling between processes that operate on different spatial and temporal scales.

Patterns that are similar on many scales and display continuous scale invariance are often described in terms of *power laws* and patterns displaying power law scaling are often termed *fractals* (Mandelbrot, 1982; Feder, 1988; Schroeder, 1991). Consider a power law relationship between two variables x and y, with exponent N and a scaling factor a:

$$y = ax^N. \tag{10.1}$$

Now, if we scale up x by a factor s, we obtain:

$$y = a(sx)^N = s^N(ax^N), \tag{10.2}$$

such that the power law remains invariant up to a constant factor. Moreover, by transforming to logarithmic variables, we find that

$$\log y = \log a + N \log x \tag{10.3}$$

and a plot of log y vs. log x is a straight line with slope N. Thus we arrive at the ubiquitous but somewhat infamous *log-log* plots, which have been greatly overused in many research fields. The perils of log-logging are now well known, including the statistical difficulties of identifying a power law in nature without controls, fitting straight lines to data that is obviously better represented by a curve than a straight line on a log-log scale and the common lack of a mechanistic explanation (Stumpf and Porter, 2012).

When two different systems, such as travertine and ice terraces, can be described by a similar power law exponent, they are often said to belong to the same *universality class*, and this could indicate common dynamic principles. Although the fundamental mechanisms controlling the formation of very similar patterns in various systems can be different, understanding the processes behind the patterns in one system can still provide important information about the origin of similar patterns in the other system. In many cases, the mathematical models describing pattern formation are similar, even though the mechanisms are very different. Laplacian growth processes, which generate dendritic patterns, and can be simulated using the diffusion limited aggregation model or the closely related aggregation models provide a notable example. When patterns are more

or less scale invariant over a wide range of scales, it is still possible that the actual mechanisms are different at large and small scales. Consequently it is important to differentiate between scale invariant *patterns* and scale invariant *processes*.

In the case of travertines (Fig. 4.2), the scaling behaviour was studied quantitatively by Veysey and Goldenfeld (2008). They found that the size of water filled pools can be represented by a power law where the number of dams with area, A, scales with A to the power of -2.2. In other words, there are many more small dams than big dams. They furthermore provided a model based on a "Cell Dynamical System", which is a set of rules that controls the local growth in each cell as a function of surface geometry and fluid transport, to explain the scaling behaviour. However, a similar distribution can be predicted from a simple "null model" where larger dams form by the aggregation of two smaller dams. Thus, there could be many paths toward the same scaling behaviour and the scaling behaviour alone generally does not provide sufficient information to deduce the mechanism of the pattern forming process.

Ideal scale invariant (fractal) geometry is inconsistent with the characteristic lengths that are typical of many patterns. However, real systems are scale invariant over only a limited range of scales and the upper and lower limits of the range of lengths over which the system is scale invariant are two characteristic lengths. In the case of travertine terraces, such as those at Yellowstone, USA, the largest terraces are on the order of a few tens of metres and the smallest are on the order of a few centimetres. However, a power law distribution of areas has been established only for small terraces, which appear to have a significantly different geometry than that of large terraces, over less than two orders of magnitude (one order of magnitude in length). In natural systems, where different processes can affect patterns at different scales, it is probably common that the overall structure, such as a travertine terrace system, contains components with characteristic lengths mixed into scale free structures. This is the case for terraced travertine systems. For example, the lips of large terraces are often decorated with stalactite like features that have a characteristic dimension and are absent from small terraces. Hammer *et al.* (2007; 2010) described characteristic lengths in the downstream distance between travertine dams arising from upstream drowning of dams (lateral inhibition, Section 1.1.1). Thus, the terrace landscape is not scale free at small scales and several processes of varying importance depending on scale are involved.

For systems in which fluid flow is important, it is common that surface tension plays an important role at small scales, whereas gravity becomes increasingly important at larger scales. It is therefore often practical to address the pattern forming process with different tools depending on the scale. Particle models and other discrete element models are often applied to small scale processes, whereas continuum models are applied to larger systems. Effective coupling between modelling tools optimised to handle problems at different spatial and temporal scales in a way that accurately conserves mass, energy and momentum remains a major computational challenge.

Scale free patterns across many orders of magnitude in length scale are uncommon in geological systems. Much more common is the situation in which a pattern observed in one system appears qualitatively similar to a pattern observed at a completely different scale in another system. Sometimes, this reflects that the patterns are generated by processes that, albeit different in detail, have some key features in common.

Some examples of patterns from this issue that are similar on different scales are shown in Figure 10.1. Pseudomorphism is a volume for volume replacement process that operates on several lengths scales. Two examples, with characteristic length scales that differ by 3 orders of magnitude, are shown in Figures 10.1a and b. Usually, the reactant and the product phase (or rock) involved in a pseudomorphic replacement have different composition and a prerequisite for replacement is effective transport of components to and from the reacting interface to conserve volume. An additional requirement is that for the reaction to proceed over time, reactive fluids must maintain contact with the parent phase. This implies that the product must contain connected porosity. These two requirements are the only common ingredient of pseudomorphic replacement.

The similarities between the patterns shown in Figures 10.1c and d do not imply that the replacement of leucite by analcime shown in Figure 10.1c is controlled by the same mechanism as the one that produced the spheroidally weathered dolerite outcrop shown in Figure 10.1d. However, both patterns do share the statistical and visual characteristics of a hierarchical fracturing process accompanied by a replacement processes starting at the fracture surfaces.

Figures 10.1e and f both show the characteristic patterns that formed when growth in pits or wedges caused stress concentration and fracturing at a reactive interface. Finally, Figures 10.1g and h show two apparently unrelated, yet somewhat similar, patterns on length scales that differ by five orders of magnitude. One displays the porosity distribution generated during the replacement of KBr with a KBr-KCl solid solution, while the other shows the distribution of charnockite formed during fluid infiltration into amphibolite facies rocks. Both transformations require the presence of fluids at the reacting interface. Thus, Figures 10.1e and f illustrate how complex porosity distributions are generated by an advancing reactive interface on scales that range from 100 micrometres to almost 100 metres. Both of these porosity pattern forming processes remain poorly understood. This is the case for a wide variety of patterns formed in many Earth systems, including many of the most familiar structures that can be observed with our own eyes.

To some of us, it is of fundamental importance to understand the origin of the things that we see around us and this is certainly true for the general public. This is *our* big challenge. Whether it is *your* big challenge or even *the* big challenge in Earth sciences is another matter. Irrespective of the role of pattern formation in the Earth sciences, it is fertile ground for curiosity driven research and it stimulates the development of concepts, understanding and information that can be broadly applied.

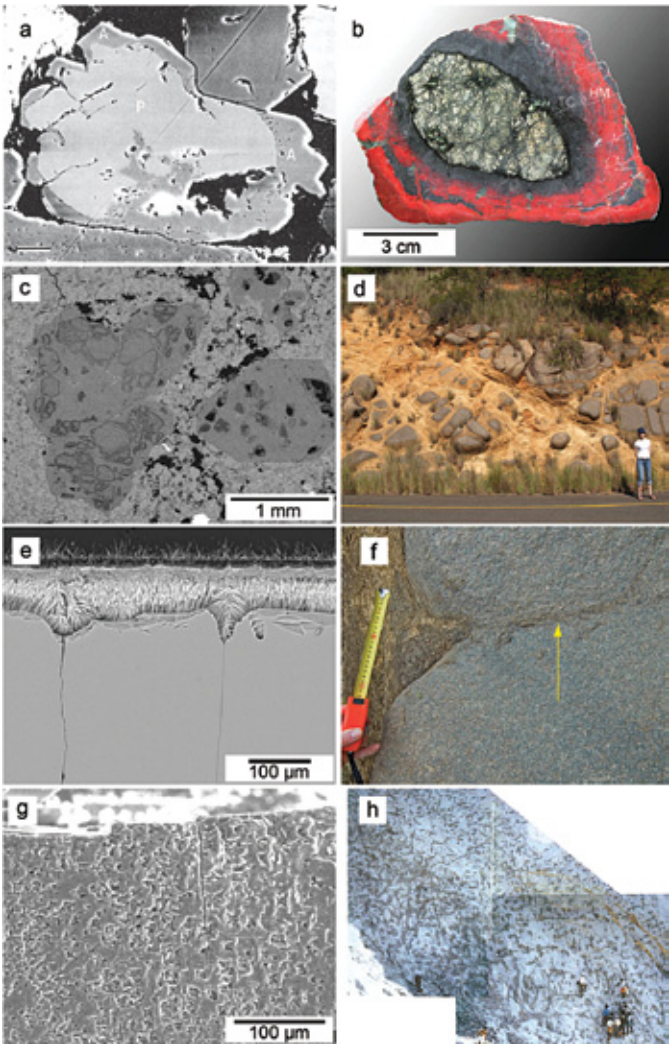

Figure 10.1 Similarities across scales. *a* and *b* show examples of pseudomorphism. A plagioclase grain is replaced by albite in *a* (scale bar 50 μm), while an ultramafic clast (green) is replaced by a red haematite containing alteration product in *b*. *c* shows replacement of leucite crystals by analcime, while *d* shows patterns formed by spheroidal weathering of dolerite. Jamtveit *et al.* (2009) interpreted both to be the results of hierarchical fracturing in a system in which stresses were generated slowly by replacement reactions. *e* and *f* illustrate the importance of interface morphology during reaction driven fracturing at length scales that differ by three orders of magnitude. If the incipient replacement

process produces pits or depressions on the surface of the parent mineral or parent rock, growth of replacement products in these regions can produce stress concentrations, as in a wedging process. Cracks tend to form at wedge tips and reactive fluids gain access to fresh surface area where the process can be repeated. Finally, *g* and *h* show replacement patterns at two extremely different length scales, the pore structure in K(Cl,Br) solid solution replacing a KBr crystal and the charnockite patches in amphibolites from Kerala in India. These patterns surely form by completely different processes and are also visually quite different. However, the progress of both replacement processes depends completely on fluid transport between a fluid reservoir and the reactive interfaces. In both examples, the replacement is pervasive and thus the systems somehow manage to produce porosity during the reaction. The mechanism of porosity production during replacement in the KBr-KCl system is known from the recent experiments of Raufaste *et al.* (2011), while the mechanism of pervasive porosity generation during charnockitisation is unknown. Is it possible to understand patterns similar to what is seen in *h* without invoking small scale processes? This remains to be seen.

REFERENCES

Abart, R., Petrishcheva, E., Joachim, B. (2012) Thermodynamic model for growth of reaction rims with lamellar microstructure. *American Mineralogist* 97, 231-240.

Agrinier, P., Cannat, M. (1997) Oxygen-isotope constraints on serpentinisation processes in ultramafic rocks from the Mid-Atlantic ridge (23ºN). In: Karson, J.A., Cannat, M., Elthon, D. (Eds.) *Proceedings of the Ocean Drilling Program, Scientific Results* 153, pp. 381-388.

Aharonov, E., Whitead, J., Kelemen, P.B., Spiegelman, M. (1995) Channeling instability of upwelling melt in the mantle. *Journal of Geophysical Research* 100, 20433-20450.

Aharonov, E., Spiegelman, M., Kelemen, P.B. (1997) Three-dimensional flow and reaction in porous media: Implications for the Earth's mantle and sedimentary basins. *Journal of Geophysical Research* 102, 14821-14833.

Alcantar, N., Israelachvili, J., Boles, J. (2003) Forces and ionic transport between mica surfaces: implications for pressure solution. *Geochimica et Cosmochimica Acta 67,* 1289-1304.

Alt, J.C., Teagle, D.A.H. (1999) The uptake of carbon during alteration of ocean crust. *Geochimica et Cosmochimica Acta* 63, 1527-1535.

Anzalone, A., Boles, J., Greene, G., Young, K., Israelachvili, J., Alcantar, N. (2006) Confined fluids and their role in pressure solution. *Chemical Geology* 230, 220-231.

Atkinson, B.K. (1984) Subcritical crack growth in geological materials. *Journal of Geophysical Research* 89, 4077-4114.

Aydin, A., DeGraff, J.M. (1988) Evolution of polygonal fracture patterns in lava flows. *Science* 239, 471–476.

Bach, W., Oaulick, H., Garrido, C.J., Ildefonse, B., Meurer, W.P., Humphris, S.E. (2006) Unravelling the sequence of serpentinisation reactions: petrography, mineral chemistry, and petrophysics of serpentinites from MAR 15 °N (ODP Leg 209, Site 1274). *Geophysical Research Letters* 33, L13306.

Ballhaus, C., Gee, C.T., Bockrath, C., Greef, K., Mansfelft, T., Rhede, D. (2012) The silification of trees in volcanic ash – An experimental study. *Geochimica et Cosmochimica Acta 84*, 62-74.

Barge, L.M., Hammond, D.E., Chan, M.A., Potter, S., Petruska, J., Nealson, K.H. (2011) Precipitation patterns formed by self-organizing processes in porous media. *Geofluids* 11, 124-133.

Barnes, I., LaMArche, V.C., and Himmelbe, G. (1967) Geochemical evidence of present-day serpentinization. *Science* 156, 830-832.

Baumgartner, L.P., Rumble, D. (1988) Transport of stable isotopes: I: Development of a kinetic continuum theory for stable isotope transport. *Contributions to Mineralogy and Petrology* 98, 417-430.

Becker, G.F., Day, A.L. (1905) The linear force of growing crystals. *Proceedings of the Washington Academy of Sciences* 8, 283-288.

Beinlich, A., Austrheim, H., Glodny, J., Erambert, M., Andersen, T.B. (2010) CO_2 sequestration and extreme Mg depletion in serpentinized peridotite clasts from the Devonian Solund basin, SW Norway. *Geochimica et Cosmochimica Acta 74*, 6935-6964.

Beinlich, A., plümper, o., hövelmann, j., Austrheim, H., Jamtveit, B. (2012) Massive carbonation of serpentinite at Linnajavri, N-Norway. *Terra Nova* (in press).

Bekri, S., Thovert, F., Adler, P. (1995) Dissolution in porous media. *Chemical Engineering Science* 50, 2765-2791.

Bezacier, L., Reynard, B., Bass, J.D., Sanchez-Valle, C., Van de Moortele, B.V. (2010) Elasticity of antigorite, seismic detection of serpentines, and anisotropy in subduction zones. *Earth and Planetary Science Letters* 289, 198-208.

Bickle, M.J. (1992) Transport mechanisms by fluid-flow in metamorphic rocks – oxygen and strontium decoupling in the Trois-Seigneurs Massif – A consequence of kinetic dispersion. *American Journal of Science* 292, 289-316.

Bickle, M.J., McKenzie, D. (1987) The transport of heat and matter by fluids during metamorphism. *Contributions to Mineralogy and Petrology* 95, 384-392.

Bird, A.J., Springer, G.S., Bosch, R.F., Curl, R.L. (2009) Effects of surface morphologies on flow behaviour in karst conduits. *Proceedings, 15th International Congress of Speleology* 1417-1421.

Bisdom, E.B.A. (1967) The role of micro-crack systems in the spheroidal weathering of an intrusive granite in Galicia (NW Spain). *Geologie en Mijnbouw* 46, 333-340.

Blackwelder, E. (1925) Exfoliation as a phase of rock weathering. *Journal of Geology* 33, 793-836.

Blattner, P., Lassey, K.R. (1989) Stable-isotope exchange fronts, Damköhler numbers, and fluid to rock ratios. *Chemical Geology* 78, 381-392.

Blumberg, P.N., Curl, R.L. (1974) Experimental and theoretical studies of dissolution roughness. *Journal of Fluid Mechanics* 65, 735-751.

Böhm, F., Westphal, H., Bornholdt, S. (2003) Required but disguised: Environmental signals in limestone-marl alternations. *Palaeogeography, Palaeoclimatology, Palaeoecology* 189,161-178.

Bohn, S., Douady, S., Couder, Y. (2005) Four sided domains in hierarchical space diving patterns. *Physical Review Letters* 94, 054503.

Bowman, J.R., Willett, S.D., Cook, S.J. (1994) Oxygen isotopic transport and exchange during fluid-flow – one dimensional models and applications. *American Journal of Science* 294, 1-55.

Bradley, W.C, Hutton, J.T., Twidale, C.R. (1978) Role of salts in development of granitic tafoni, South Australia. *Journal of Geology* 86, 647–654.

Briggs, D.E. (2003) The role of decay and mineralization in the preservation of soft-bodied fossils. *Annual Reviews of Earth and Planetary Sciences* 31, 275-301.

Bucher, K. (1998) Growth mechanisms of metasomatic reaction veins in dolomite marbles from the Bergell Alps. *Mineralogy and Petrology* 63, 151-171.

Buhmann, D., Dreybrodt, W. (1985) The kinetics of calcite dissolution and precipitation in geologically relevant situations of karst areas. 1. Open system. *Chemical Geology* 48, 189-211.

Carlson, W.D., Rosenfeld, J.L. (1981) Optical determination of topotactic aragonite-calcite growth kinetics: metamorphic implications. *Journal of Geology* 89, 615-638.

Chadam, J., Hoff, D., Meriono, E., Ortoleva, P. (1986) Reactive infiltration instabilities. *IMA Journal of Applied Mathematics* 36, 207-221.

Chapman, R.W., Greenfield, M.A. (1949) Spheroidal weathering of igneous rocks. *American Journal of Sciences* 247, 407-429.

Charlou, J.L., Fouquet, Y., Bougault, H., Donval, J.P., Etou, J., Jean-Baptiste, P., Dapoigny, A., Appriou, P., Rona, P.A. (1998) Intense CH_4 plumes generated by serpentinisation of ultramafic rocks at the intersection of the 15°20′N fracture zone and the Mid-Atlantic Ridge. *Geochimica et Cosmochimica Acta* 62, 2323-2333.

Chopard, B., Herrmann, H.J., Vicsek, T. (1991) Structure and growth mechanism of mineral dendrites. *Nature* 353, 409-412.

Correns, C.W., Steinborn, W. (1939) Experimente zur Messung und Erklärung der sogenannten Kristallisationskraft. *Zeitschrift für Kristallographie* 101, 117-133.

Curl, R.L. (1966) Scallops and flutes. *Transactions of Cave Research Group* 7, 121-160.

Daccord, G. (1987) Chemical dissolution of a porous-medium by reactive fluids. *Physical Review Letters* 58, 479-482.

Daccord, G., Lenormand, R. (1987) Fractal patterns from chemical dissolution. *Nature* 325, 41-43.

Dana, J.D. (1896) *Manual of Geology*, 4th ed. American Book Company.

Dash, J.G., Fu, H.Y., Wettlaufer, J.S. (1995) The premelting of ice and its environmental consequences. *Reports on Progress in Physics* 58, 115-167.

Davis, J.C. (1986) *Statistics and Data Analysis in Geology*. John Wiley & Sons.

Delescluse, M., Chamot-Rooke, N. (2008) Serpentinization pulse in the actively deforming Central Indian Basin. *Earth and Planetary Science Letters* 276, 140-151.

Delvigne, J., Bisdom, E.B.A., Sleeman, J., Stoops, G. (1979) Olivines, their pseudomorphs and secondary products. *Pedologie XXIX* 3, 247-309

Eden, M. (1961) A two-dimensional growth process. In: F. Neyman (Ed.) *Biology and Problems of Health*. Vol. 4 of Proceedings of the Fourth Berkeley Symposium on Mathematical Statistics and Probability, University of California Press, Berkeley, pp. 4:223-239.

Emmanuel, S., berkowitz, B. (2007) Effects of pore-size controlled solubility on reactive transport in heterogeneous rock. *Geophysical Research Letters* 34, L06404.

Emmanuel, S., Ague, J.J. (2009) Modelling the impact of nanopores on mineralization in sedimentary rocks. *Water Resources Research* 45, W04406.

Emmanuel, S., Ague, J.J., Walderhaug, O. (2010) Interfacial energy effects and the evolution of pore size distribution during quartz precipitation in sandstone. *Geochimica et Cosmochimica Acta* 74, 3539-3552.

Engvik, A.K., Putnis, A., Fitz Gerald, J.D., Austrheim, H. (2008) Albitisation of granitic rocks: The mechanism of replacement of oligoclase by albite. *Canadian Mineralogist* 46, 1401-1415.

Escartin, J., Hirth, G., Evans, B. (2001) Strength of slightly serpentinized periodotites: Implications for the tectonics of oceanic lithosphere. *Geology* 29, 1023-1026.

Espinosa-Marzal, R.M., Scherer, G.W. (2010) Advances in understanding damage by salt crystallization. *Accounts of Chemical Research* 43, 897-905.

Evans, B.W. (2004) The serpentinite multisystem revisited: Chrysotile is metastable. *International Geology Review* 46, 479-506.

Everett, D.H. (1961) The thermodynamics of frost damage to porous solids. *Faraday Society Transactions* 57, 1541-1550.

Feder, J. (1988) *Fractals*. Plenum Press, New York.

Ferréol. B., Rothman, D.H. (1995) Lattice-Boltzmann simulations of flow though Fountainebleau sandstone. *Transport in Porous Media* 20, 3-20.

Fisher, G.W. (1973) Nonequilibrium thermodynamics as a model for diffusion-controlled metamorphic processes. *American Journal of Science* 273, 897-924.

Fisher, G.W. (1978) Rate laws in metamorphism. *Geochimica et Cosmochimica Acta* 42, 1035-1050.

Fisher, G.W., Lasaga, A. (1981) Irreversible thermodynamics in petrology. *Reviews in Mineralogy* 8, 171-209.

Flatt, R.J., Steiger, M., Scherer, G.W. (2007) A commented translation of the paper by C.W. Correns and W. Steinbor on crystallization pressure. *Environmental Geology* 52, 221-237.

Fletcher, R.C., Merino, E. (2001) Mineral growth in rocks: Kinetic-rheological models of replacement, vein formation, and syntectonic crystallization. *Geochimica et Cosmochimica Acta* 65, 3733-3748.

Fletcher, R. C., Brantley, S.L. (2010) Reduction of bedrock blocks as corestones in the weathering profile: observations and model. *American Journal of Science* 310, 131-164.

Fletcher, R. C., Buss, H. L., Brantley, S.L. (2006) A spheroidal weathering model coupling porewater chemistry to soil thickness during steady-state denudation. *Earth and Planetary Science Letters* 244, 444-457.

Foster, C.T. (1981) A thermodynamic model of mineral segregations in the lower sillimanite zone near Rangeley, Maine. *American Mineralogist* 66, 260-277.

Fukoda, M. (1983) The pore water pressure in porous rocks during freezing. In: *Proceedings, International Conference on Permafrost, 4th, Fairbanks, Alaska*. Washington D.C. National Academy Press, pp. 322-327.

Fyfe, W.S., Bischoff, J.L. (1965) The calcite-aragonite problem. *Society of Economic Paleontologists and Mineralogists Special Publication* 13, 3-13.

Gabrovšek, F. Dreybrodt, W. (2001) A model of the early evolution of karst aquifers in limestone in the dimensions of length and depth. *Journal of Hydrology* 240, 206-224.

Gaillardet, J., Dupre, B., Louvat, P., Allègre, C.J. (1999) Global silicate weathering and CO_2 consumption rates deduced from the chemistry of large rivers. *Chemical Geology* 159, 3-30.

Garcia-Ruiz, J.M., Otálora, F., Sanchez-Navas, A., Higes-Rolando, F.J. (1994) The formation of manganese dendrites as the mineral record of flow structures. In: Kruhl, J.H. (Ed.) *Fractals and dynamic systems in geoscience*. Springer-Verlag, Berlin, pp. 207-318.

De Gennes, P.G. (1985) Wetting: statics and dynamics. *Reviews in Modern Physics* 57, 827-863.

Gerdemann, S.J., O'Connor, W.K., Dahlin, D.C., Penner, L.R., Rush, H. (2007) Ex situ aqueous mineral carbonation. *Environmental Science Technology* 41, 2587-2593.

Giammar, D.E., Bruant, R.G., Peters, C.A. (2005) Forsterite dissolution and magnesite precipitation at conditions relevant for deep saline storage and sequestration of carbon dioxide. *Chemical Geology* 217, 257-276.

Gilpin, R.R. (1979) A model for the 'liquid-like' layer between ice and substrate with application to wire regelation and particle migration. *Journal of Colloid and Interface Science* 68, 235-251.

Gilpin, R.R. (1980) A model for the prediction of ice lensing and frost heave in soils. *Water Resources Research* 16, 918-930.

Goldenfeld, N., Chan, P.-Y., Veysey, J. (2006) Dynamics of precipitation pattern formation at geothermal hot springs. *Physical Review Letters* 96, 254501.

Goldschmidt, V.M. (1911) Die Kontaktmetamorphose im Kristianiagebiet. *Skr. Nor. Vitensk. Akad. Oslo Mat., naturv.* Kl. 1911, No.11.

Goodchild, M.F., Ford, D.C. (1971) Analysis of scallop patterns by simulation under controlled conditions. *Journal of Geology* 79, 52-62.

Grguric, B.A., Rosengren, N.M., Fletcher, C.M., Hronsky, J.M.A. (2006) Type 2 Deposits: Geology, mineralogy, and processing of the Mount Keith and Yakabindie orebodies, Western Australia. In: Barnes, S.J. (Ed.) *Nickel Deposits of the Yilgarn Craton*. Society of Economic Geologists, Littleton, Colorado, pp. 119–138.

Grotzinger, J.P., Rothman, D.H. (1996) An abiotic model for stromatolite morphogenesis. *Nature* 383, 423-425.

GROTZINGER, J.P., KNOLL, A.H. (1999) Stromatolites in Precambrian carbonates: Evolutionary mileposts or environmental dipsticks? *Annual Review of Earth and Planetary Sciences* 27, 313-358.

HAASE, C.S., CHADAM, J., FEINN, D., ORTOLEVA, P. (1980) Oscillatory zoning in plagioclase feldspar. *Science* 209, 272-274.

HACKER, B.R., ABERS, G.A., PEACOCK, S.M. (2003) Subduction factory – 1. Theoretical mineralogy, densities, sesismic wave speeds, and H_2O contents. *Journal of Geophysical Research* 108, 2029.

HAMMER, Ø. (1998) Regulation of astogeny in halysitid tabulates. *Acta Palaeontologica Polonica* 43, 635-651.

HAMMER, Ø. (2008) Pattern formation: Watch your step. *Nature Physics* 4, 265-266.

HAMMER, Ø. (2009) Pattern formation by local amplification and lateral inhibition: examples from biology and geology. *European Physical Journal, Special Topics* 178, 5-12.

HAMMER, Ø., DYSTHE, D.K., JAMTVEIT, B. (2007) The dynamics of travertine dams. *Earth and Planetary Science Letters* 256, 258-263.

HAMMER, Ø., DYSTHE, D.K., LELU, B., LUND, H., MEAKIN, P., JAMTVEIT, B. (2008) Calcite precipitation instability under laminar, open-channel flow. *Geochimica et Cosmochimica Acta* 72, 5009-5021.

HAMMER, Ø., DYSTHE, D.K., JAMTVEIT, B. (2010) Travertine terracing: patterns and mechanisms. In: Pedley, H.M., Rogerson, M. (Eds) *Tufas and Speleothems: Unravelling the Microbial and Physical Controls*. Geological Society of London Special Publication 336, pp. 345-355.

HAMMER, Ø., LAURITZEN, S.E., JAMTVEIT, B. (2012) Stability of dissolution flutes under turbulent flow. *Journal of Cave and Karst Studies*, doi: 10.4311/2011JCKS0200 (in press).

HANCHEN, M., PRIGIOBBE, V., BACIOCCHI, R., MAZZOTTI, M. (2008) Precipitation in the Mg-carbonate system – effects of temperature and CO_2 pressure. *Chemical Engineering Science* 63, 1012-1028.

HARTMANN, J., JANSEN, N., DÜRR, H.H., KEMPE, S., KÖHLER, P. (2009) Global CO_2-consumption by chemical weathering: What is the contribution of highly active weathering regions? *Global and Planetary Change* 69, 185-194.

HEIBERG, J.L. (1912) *Heronis Alexandrini opera quae supersunt omnia*, vol. 4. Teubner, Stuttgart.

HELGESON, H.C. (1968) Evaluation of irreversible reactions in geochemical processes involving minerals and aqueous solutions – I: Thermodynamic relations. *Geochimica et Cosmochimica Acta* 32, 853-877.

HILAIRET, N., REYNARD, B. (2009) Stability and dynamics of serpentinite layer in subduction zone. *Tectonophysics* 465, 24-29.

HOEFNER, M., FOGLER, H. (1988) Pore evolution and channeling formation during fluid flow and reaction in porous media. *AIChE Journal* 34, 45-54.

HOSE, L.D., PALMER, A.N., PALMER, M.V., NORTHUP, D.E., BOSTON, P.J., DUCHENE, H.R. (2000) Microbiology and geochemistry in a hydrogen-sulphide-rich karst environment. *Chemical Geology* 169, 399-423.

Hövelmann, J., Putnis, A., Geisler, T., Schmidt, B.C., Golla-Schindler, Y. (2010) The replacement of plagioclase by albite; observations from hydrothermal experiments. *Contributions to Mineralogy and Petrology* 159, 43-59.

Hövelmann, J., Austrheim, H., Beinlich, A., Munz, I.A. (2011) Experimental study of the carbonation of partially serpentinized and weathered peridotites. *Geochimica et Cosmochimica Acta* 75, 6760-6779.

Huinink, H.P., Pel, L., Kopinga, K. (2004) Simulating the growth of tafoni. *Earth Surface Processes and Landforms* 29,1225-1233.

Iyer, K., Jamtveit, B., Mathiesen, J., Malthe-Sørenssen, A., Feder, J. (2008) Reaction-assisted hierarchical fracturing during serpentinisation. *Earth and Planetary Science Letters* 267, 503-516.

Jamtveit, B., Austrheim, H. (2010) Metamorphism: The role of fluids. *Elements* 6, 153-158.

Jamtveit, B., Bucher-Nurminen, K. Stijfhoorn, D.E. (1992) Contact metamorphism of layered shale-carbonate sequences in the Oslo rift: I. Buffering, infiltration and the mechanisms of mass-transport. *Journal of Petrology* 33, 377-422.

Jamtveit, B., Austrheim, H., Malthe-Sørensen, A. (2000) Accelerated hydration of the Earth's deep crust induced by stress perturbations. *Nature* 408, 75-78.

Jamtveit, B., Malthe-Sørenssen, A., Kostenko, O. (2008) Reaction enhanced permeability during retrogressive metamorphism. *Earth and Planetary Science Letters* 267, 620-627.

Jamtveit, B., Putnis, C., Malthe-Sørenssen, A. (2009) Reaction induced fracturing during replacement processes. *Contributions to Mineralogy and Petrology* 157, 127-133.

Jamtveit, B., Kobchenko, M., Austrheim, H., Malthe-Sørenssen, A., Røyne, A., Svensen, H. (2011) Porosity evolution and crystallization-driven fragmentation during weathering of andesite. *Journal of Geophysical Research* 116, B12204.

Jettestuen, E., Jamtveit, B., Podladchikov, Y.Y., deVilliers, S., Amundsen, H.E.F., Meakin, P. (2006) Growth and characterization of complex mineral surfaces. *Earth and Planetary Science Letters* 249, 108-118.

Johnson, J.W., Oelkers, E.H., Helgeson, H.C. (1992) SUPCRT92: A software package for calculating the standard molal thermodynamic properties of minerals, gases and aqueous species and reactions from 1 to 5000 bar and 0 to 1000°C. *Computers & Geosciences* 18, 899-947

Joesten, R. (1977) Evolution of mineral assemblage zoning in diffusion metasomatism. *Geochimica et Cosmochimica Acta* 41, 649-670.

Kaandorp, J.A., Koopman, E.A., Sloot, P.M.A., Bak, R.P.M., Vermeij, M.J.A., Lampmann, L.E.H. (2003) Simulation and analysis of flow patterns around the scleractinian coral *Madracis mirabilis* (Duchassaing and Michelotti). *Philosophical Transactions of the Royal Society of London B* 358, 1551-1557.

Kaandorp, J.A., Sloot, P.M.A., Merks, R.M.H., Bak, R.P.M., Vermeij, M.J.A., Maier, C. (2005) Morphogenesis of the branching coral *Madracis mirabilis*. *Proceedings of the Royal Society B* 272, 127-133.

Kang, Q., Lichtner, P.C., Janecky, D.R. (2010) Lattice Boltzmann method for reacting flows in porous media. *Advances in Applied Mathematics and Mechanics* 2, 545-563.

KATZAV, E., EDWARDS, S.F., SCHWARTZ, M. (2006) Structure below the growing surface. *Europhysics Letters* 75, 29-35.

KENDRICK, M.A., SCAMBELLURI, M., HONDA, M., PHILLIPS, D. (2011) High abundances of noble gas and chlorine delivered to the mantle by serpentine subduction. *Nature Geosciences* 4, 807-812.

KELEMEN, P.B., MATTER J. (2008) In situ carbonation of peridotite for CO_2 storage. *Proceedings of the National Academy of Sciences of the United States of America* 105, 17295-17300.

KELEMEN, P.B., HIRTH, G. (2012) Force of crystallization during retrograde metamorphism: Olivine hydration and carbonation. *Earth and Planetary Science Letters* (in press).

KELEMEN, P.B., WHITEHEAD, J., AHARONOV, E., JORDAHL, K. (1995) Experiments on flow focusing in soluble porous media with applications to melt extraction from the mantle. *Journal of Geophysical Research – Solid Earth* 100, 475-496.

KELEMEN, P.B., MATTER, J., STREIT, E.E., RUDGE, J.F., CURRY, W.B., BLUSZTJAN, J. (2011) Rates and mechanisms of mineral carbonation in peridotite: Natural processes and receipts for enhanced, in situ CO_2 capture and storage. *Annual Reviews of Earth and Planetary Sciences* 39, 545-576.

KESSLER, M.A., WERNER, B.T. (2003) Self-organization of sorted patterned ground. *Science* 299, 380-383.

KING, H.E., PLUMPER, O., GEISLER, T., PUTNIS, A. (2011) Experimental investigations into the silicification of olivine: Implications for the reaction mechanism and acid neutralization. *American Mineralogist* 96, 1503-1511.

KONN, C., CHARLOU, J.L., DONVAL, J.P., HOLM, N.G., DEHAIRS, F., BOUILLON, S. (2009) Hydrocarbons and oxidized organic compounds in hydrothermal fluids from Rainbow and Lost City ultramafic- hosted vents. *Chemical Geology* 258, 299-314.

KORZHINSKII, D.S. (1957) *Physicochemical basis of the analysis of the paragenesis of minerals*. Academy of Sciences Press, Moscow (English translation by Consultants Bureau, Inc., New York, 1959).

KURODA, T. (1999) Characteristics of the reutilized ruins of the Roman amphitheatre for housing by an analysis of the urban history and context. Study on the reutilization of the ruins of the Roman amphitheatre in Lucca for housing. *Journal of Architecture, Planning and Environmental Engineering* 517, 299-306.

LACHENBRUCH, A.H. (1963) Contraction theory of ice-wedge polygons: a qualitative discussion. Permafrost International Conference. *Proceedings of the National Academy of Science*, 63–71.

LAPHAM, D.M. (1961) New data on Deweylite. *American Mineralogist* 46, 168-188.

LASAGA, A.C. (1998) *Kinetic Theory in the Earth Sciences*. Princeton University Press, Princeton, New Jersey.

LAVALLE, J. (1853) Recherches sur la formation lente des cristaux à la température ordinaire. *Comptes Rendus de l'Academie des Sciences* 36, 49-495.

LEBEDEVA, M.I., FLETCHER, R.C., BRANTLEY, S.L. (2010) A mathematical model for steady-state regolith production at constant erosion rate. *Earth Surface Processes and Landforms* 35, 508-524.

LIBBRECHT, K. G. (2010) *The secret life of a snowflake: An up-close look at the art and science of snowflakes*. Voyageur Press, Minneapolis, USA.

LICHTNER, P.C. (1985) Continuum model for simultaneous chemical reactions and mass transport in hydrothermal systems. *Geochimica et Cosmochimica Acta* 49, 779-800.

LICHTNER, P.C. (1988) The quasi-stationary state approximation to coupled mass transport and fluid-rock interaction in a porous medium. *Geochimica et Cosmochimica Acta* 52, 143-165.

LICHTNER, P.C., KANG, Q. (2007) Upscaling pore-scale reactive transport equations using a multiscale continuum formulation. *Water Resources Research* 43, W12S15.

LICHTNER, P.C., STEEFEL, C.I., OELKERS, E.H. (1996) Reactive transport in porous media. *Reviews in Mineralogy* 34, 438.

LIESEGANG, R.E. (1896) Über einige Eigenschaften von Gallerten. *Naturwissenschaftliche Wochenschrift* 11, 353-362.

LOWE, C.P., FRENKEL, D. (1996) Do hydrodynamic dispersion coefficients exist? *Physical Review Letters* 77, 4552-4555.

MACDONALD, A.H., FYFE, W.S. (1985) Rate of serpentinization in seafloor environments. *Tectonophysics* 116, 123-135.

MALTHE-SØRENSSEN, A., JAMTVEIT, B., MEAKIN, P. (2006) Fracture patterns generated by diffusion-controlled volume changing reactions. *Physics Review Letters* 96, art no. 245501.

MALVOISIN, B., BRUNET, F., CARLUT, J., ROUMÉJON, S., CANNAT, M. (2012) Serpentinization of oceanic peridotites: 2. Kinetics and processes of San Carlos olivine hydrothermal alteration. *Journal of Geophysical Research* 117, B04102.

MANDELBROT, B.B. (1982) *The Fractal Geometry of Nature*. W.H.Freeman, New York.

MARTIN, B., FYFE, W.S. (1970) Some experimental and theoretical observations on the kinetics of hydration reactions with particular reference to serpentinisation. *Chemical Geology* 6, 185-202.

MATTER, J., KELEMEN, P.B. (2009) Permanent CO_2 storage and mineral carbonation in geological reservoirs. *Nature Geosciences* 2, 837-841.

MCBRIDE, E. F. (2003) Pseudofaults resulting from compartmentalized Liesegang bands: update. *Sedimentology* 50, 725–730.

MCBRIDE, E.F, PICARD, M.D. (2004) Origin of honeycombs and related weathering forms in Oligocene Macigno sandstone, Tuscan coast near Livorno, Italy. *Earth Surface Processes and Landforms* 29, 713–735.

MEAKIN, P. (1998) *Fractals, scaling and growth far from equilibrium*. Cambridge University Press.

MEAKIN, P., JAMTVEIT, B. (2010) Geological pattern formation by growth and dissolution in aqueous systems. *Proceedings of the Royal Society of London A* 466, 659-694.

MEAKIN, P., KRUG, J. (1990) Columnar microstructure in three-dimensional ballistic deposition. *Europhysics Letters* 11, 7-12.

MERINO, E., ORTOLEVA, P., STRICKHOLM, P. (1983) Generation of evenly spaced pressure-solution seams during (late) diagenesis – a kinetic theory. *Contributions to Mineralogy and Petrology* 82, 360-370.

MULLINS, W.W., SEKERKA, R.F. (1963) Morphological stability of a particle growing by diffusion or heat flow. *Journal of Applied Physics* 34, 323-329

MÅLØY, K.J., FEDER, J., BOGER, F., JØSSANG, T. (1988) Fractal structure of hydrodynamic dispersion in porous media. *Physical Review Letters* 61, 2925-2928.

NAVARRE-SITCHLER, A., STEEFEL, C.I., YANG, L., TOMUTSA, L., BRANTLEY, S.L. (2009) Evolution of porosity and diffusivity associated with chemical weathering of a basalt clast. *Journal of Geophysical Research* 114, F02016.

NAVARRE-SITCHLER, A., STEEFEL, C.I., SAK, P.B., BRANTLEY, S.L. (2011) A reactive-transport model for weathering rind formation on basalt. *Geochimica et Cosmochimica Acta* 75, 7644-7667.

NAVROTSKY, A., MAZEINA, L., MAJZLAN, J. (2008) Size-driven structural and thermodynamic complexity in iron oxides. *Science* 319, 1635-1638.

NEWTON, R.C., SMITH, J.V., WINDLEY, B.F. (1980) Carbonic metamorphism, granulites and crustal growth. *Nature* 288, 45-50.

NICOLIS, G., ERNEUX, T., HERSCHKOWITZ-KAUFMAN, M. (1978) Pattern formation in reacting and diffusing systems. *Advances in Chemical Physics* 38, 263-315.

NISHIYAMA, T. (1983) Steady diffusion-model for olivine-plagioclase corona growth. *Geochimica et Cosmochimica Acta* 47, 283-294.

NORBERG, N., NEUSSER, G., WIRTH, R., HARLOV, D. (2011) Microstructural evolution during experimental albitization of K-rich alkali feldspar. *Contributions to Mineralogy and Petrology* 162, 531-546.

O'HANLEY, D.S. (1992) Solution to the volume problem in serpentinization. *Geology* 20, 705–708.

OKAMOTO, A., OGASAWARA, Y., OGAWA, Y., TSUCHIYA, N. (2011) Progress of hydration reactions in olivine-H_2O and orthopyroxene-H_2O at 250°C and vapor-saturated pressure. *Chemical Geology* 289, 245-255.

OLLIER, C.D. (1971) Causes of spheroidal weathering. *Earth Science Reviews* 7, 127-141.

O'NEILL, J.R., TAYLOR, H.P. (1967) The oxygen isotope and cation exchange chemistry of feldspars. *American Mineralogist* 52, 1414-1437.

ONSAGER, L. (1931) Reciprocal relations in irreversible processes. I. *Physical Review* 37, 405-426.

ORTOLEVA, P., CHADAM, J., MERINO, E., SEN, A. (1987a) Geochemical self-organization. 1. Reaction-transport feedbacks and modelling approach. *American Journal of Science* 287, 979-1007.

ORTOLEVA, P., MERINO, E., MOORE, C., CHADAM, J. (1987b) Geochemical self-organization. 2. The reactive-infiltration instability. *American Journal of Science* 287, 1008-1040.

ORTOLEVA, P., MERINO, E., STRICKHOLM, P. (1982) Kinetics of metamorphic layering in anisotropically stressed rocks. *American Journal of Science* 282, 619-643.

ORVILLE, P.M. (1963) Alkali ion exchange between vapor and feldspar phases. *American Journal of Science* 261, 201-237.

OSTWALD, W. (1897). *Lehrbuch der Allgemeinen Chemie*. Verlag von Wilhelm Engelmann, Leipzig.

OUFI, O., CANNAT, M., HOREN, H. (2002) Magnetic properties of variably serpentinized abyssal peridotites. *Journal of Geophysical Research* 107, 2095.

Palmer, A.N. (2011) Distinction between epigenic and hypogenic maze caves. *Geomorphology* 134, 9-22.

Perdikouri, C., Kasioptas, A., Geisler, T., Schmidt, B.C., Putnis, A. (2011) Experimental study of the aragonite to calcite transition in aqueous solution. *Geochimica et Cosmochimica Acta* 75, 6211-6224.

Peretti, A., Dubessy, J., Mullis, J., Frost, B.R., Trommsdorff, V. (1992) Highly reducing conditions during alpine metamorphism of the Malenco peridotite (Sondrino, Northern Italy) indicated by mineral paragenesis and H_2 in fluid inclusions. *Contributions to Mineralogy and Petrology* 112, 329-340.

Plümper, O., Røyne, A., Sola, A.M., Jamtveit, B. (2012) The interface-scale mechanism of reaction-induced fracturing during upper mantle serpentinisation. *Geology* (in press).

Pollok, K., Putnis, C.V., Putnis, A. (2011) Mineral replacement reactions in solid solution – aqueous solution systems: Volume changes, reaction paths and end-points using the example of model salt systems. *American Journal of Science* 311, 211-236.

Pons, M.L., Quitte, G., Fujii, T., Rosing, M.T., Reynard, B., Moynier, F., Douchet, C., Albarède, F. (2011) Early Archean serpentine mud volcanoes at Isua, Greenland, as a niche for early life. *Proceedings of the National Academy of Science* 108, 17639-17643.

Putnis, A. (2002) Mineral replacement reactions: from macroscopic observations to microscopic mechanisms. *Mineralogical Magazine* 66, 689–708.

Putnis, A. (2009) Mineral replacement reactions. *Reviews in Mineralogy & Geochemistry* 70, 87-124.

Putnis, A., Mauthe, G. (2001) The effect of pore size on cementation in porous rocks. *Geofluids* 1, 37-41.

Putnis, A., Prieto, M., Fernandez-Diaz, L. (1995) Supersaturation and crystallization in porous media. *Geological Magazine* 132, 1-13.

Putnis, C. V., Mezger, K. (2004) A mechanism of mineral replacement: isotope tracing in the model system KCl-KBr-H_2O. *Geochimica et Cosmochimica Acta* 68, 2839–2848.

Putnis, C. V., Tsukamoto, K., Nishimura, Y. (2005) Direct observations of pseudomorphism: compositional and textural evolution at a fluid-solid interface. *American Mineralogist* 90, 1909–1912.

Putnis, C.V., Geisler, T., Schmid-Beurmann, P., Stephan, T., Giampaolo, C. (2007) An experimental study of the replacement of leucite by analcime. *American Mineralogist* 92, 19-26.

Raith, M., Srikantappa, C. (1993) Arrested charnockite formation at Kottavattam, Southern India. *Journal of Metamorphic Geology* 11, 815-832.

Raufaste, C., Jamtveit, B., John, T., Meakin, P., Dysthe, D.K. (2011) The mechanism of porosity formation during solvent-mediated phase transformations. *Proceedings of the Royal Society A* 467, 1408-1426.

Raviv, U., Klein, J. (2002) Fluidity of bound hydrate layers. *Science* 297, 1540-1543.

Rempel, A.W. (2011) A model for the diffusive growth of hydrate saturation anomalies in layered sediments. *Journal of Geophysical Research* 116, B10105.

Rempel, A.W., Wettlaufer, J.S., Worster, M.G. (2004) Premelting dynamics in a continuum model of frost heave. *Journal of Fluid Mechanics* 498, 227-244.

Richards, L.A. (1931) Capillary conduction in liquids through porous mediums. *Journal of Applied Physics* 1, 318-333.

Ripley, B.D. (1979) Tests of 'randomness' for spatial point patterns. *Journal of the Royal Statistical Society, series B* 41, 368-374.

Rittmann, B.E., VanBriesen, J.M. (1996) Microbial processes in reactive modelling. *Reviews in Mineralogy* 34, 311-334.

Robin, P.-Y.F. (1978) Pressure solution at grain-to-grain contacts. *Geochemica et Cosmochimica Acta* 42, 1383-1389 .

Rudge, J.F., Kelemen, P.B., Spiegelman, M. (2010) A simple model of reaction-induced cracking applied to serpentinisation and carbonation of peridotite. *Earth and Planetary Science Letters* 291, 215-227.

Rumori, C., Mellini, M., Viti, C. (2004) Oriented, non-topotactic olivine serpentine replacement in mesh-textured, serpentinized peridotites. *European Journal of Mineralogy* 16, 731-741.

Røyne, A., Jamtveit, B., Mathiesen, J., Malthe-Sørenssen, A. (2008) Controls on weathering rates by reaction induced hierarchical fracturing. *Earth and Planetary Science Letters* 275, 364-369.

Røyne, A., Malthe-Sørenssen, A., Jamtveit, B., Dysthe, D.K., Meakin, P. (2011) Critical crack propagation driven by crystal growth. *Europhysics Letters* 96, 24003.

Sagemann, J., Bale, S.J., Briggs, D.E.G., Parkes, R.J. (1999) Controls on the formation of authigenic minerals in association with decaying organic matter: An experimental approach. *Geochimica et Cosmochimica Acta* 63, 1083-1095.

Saldi, G.D., Schott, J., Pokrovsky, O.S., Gautier, Q., Oelkers, E.H. (2012) An experimental study of magnesite precipitation rates at neutral to alkaline conditions and 100-200°C as a function of pH, aqueous solution composition and chemical affinity. *Geochimica et Cosmochimica Acta* 83, 93-109.

Sarracino, R., Prasad, G. (1989) Investigation of spheroidal weathering and twinning. *GeoJournal*, 19, 77-83.

Scherer, G.W. (1999) Crystallization in pores. *Cement and Concrete Research* 29, 1347-1358.

Scherer, G.W. (2004) Stress from crystallization of salt. *Cement and Concrete Research* 34, 1613-1624.

Schopf, J.M. (1975) Models for fossil preservation. *Review of Palaeobotany and Palynol*ogy 20, 27-53.

Schroeder, M.R. (1991) *Fractals, chaos, power laws: Minutes from an infinite paradise*. Freeman, New York.

Short, M.B., Baygents, J.C., Beck, J.W., Stone, D.A., Toomey, R.S., Goldstein, R.E. (2005) Stalactite growth as a free-boundary problem: A geometric law and its Platonic ideal. *Physical Review Letters* 94, 018501.

Schuiling, R.D. (1964) Serpentinization as a possible source of high heat-flow values in and near oceanic ridges. *Nature* 201, 807-808.

Smith, D. A. (1984) On Ostwald's supersaturation theory of rhythmic precipitation (Liesegang's rings). *Journal of Chemical Physics* 81, 3102–3115.

Spotl, C., Matter, A., Brevart, O. (1993) Diagenesis and pore water evolution in the Keuper Reservoir, Paris Basin, France. *Journal of Sedimentary Petrology* 63, 909-928.

Steefel, C.I., lasaga, A.C. (1992) Putting transport into water-rock interaction models. *Geology* 20, 680-684.

Steefel, C.I., lasaga, A.C. (1994) A coupled model for transport of multiple chemical species and kinetic precipitation dissolution reactions with applications to reactive flow in single-phase hydrothermal systems. *American Journal of Science* 294, 529-592.

Steefel, C.I., MacQuarrie, K.T.B. (1996) Approaches to modelling of reactive transport in porous media. *Reviews in Mineralogy* 34, 83-129.

Steefel, C.I., Maher, K. (2009) Fluid-Rock interactions: A reactive transport approach. *MSA Reviews in Mineralogy* 70, 485-532.

Steefel, C.I., DePaolo, D.J., Lichtner, P.C. (2005) Reactive transport modelling: An essential tool and a new research approach for the Earth Sciences. *Earth and Planetary Science Letters* 240, 539-558.

Steiger, M. (2005) Crystal growth in porous materials–II: Influence of crystal size on the crystallization pressure. *Journal of Crystal Growth* 282, 470–481.

Stern, K.H. (1954) The Liesegang phenomenon. *Chemical Reviews* 54, 79-99.

Stesky, R.M., Brace, W.F. (1973) Electrical conductivity of serpentinized rocks to 6 kilobars. *Journal of Geophysical Research* 78, 7614-7621.

Stewart, P.S. (2003) Diffusion in biofilms. *Journal of Bacteriology* 185, 1485-1491.

Streitz, J.T., Ettema, R. (2002) Observations from an aufeis windtunnel. *Cold Regions Science and Technology* 34, 85-96.

Stroock, A.D., Dertinger, S.K.W., Ajdari, A., Mezic, I., Stone, H.A., and Whitesides, G.M. (2002) Chaotic mixers for microchannels. *Science* 295, 647-651.

Stumm, W., Morgan, J.J. (1996) *Aquatic Chemistry*. Third edition, Wiley Interscience.

Stumpf, M.P.H., Porter, M.A. (2012) Critical truths about power laws. *Science* 335, 665-666.

Sultan, R., Ortoleva, P. (1993) Periodic and aperiodic macroscopic patterning in two precipitate post-nucleation systems. *Physica D* 63, 202-12.

Szymczak, P., Ladd, A.J.C. (2011) Instabilities in the dissolution of a porous matrix. *Geophysical Research Letters* 38, L07403.

Taber, S. (1916) The growth of crystals under external pressure. *American Journal of Science* 41, 532-556.

Taber, S. (1929) Frost heaving. *Journal of Geology* 37, 428-461.

Taber, S. (1930) The mechanics of frost heaving. *Journal of Geology* 38, 303-317.

Taber, S. (1950) Intensive frost action along lake shores. *American Journal of Science* 248, 784-793.

Takai, K., Gamo, T., Tsunogai, U., Nakayama, N., Hirayama, H., Nealson, K.H., Horikoshi, K. (2004) Geochemical and microbiological evidence for a hydrogen-based, hyperthermophilic subsurface lithoautotrophic microbial ecosystem (HyperSLiME) beneath an active deep sea hydrothermal field. *Extremophiles* 8, 269-282.

Thompson, J.B. (1959) Local equilibrium in metasomatic processes. In: Abelson, P.H. (Ed.) *Researches in Geochemistry*. Wiley, New York.

Toga, K.B., Alaca, B.E. (2006) Junction formation during desiccation cracking. *Physical Review E* 74, 021405.

Tompson, A.F.B. (1993) Numerical simulation of chemical migration in physically and chemically heterogeneous porous media. *Water Resources Research* 29, 3709-3726.

Turner, B.F., Stallard, R.F., Brantley, S.L. (2003) Investigation of in situ weathering of quartz diorite bedrock in the Rio Icacos basin, Luquillo Experimental Forest, Puerto Rico. *Chemical Geology* 202, 313-341.

Ueno, K., Farzaneh, M., Yamaguchi, S., Tsuji, H. (2010). Numerical and experimental verification of a theoretical model of ripple formation in ice growth under supercooled water film flow. *Fluid Dynamics Research* 42, 025508.

Van Cappellen, P., Gaillard, J.F. (1996) Biogeochemical dynamics in aquatic sediments. *Reviews in Mineralogy and Geochemistry* 34, 335-376.

Veysey, J., Goldenfeld, N. (2008) Watching rocks grow. *Nature Physics* **4**, 310-313.

Villien, B., Zheng, Y., Lister, D. (2005) Surface dissolution and the development of scallops. *Chemical Engineering Communications* 192,125-136.

Walder, J., Hallet, B. (1985) A theoretical model of the fracture of rock during freezing. *Geological Society of America Bulletin* 96, 336-346.

Wary, J.L., Daniels, F. (1957) Precipitation of calcite and aragonite. *Journal of American Chemical Society* 79, 2031-2034.

Webb, M.B., Garofalini, S.H., Scherer, G.W. (2011) Molecular dynamics investigation of solution structure between NaCl and quartz crystals. *Journal of Physical Chemistry C* 115, 19724-19732.

Weill, D.F., Fyfe, W.S., (1964) A discussion of the Korzhinskii and Thompson treatment of thermodynamic equilibrium in open systems. *Geochimica et Cosmochimica Acta* 28, 565-576.

Williams, P.J., Smith, M.W. (1991) *The Frozen Earth: Fundamentals of Geocryology*. Cambridge University Press, Cambridge.

Wooding, R.A. (1991) Growth of natural dams by deposition from steady supersaturated shallow flow. *Journal of Geophysical Research* 96, 667-682.

Xia, F., Brugger, J., Ngothai, Y., O'Neill, B., Chen, G., Pring, A. (2009) Three dimensional ordered arrays of nanozeolites with uniform size and orientation by a pseudomorphic coupled dissolution-reprecipitation replacement route. *Crystal growth and design* 9, 4902-4906.

Yakobson, B.I. (1991) Morphology and rate of fracture in chemical decomposition of solids. *Physical Review Letters* 67, 1590-1593.

SUPPLEMENTARY INFORMATION

THE STATISTICS OF PATTERNS

By a *pattern*, we often mean a more or less regular spacing of elements. This could indicate a lateral inhibition process that could be explained *e.g.* by depletion and diffusion of chemical species. The machinery of spatial statistics can be helpful to identify and characterise such patterns in a rigorous manner.

A useful starting point is the null hypothesis of a so called *Poisson process* which places points independently and with uniform probability over the domain of interest. This results in complete spatial randomness (CSR) and the distribution of distances between nearest neighbours has a decaying exponential form. Under CSR, perhaps contrary to intuition, very small distances between nearest points are commonly observed, while larger distances are progressively less common. If a lateral inhibition process has played a role in the process, the average nearest neighbour distance (the distance between a point and the nearest different point) is larger. This observation forms the basis for a simple test of spatial randomness (*e.g.* Davis, 1986). The observed average nearest neighbour distance is compared with the expected value under CSR, which is

$$\mu = \frac{\sqrt{A/n}}{2}, \qquad \text{(SI-1)}$$

where A represents the area (often difficult to estimate precisely) and n, the number of points. The difference between observed and expected average distance can be subjected to a statistical significance test (Z test). A correction should be made for the fact that points near the boundary have neighbours only on the inner side.

A simple example illustrates the procedure. Figure SI-1 shows the digitised positions of garnet crystals in a garnet schist. The average nearest neighbour distance is 11.1 mm (using a toroidal edge correction), slightly larger than the expected distance of 9.45 mm. The difference is significant at p=0.018.

Nearest neighbour analysis is a local procedure. However, the point pattern parameters often change with scale, for example with over dispersion (lateral inhibition) at small scales but clustering at larger scales. Information on such effects can be obtained by Ripley's K analysis (Ripley, 1979). The function, $K(d)$, is simply the number of points within increasing distance, d, averaged over all central points and scaled by a density parameter. Under CSR, it is expected to increase as the square of d. The black curve in Figure SI-2a shows Ripley's K for the garnet data set, together with 95% confidence intervals under the null hypothesis of CSR (obtained by a Monte Carlo procedure). To make the graphs clearer, we can transform the curve by $L(d)=\sqrt{K(d)}$. The function $L(d)$-d is expected to be zero under CSR. As seen in Figure SI-2b, the garnet data are below zero for all distances, indicating over dispersion, but are mostly inside the 95% confidence interval, *i.e.* not significantly different from CSR. However, at the smallest scales, below ~10 mm, there is stronger evidence for

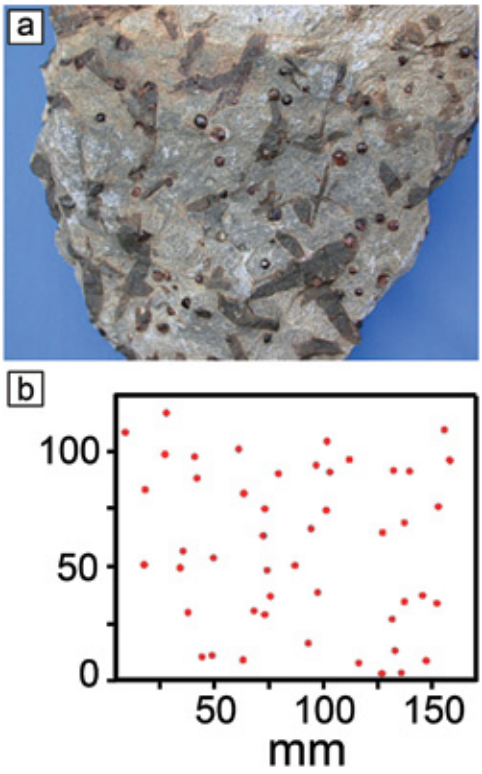

Photo: Charles Jones, University of Pittsburgh.

Figure SI-1 a) Garnet-staurolite schist. b) Digitised positions of the garnets in a).

lateral inhibition. This distance is still much larger than the size of the crystals. We can conclude that there is (somewhat weak) statistical evidence for lateral inhibition in this case but it has a relatively short range.

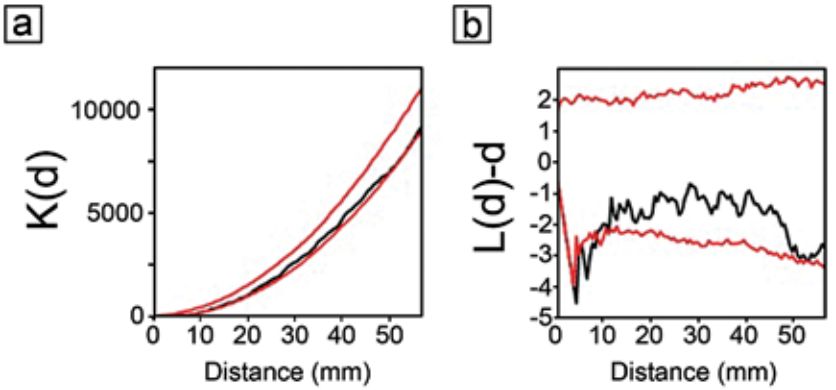

Figure SI-2 Ripley's *K* analysis of the garnet data set. a) Observed *K*(*d*) (black), with 95% confidence limits for CSR (red). b) The transformed curve *L*(*d*)-*d*, with confidence limits.

Similar procedures can be carried out in one dimension (such as a transect across a banded structure) and in three dimensions (*e.g.* from tomographic data).

INDEX

Geochemical Perspectives is an official journal of the European Association of Geochemistry

The European Association of Geochemistry, EAG, was established in 1985 to promote geochemistry, and in particular, to provide a platform within Europe for the presentation of geochemistry, exchange of ideas, publications and recognition of scientific excellence.

Officers of the EAG Council

President	Bernard Bourdon, ENS Lyon, France
Vice-President	Chris Ballentine, University of Manchester, UK
Past-President	Eric H. Oelkers, CNRS Toulouse, France
Treasurer	Christa Göpel, IPG Paris, France
Secretary	Liane G. Benning, University of Leeds, UK
Goldschmidt Officer	Bernard Marty, CNRS Nancy, France
Goldschmidt Officer	Bernie Wood, University of Oxford, UK

www.eag.eu.com

BJØRN JAMTVEIT is professor of petrology and director of Physics of Geological Processes (PGP), a Norwegian Center of Excellence at the University of Oslo. Bjørn's research focuses on the coupling between fluid migration, reactions and deformation processes. Applications include the mechanisms of retrograde metamorphism, weathering, growth of emergent patterns by coupled fluid flow and growth or dissolution in near surface environments (eg. travertines), pressure solution, compaction and crystal growth. He has also worked on the generation of hydrothermal vent complexes driven by sill intrusions in sedimentary basins.
In contrast to many Scandinavian geology colleagues, Bjørn enjoys mingling with physicists and prefers field work at low latitudes. Nonscientific activities include literature, gardening and single malts.
He was elected Fellow of the European Association of Geochemistry and the Geochemical Society in 2012.

ØYVIND HAMMER was born when atmospheric CO_2 was 320 ppm. A mathematical modeller turned paleontologist, he is now associate professor in paleontology at the Natural History Museum, and senior researcher in geology at PGP, both at the University of Oslo. Øyvind has published in palæontology, stratigraphy, geochemistry, oceanography, climatology, zoology, botany, theoretical biology and statistics. Some points of focus are the Lower Palæozoic, Jurassic and Holocene of Norway (including the Arctic and offshore areas), precipitation and dissolution under flow, pattern formation in biology and geology and quantitative data analysis. Currently, his favourite projects are Recent and Jurassic methane seepage and Ordovician cyclostratigraphy.
In common with many Scandinavian geology colleagues, Øyvind prefers field work at high latitudes. Nonscientific interests include history and music, his son, and his saltwater aquarium.